Modeling and Mitigating Spatial Disorientation in Low G Environments: Final Report

Submitted to NASA's National Space Biomedical Research Institute (NSBRI)

Under NASA Cooperative Agreement NCC 9-58, sub-agreement 511
NSBRI Project Number SA 01302

By
Ronald L. Small; Charles M. Oman, PhD; Christopher D. Wickens, PhD; John W. Keller; Brian Curtis; Thomas D. Jones, PhD; Mark Brehon

August 2011

Alion Science and Technology Corp.
4949 Pearl East Circle, Suite 200
Boulder, Colorado 80301
303.442.6947

and

Massachusetts Institute of Technology
Man Vehicle Laboratory, Room 37-219
77 Mass. Ave., Cambridge, MA 02139
617.253.7508

Table of Contents

Acknowledgements

We are indebted to the anonymous Space Shuttle flight crewmembers who responded to our survey about spatial orientation problems and illusory sensations. We also greatly appreciate receiving helicopter data sets from an anonymous source, and the time and effort from a specific individual who helped us better understand helicopter spatial disorientation illusions, and their manifestations in helicopter operations. Drs. Larry Young of MIT and Art Estrada of USAARL were helpful throughout the project's four years. Torin Clark of MIT provided data sets from a lunar landing simulation. MIT graduate students Mike Newman, Raghav Venkatesan, and Alex Donaldson worked to improve Observer, as did post-doctoral student Pierre Selva. Alion's Andrew Hamilton and Angie Eckdahl helped with software improvements to SDAT. Angie also was the main developer of the FORT tool. As with our previous spatial disorientation research for AFRL, discussions of vestibular perception nuances with Drs. Bill Ercoline and Bob Cheung made seemingly insurmountable problems less so.

Executive Summary

This report describes the goals and accomplishments of the project entitled *Modeling and mitigating spatial disorientation in low g environments* for NASA's National Space Biomedical Research Institute (NSBRI) by the team of Alion Science and Technology Corporation's MA&D Operation, and the Massachusetts Institute of Technology's (MIT's) Man Vehicle Laboratory. The report comprehensively captures the team's methods and accomplishments over the four years of the project (9/1/07-8/31/11).

The goal of this industry-university research and development project was to extend Alion's spatial disorientation mitigation software – originally developed for aeronautical use – to NASA space applications. Alion's Spatial Disorientation Analysis Tool (SDAT) was designed for post hoc analyses of aircraft flight data to determine the likelihood of the pilot experiencing vestibular SD. Companion software, SOAS (Spatial Orientation Aiding System), is a real-time cockpit aid that has been evaluated in simulators with rated pilots. Both tools incorporate models of the vestibular system and SD illusion models to predict the epoch and probability of an SD event, as well as any other significant disparities between actual and perceived pitch attitude (somatogravic), and roll or yaw/heading rates (somato-gyral). Additionally, SOAS assesses the pilot's multi-sensory workload to determine the types of countermeasures to trigger and when to trigger them.

MIT's *Observer* model of human orientation physiology predicts attitude and displacement perceptions using experimental data to explain known terrestrial (e.g., Coriolis) and space flight illusions (e.g., ROTTR).

The objectives of the project were to improve both Observer and SDAT and to integrate the two models to achieve better predictions of SD illusion epochs and probabilities than either model could do separately. All improvements were to be verified and validated using existing aeronautical and experimental data sets, and if feasible, newly acquired data sets from space vehicles. Simulator and flight experiments would be planned and conducted, if needed, for further validations. A final aim was to consider multiple visual frames of reference, the effects of visual attention and sensory workload, and the cognitive costs of mental rotation and reorientation.

The four overall specific aims of the project and accomplishments for each were:

1. Extend Alion's Spatial Disorientation Analysis Tool (SDAT) by incorporating an enhanced MIT *Observer* model into SDAT. Validate enhancements with existing and new flight data sets.
   - Accomplishments: SDAT now includes a user selection for using an Observer .dll (dynamically linked library) to calculate perceptions. In addition, SDAT's otolith perception model was enhanced with gravito-inertial force calculations. The pre-existing semi-circular canal (SCC) perception model was unchanged, but the pitch and roll perception angles are now a result of combining SCC and otolith perceptions in a unique way.

     Observer was enhanced by adding static and dynamic visual cue inputs, estimate of perceived velocity, displacement and azimuth, improvements to vestibular model coefficients, and a new GUI. The relationship between Observer and Kalman Filter models was also explored. As an intermediate step toward fully integrating Observer into SDAT, a stand-alone compiled version, called *eObserver*, was developed and tested. Finally, MIT created an Observer 10Hz model .dll for integration into SDAT.

All enhancements were verified and validated with existing data sets from simulators, laboratory experiments, and real SD mishaps.

2. Extend SDAT assessments to include typical space vehicle illusions. Validation will include assessment of Space Shuttle landing data, and Altair simulator data.
   - Accomplishments: We designed new illusion models for vertical landing vehicles (e.g., helicopters and lunar landers) and obtained actual helicopter flight data sets that include SD events. Shuttle data sets were unusable. Altair (lunar lander) simulator data (from the NASA-Ames vertical motion simulator) were used for verifying and validating Observer enhancements. Furthermore, we distributed a survey to Shuttle commanders and pilots to quantify their experiences with illusory sensations resulting from the transition from 1-g to 0-g and back.

3. Further extend SDAT by examining alternative visual reference frames. FORT is used to predict the cognitive cost of transitioning between reference frames. Validation of Aims 1-3 for SDAT may include parabolic flight experiments.
   - Accomplishments: A frame of reference transformation (FORT) tool was designed, developed, verified, and validated. Flight experiments did not occur since 0-g adapted humans are only available on the International Space Station (ISS). The FORT tool and concepts were not integrated into SDAT because it is not appropriate to do so. The FORT tool is for system designers; it examines human performance issues separate from vestibular-based spatial disorientation, which is the primary purpose of SDAT.

4. To further enhance SDAT assessor performance, pilot multi-sensory workload is considered in countermeasure selection. Validation experiments are not detailed, but will involve evaluations in ground-based simulators.
   - Accomplishments: In addition to existing countermeasure logic within SDAT, which is based upon pilot multi-sensory (visual, auditory, tactile, and cognitive) workload, we incorporated a representation of the N-SEEV (noticing - salience, effort, expectancy, value) pilot attention model into SDAT to improve countermeasure triggering logic.

To summarize: (1) The first year of the four-year project was spent trying to understand each other's models (Observer and SDAT) in sufficient detail to figure out how to merge them. Data set results were analyzed and compared. Observer was enhanced with an improved GUI and visual orientation cues. (2) The second year emphasized Observer-SDAT comparisons and contrasts, and the theoretical design of a FORT tool. (3) The third year emphasized FORT tool development and merging a compiled stand-alone version of Observer (aka *eObserver*) into SDAT. We also designed and partially developed a method to make use of the N-SEEV pilot attention model within SDAT. (4) In the fourth year we concluded that the two models (Observer and SDAT) could not be fully integrated due to their philosophical differences and disparate data needs. However, MIT developed a .dll version of Observer to be integrated within SDAT so that users can select which perception model to use when analyzing a specific data set. In addition, the FORT tool was validated, and the N-SEEV addition to SDAT was completed. We also added new SD illusion models to SDAT and completely re-worked its otolith (GIF) model. Finally, we enhanced SDAT to provide a total combined prediction of perceived pitch and roll from the previously separate otolith and SCC models.

Introduction

This report describes the goals and progress of the project entitled *Modeling and mitigating spatial disorientation in low g environments* for NASA's National Space Biomedical Research Institute (NSBRI) by the team of Alion Science and Technology Corp., and the Massachusetts Institute of Technology's (MIT's) Man Vehicle Laboratory (MVL).

The project's original four goals and summaries of our accomplishments are in the Executive Summary. The following sections of this report will elaborate on the methods used and progress for each goal. Specifically, we will describe: the enhancements to MIT's model of human orientation perception, Observer; the enhancements to Alion's SDAT; how we integrated the two distinct models; ancillary accomplishments; recommendations for future related research and development; and, conclusions.

MIT's Observer

This section first recounts the history of Observer and then describes its enhancements due to this project.

Observer model history

Quantitative *observer* models for spatial orientation and eye movements have been developed based on 1-g data from humans and animals (e.g., Oman, 1982, 1991; Merfeld et al., 1993; Merfeld & Zupan, 2002; Haslwanter et al., 2000; Vingerhoets et al., 2006). These models assume that the central nervous system (CNS) estimates *down*, head angular velocity, and linear accelerations using an internal model for gravity and sense organ dynamics that are continuously updated by sensory-conflict signals. Thus, this CNS function is analogous to a Luenberger (1971) state observer in engineering systems. Using a relatively small set of free parameters, Observer orientation models capture the main features of experimental data for a variety of different motion stimuli.

Observer describes the input-output relationships learned or genetically prewired in CNS neural networks, which presumably function without the explicit vector and quaternion mathematics used by the Matlab simulation at the heart of Observer. As noted by Oman (2007), electro-physiological and anatomical evidence supports the notion of brainstem "velocity storage" neurons, and limbic head direction, grid and place cells coded in a 2-D horizontal plane whose orientation is apparently determined by the perceived direction of "down."

The notion that human spatial orientation could be phenomenologically and mathematically described using "Kalman Filter" techniques borrowed from estimation and control theory was first demonstrated by Young and coworkers (Borah et al., 1979). Subsequent MVL modeling efforts (e.g., Bilien, 1993) showed that human orientation perception dynamics may not be truly "optimal" in a theoretical sense – much faster dynamics of a different order would be expected than are actually seen. Nonetheless, as noted by Oman (1991) the more general "observer" concept of state estimation – updated by sensory conflict signals derived from internal models of body and sense organ dynamics – remained useful, even if the human was not truly an "optimal" observer. The "sensory conflict" notion also provided a parsimonious hypothesis for the

essential stimulus for motion sickness. Observer-based models currently underlie the widely accepted sensory-motor conflict theory for motion sickness (Reason, 1978; Oman, 1990), and several related theories (e.g., Bos & Bles, 2002).

Observer models for vestibular cue interaction have been validated using perceptual and eye movement data from humans, and eye movement data from animals, all of whom were passively accelerated (i.e., they did not control the motions they experienced). The models capture the main features of response data for a variety of different stimuli in a 1-g environment, including off-vertical-axis rotation (OVAR), linear acceleration, and centrifugation with a single set of up to five free parameters. In this sense, Observer models have emergent properties, and can play a useful role in quantitative hypothesis testing and refinement. For example, it can be applied to the current debate (e.g., Merfeld et al., 2005) as to whether or not the human vestibular-ocular reflex (VOR) is as closely coupled to orientation perception as originally suggested by the models of Haslwanter et al. (2000) and Vingerhoets et al. (2006, 2007).

Observer enhancements

During the course of the current research and development project, Observer was enhanced with a variety of new features, as described below.

Inputs to Observer are time series data supplied via Excel spreadsheet using a specific format. After each simulation, Observer displays a family of 2-D plots of model inputs and outputs. A separate 3-D visualization window dynamically displays the time course of Observer model "down" and "azimuth" estimates.

Figure 1 is a block diagram of Observer. Observer uses a quaternion vector integrator to calculate the perceived "down" vector. For rotations about the axis of gravity, the primary drive to this quaternion rotator comes from the angular velocity estimate, weighted by a gain ("kwf"). The estimated azimuth is calculated by integrating the estimated angular velocity in a plane perpendicular to the estimated gravitational vertical. During off-gravitational-vertical-rotation of the head, the changing otolith signal provides an additional cue to angular rotation. Observer compares actual and expected otolith signals, and computes the vector difference between them. This vector, weighted by the gain "kf," provides a second important "down" rotational input to the quaternion rotator. Since the GIF error vector also provides a cue to angular motion, this is weighted by a gain, "kfw," and added into the angular velocity estimation. During constant velocity OVAR, this pathway creates sustained rotation sensations, and ultimately contributes a constant bias component to the VOR, long after SCC cues have disappeared.

In 1-g, the interaction between semicircular canal and otolith cues in the Observer model is thus determined by the four observer parameters (ka, kf, kw, and kfw) in both humans and monkeys (Merfeld et al., 1993; Vingerhoets et al., 2007) (Figure 2). A fifth GIF gain, "kwf," has been added so the model will mimic post-landing tilt-gain illusions in astronauts returning to 1-g from space. Otolith-tilt-translation-reinterpretation (OTTR) illusions after spaceflight can be approximated by setting the GIF feedback gain, kf, to a low value (e.g., 0). Observer accounts for the dynamics of these illusions; for example, it mimics the anecdotal descriptions by returning astronauts that a sustained head tilt does not yield a sustained perception of motion, only an initial illusion.

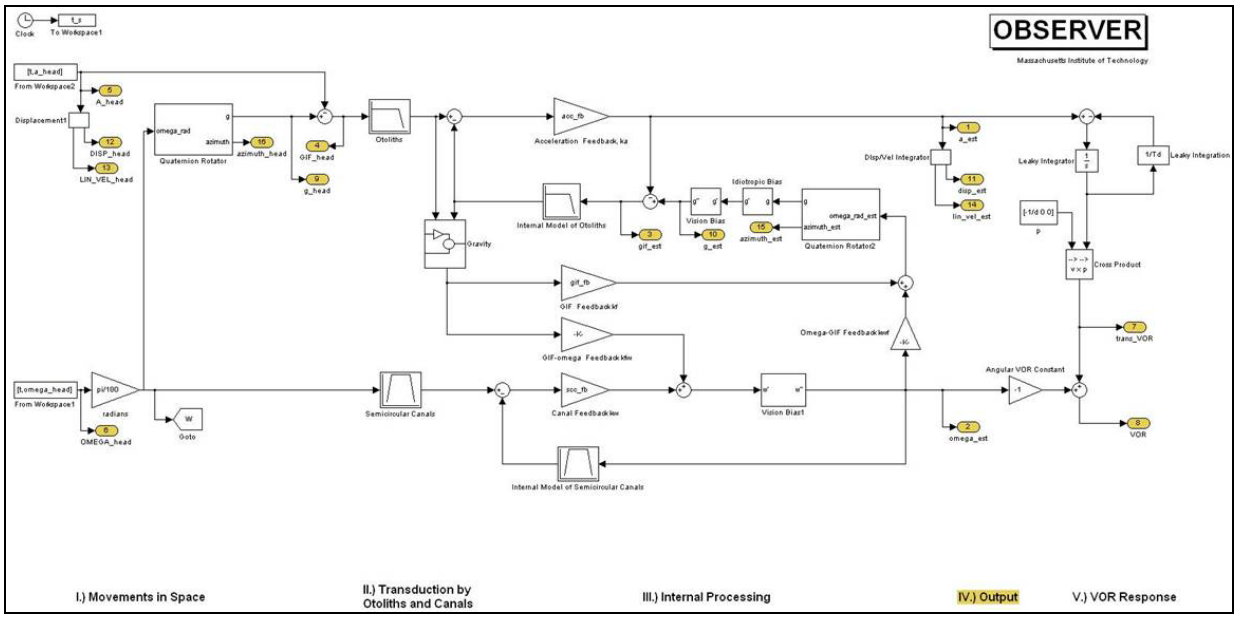

Figure 1. Observer block diagram.

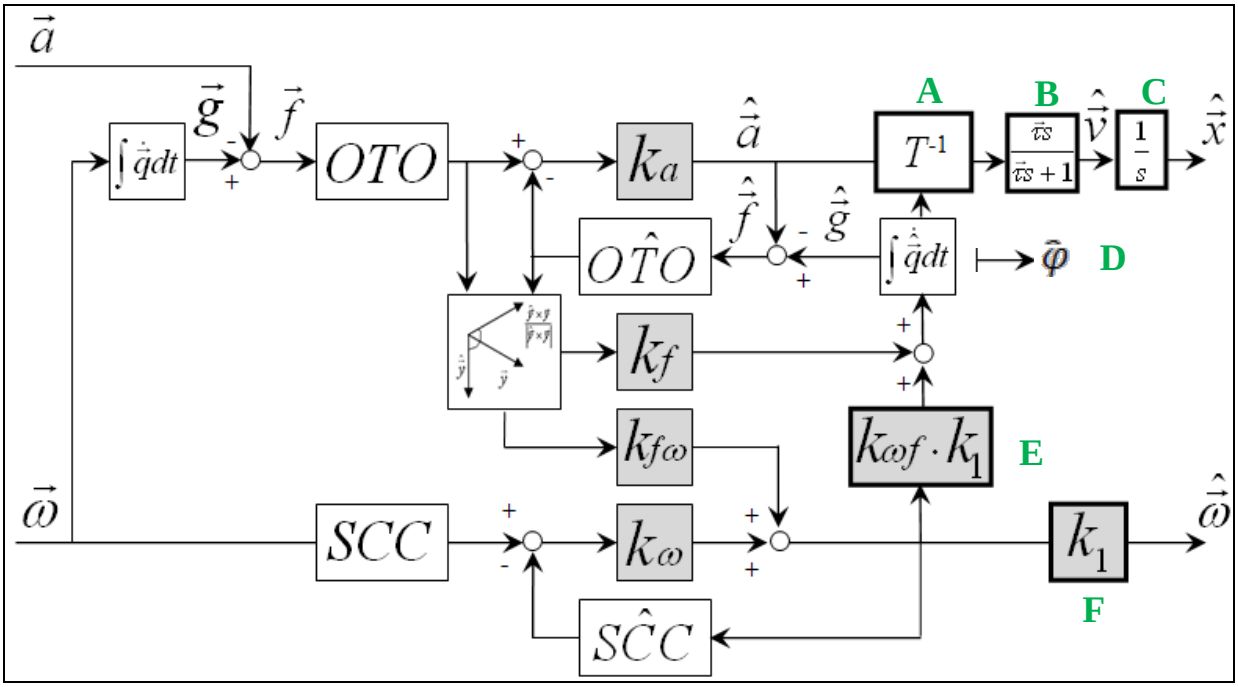

Figure 2. Core vestibular portion of Observer.

The structure of the core *vestibular portion* of Observer is based on Merfeld and Zupan's (2002) model, and is shown in Figure 2. Modifications to the original Merfeld and Zupan (2002) model are denoted by **A-F**, as follows: **A**. Head-to-limbic coordinate frame transformation. **B**. Leaky integrator for linear velocity estimate. Merfeld & Zupan included a similar leaky integrator to obtain velocity estimates for the translational component of the VOR. **C**. Integrator for displacement estimate. **D**. Estimated azimuth. **E** & **F**. Additional feedback gains $k_{\omega f}$ and k_1. The model's free parameters, shaded in grey, are set based on matches with data from laboratory

experiments conducted on humans and animals ($\vec{x}$ - position, $\vec{v}$ - velocity, $\vec{a}$ - acceleration, $\vec{g}$ - gravity, $\vec{f}$ - GIF, $\vec{\omega}$ - angular velocity, $\vec{\tau}$ - leaky integration time constant, φ - azimuth; $\hat{\square}$ denotes estimated quantity; e.g., $\hat{\vec{x}}$ - estimated position).

The vestibular core of the extended model was coded and tested, and found to reproduce results for stimulus paradigms as described in papers by Haslwanter et al. (2000), Merfeld & Zupan (2002), and Vingerhoets et al. (2006, 2007). Previous models predicted orientation and linear acceleration, but did not predict azimuth position in space. To do this, a limbic coordinate frame, aligned with the perceived vertical, was added; velocity and position *path* integration was assumed to take place in this frame. Also, the magnitude of gravity was left as a free parameter for accommodating low g environments, as found on ISS, the Moon, and Mars.

The visual pathways were added to the core model (from Figure 2), as shown in Figure 3, and further detailed in Newman (2009). Model inputs now include static visual position ($\vec{x}_v$) and gravity ($\vec{g}_v$), and dynamic visual velocity ($\dot{\vec{x}}_v$) and angular velocity ($\vec{\omega}_v$). All cues are centrally combined and used to generate internal estimates of angular velocity ($\hat{\vec{\omega}}$), acceleration ($\hat{\vec{a}}$), velocity ($\hat{\vec{v}}$), position ($\hat{\vec{x}}$) and gravity ($\hat{\vec{g}}$). Free parameters are highlighted in grey in Figure 3; values for the free parameters are shown in Table 1.

Table 1. Observer model parameters.

	Vestibular parameters					**Visual parameters**				**Leaky time constants**		
	K_a	K_f	$K_{f\omega}$	K_ω	$K_{\omega f}$	K_{x_v}	$K_{\dot{x}_v}$	K_{g_v}	K_{ω_v}	τ_x	τ_y	τ_z
Value	-4	4	8	8	1	0.1	0.75	10	10	16.67	16.67	1

Visual parameters for the Observer model were determined by simulating the same 1-g laboratory visual-vestibular interaction stimulus paradigms considered by Borah et al. (1979; i.e., linear vection, circular vection, rotation in the light, and acceleration in the light), and determining parameter values such that results matched those of Borah et al.'s (1979) Kalman filter predictions. Observer was then used to predict and compare subjective responses to vestibular Coriolis and visual pseudo-Coriolis stimuli. Most previous 3-D, 6-DOF visual-vestibular interaction models (e.g., the Kalman filter model of Borah, et al. (1979)) made small angle assumptions, so that actual or perceived head orientation remained near upright. Like the Merfeld model, Observer's real or perceived head tilt can undergo unlimited rotation from the vertical. Working with a visiting French Ph.D. student, Oman compared the nonlinear Observer model with the linear Kalman filter model family, and prepared a paper (Selva & Oman, 2011) deriving 1-D and 3-D examples of each model type for vestibular inputs. They showed that – despite apparently different structure and assumptions – the model predictions are dynamically equivalent when model parameters are adjusted to fit the same empirical data.

This enhanced version of Observer was partially validated by comparison to prior experiments and models, as noted above, and is being used by a related NSBRI project (*Sensorimotor displays and controls for lunar landing*; LR Young, PI) to model disorientation during lunar landing.

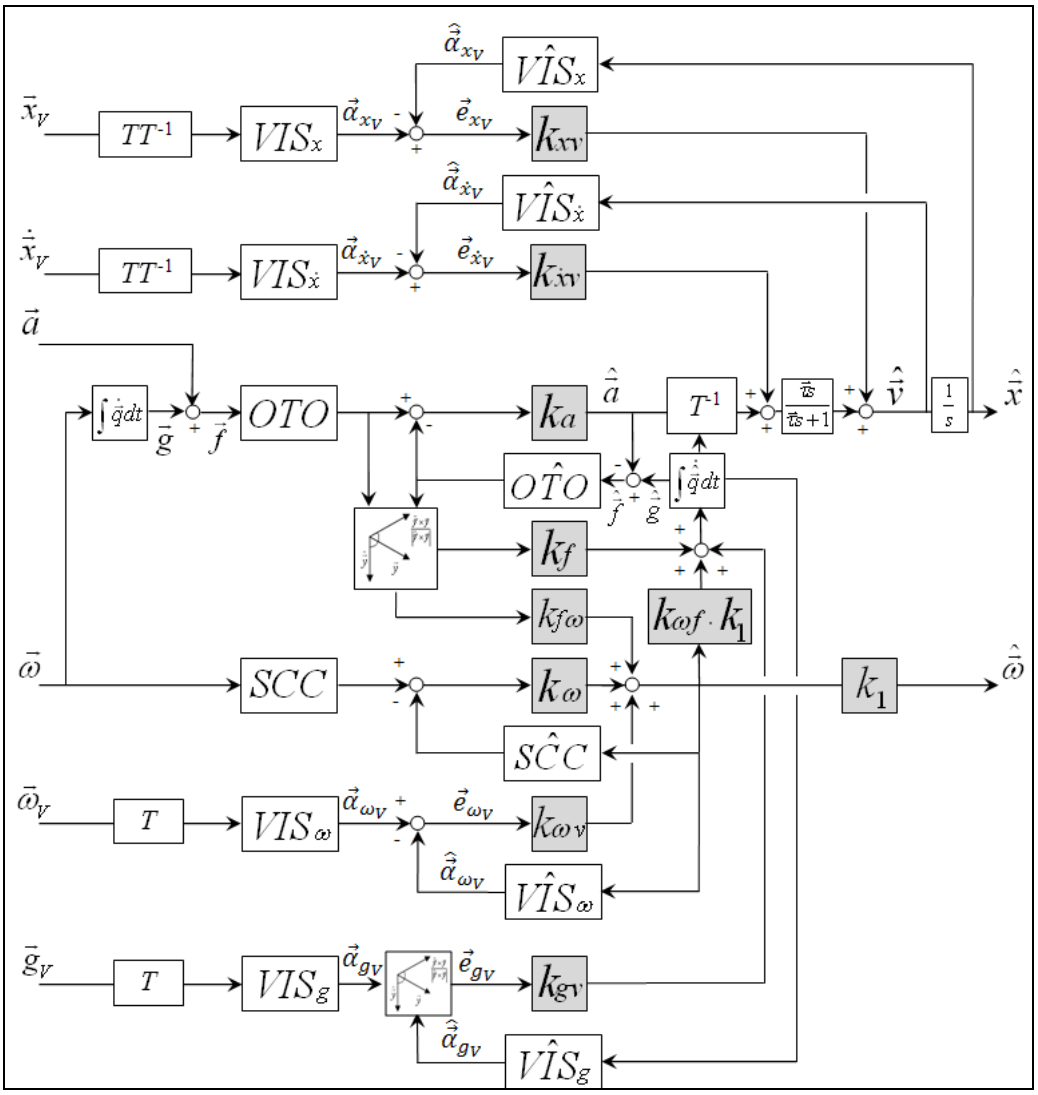

Figure 3. Observer model with static and dynamic visual inputs.

The non-visual, 1-g aspects of Observer largely derive from our 1993 multidimensional spatial orientation model (Merfeld et al., 1993) and subsequent structural and parameter value refinements by Haslwanter and colleagues (2000), and Merfeld and Zupan (2002). The idiotropic bias calculation is partly derived from Vingerhoets and colleagues (2007), and concepts articulated by Mittelstaedt (1983) and others. Visual bias effects are based on vector models suggested by Oman (2003), Laurence Harris (personal communication), and Groen and colleagues (2007). Simulations of astronaut OTTR and Gain illusions are from anecdotal descriptions and the ROTTR hypothesis proposed by Merfeld (2003). Observer can also mimic head movement contingent vertigo events after spaceflight.

Observer was further extended to include static and dynamic visual sensory information from four independent visual sensors (visual velocity, position, angular velocity, and visual *down*). Visual additions were validated against the Borah et al. (1978) Kalman filter simulation results, and other data sets, such as Earth vertical constant velocity rotation in the light, somatogravic illusion in the light, and linear and circular vection. The model predicts that circular vection

should have two dynamic components, and predicts the finding of Tokumaru et al. (1998) that visual cues influence the somatogravic illusion in ways not accounted for by the Borah model.

The model also correctly predicts both the direction of Coriolis illusion, and the magnitude of the resulting tilt illusion. It also predicts that the direction and mechanism of the pseudo-Coriolis illusion is fundamentally different from Coriolis, a prediction verified by means of a pilot experiment (Newman et al., 2011). Finally, the model accounts for the dynamics of astronaut post-flight tilt-gain and OTTR vertigos in ways not previously explained by static analyses (e.g., Merfeld, 2003).

However, the components of the present Observer model that represent the effects of vision must be considered preliminary, and require further validation. Only visual orientation and angular velocity cues are presently being considered; landmark distance cues and ambiguities in visual frames of reference due to "frame" and "polarity" cues (Oman, 2003; 2007) are not yet incorporated.

Observer graphical user interface enhancements

Observer now includes a graphical user interface, shown in Figure 4, that the user can employ to select input data files, tune model parameters, and visualize model responses. Input data files are assumed to include the inertial and visual position and orientation of the pilot's head in a world coordinate frame, the inertial and visual angular velocity of the head in head axes, and *switch* variables that allow the user to modify the character of visual stimulation, mimicking changes in the environment or instrument visibility. The format is detailed in Newman (2009).

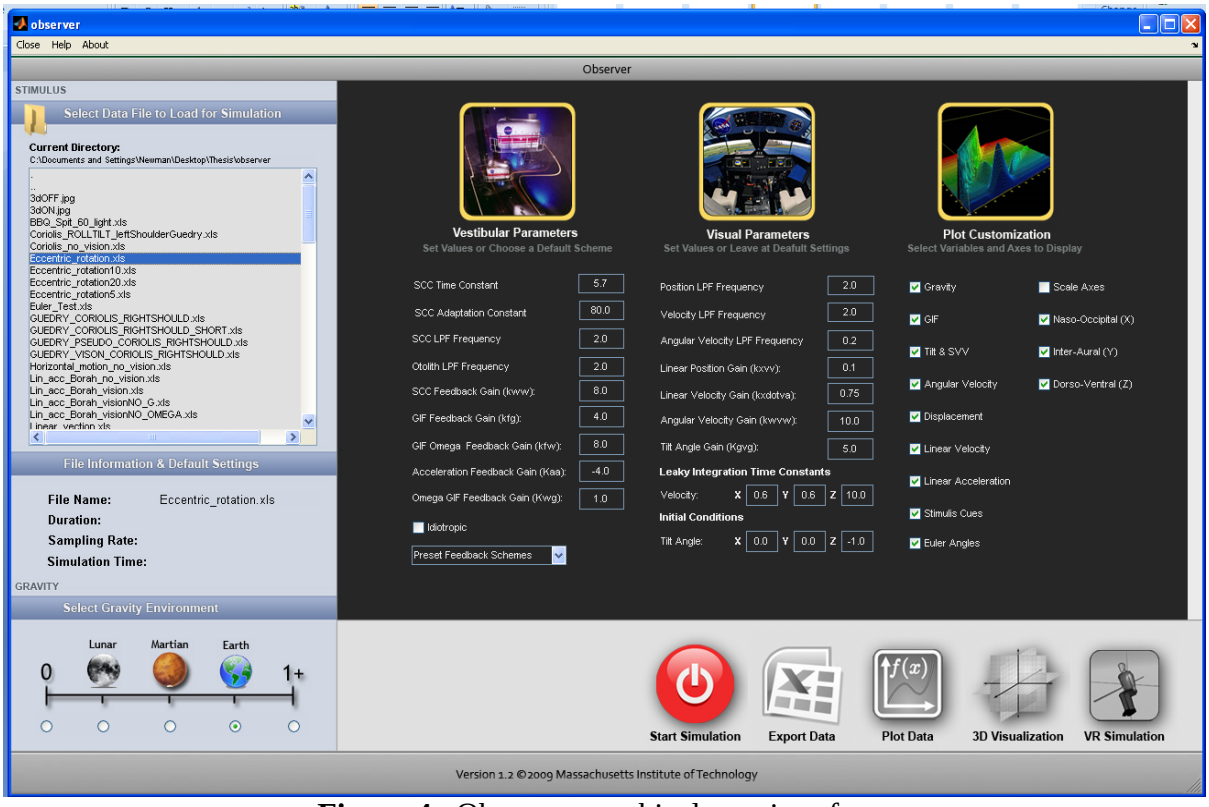

Figure 4. Observer graphical user interface.

Some outputs of Observer are as follows. Observer's *visualization* feature opens an animated vector plot of actual (red) vs. estimated (blue) direction of g and azimuth over time (Figure 5). Observer describes all head motions using a right-handed head-fixed inertial coordinate frame, with the X axis pointing forward, the positive Y axis pointing out the left ear, and the Z axis pointing upwards as noted in Figure 6.

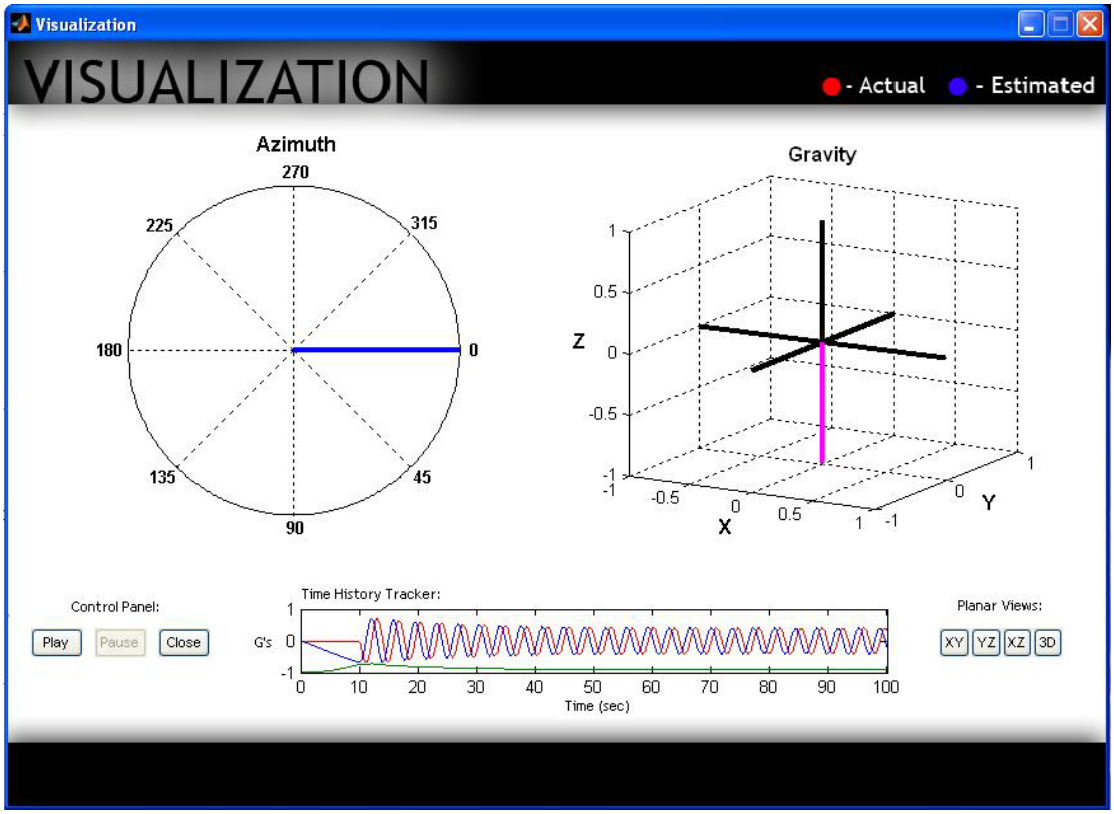

Figure 5. Observer output of estimated azimuth and "down" (labeled as Gravity).

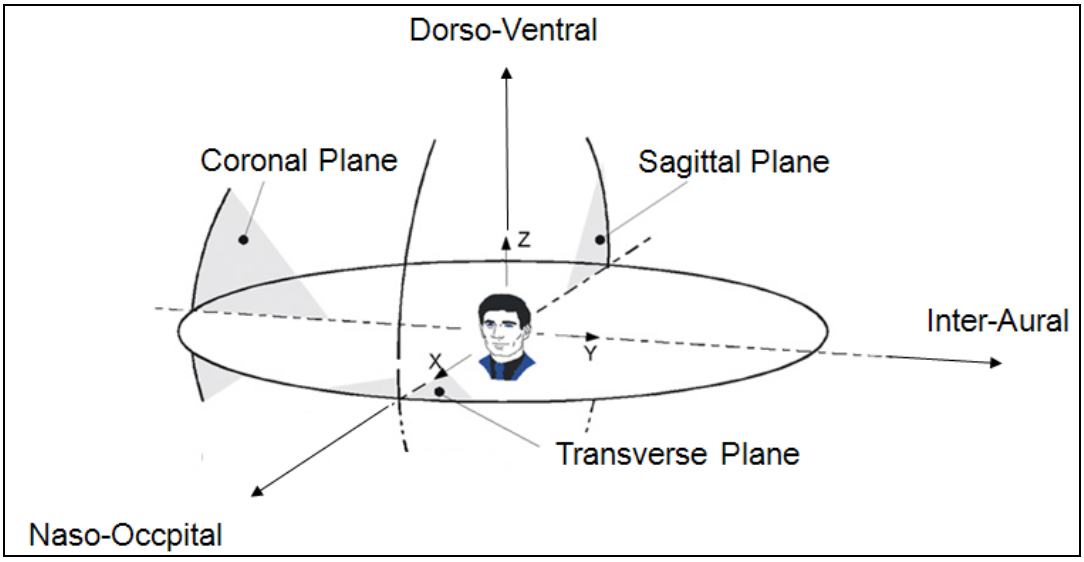

Figure 6. Observer coordinate system.

All of the new Observer outputs are illustrated in Figure 7. They include:

(a) An output data plot window where plots display the actual and estimated response for each individual vector component of a particular model output. Observer provides nine default plots: gravity, GIF, linear acceleration, linear velocity, position, angular velocity, tilt/subjective visual vertical (SVV), Euler angles, and stimulus cues.

(b) A 3-D animated vector plot of the actual and perceived direction of gravity. Users can view the vector plot in the standard 3-D isometric view and also with respect to each of the head axis planes. An animated progression of actual and predicted azimuth is also presented.

(c) and (d) Virtual reality (VR) simulation of the actual and estimated motion response. The VR simulation allows for a side-by-side comparison of the rotational (c) and translational (d) response of the subject in a true world-fixed coordinate frame.

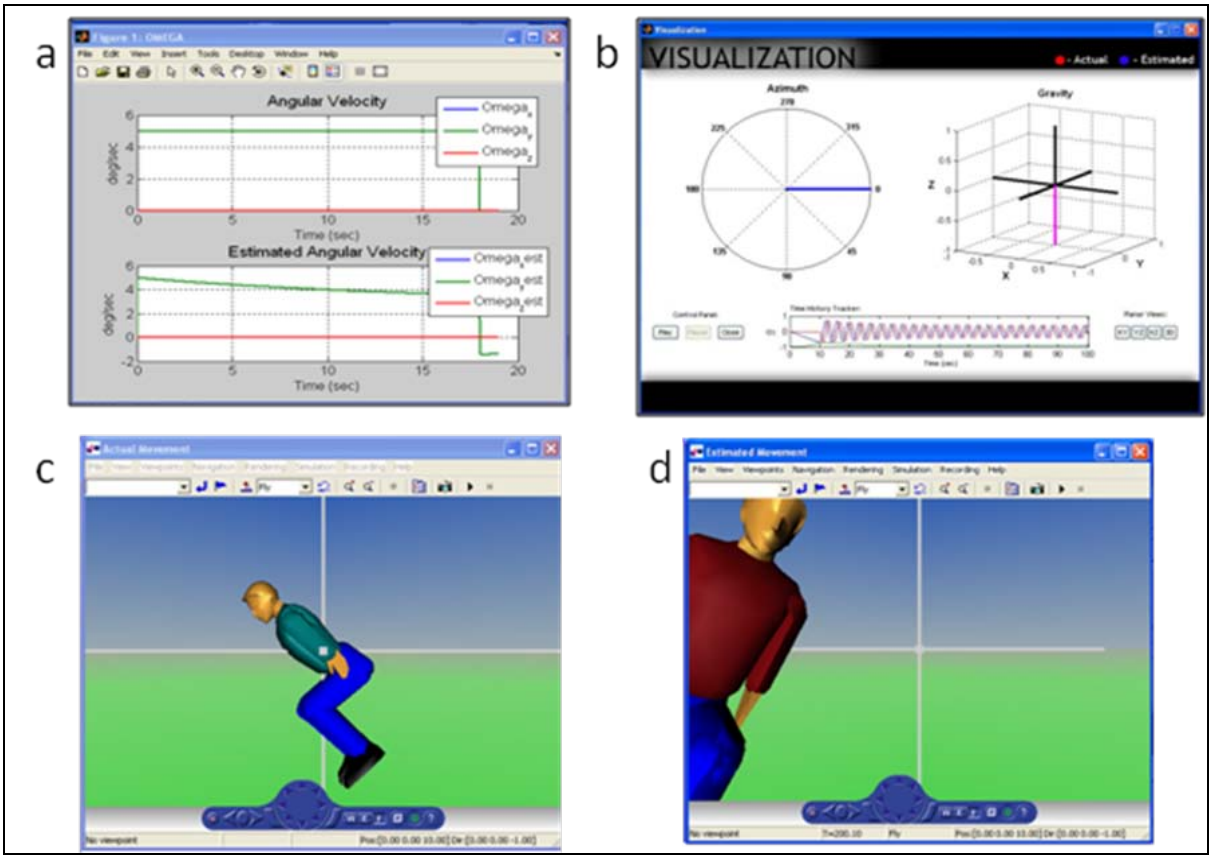

Figure 7. New Observer outputs.

Summary of Observer Enhancements

In summary, Observer is a tool developed to predict the time course of 3-D human spatial orientation and eye movements in response to complex angular velocity and linear acceleration stimuli. As compared to earlier research versions, the current version of Observer is designed to be more easily used by sensorimotor investigators, human factors engineers and by accident investigators. Although originally validated using 1-g human and animal data, the model has

been extended to predict responses in 0-g, 1/6-g (lunar) and 3/8-g (Mars), and the presence or absence of visual cues.

In addition, MIT developed *eObserver*, a stand-alone version of Observer for users who do not own a *Matlab/Simulink* license, or who need to change model parameters beyond the five choices currently built into the Observer interface (detailed above). It uses the *MatLab Component Runtime* engine (distributed royalty-free by *Mathworks*), and includes separate routines for reading, writing, and plotting Excel time series datasets.

As noted, Observer was originally developed using the Matlab/Simulink (Mathworks, Inc.) platform. This provided interactive graphical interface, and powerful variable step differential equation solvers. However it requires the user to have a Matlab license. To address this problem, MIT recompiled the Matlab/Simulink interpretive version of Newman's (2009) visual-vestibular Observer model as a self-contained dynamically linked library (.dll), utilizing the Windows .NET framework as a target, and a fixed time step differential equation solver. It was this .dll version of Observer that was integrated with SDAT, as described in the SDAT section of this report.

MIT developed a *MatLab*/*Simulink* based Observer model, including Excel spreadsheet input capability and a GUI to make the model accessible to less expert Matlab users. A stand-alone, executable version, *eObserver*, was developed for those who do not have Matlab licenses, or who need to change the model's internal code. Orientation and motion predictions can be plotted in 2-D or visualized in 3-D using virtual avatars. Observer's internal model computes azimuth, and pseudo-integrates linear motion in an allocentric reference frame (perceived north-east-down).

Validations of Observer during this research included:

- The model mimics the large perceptual errors for vertical motion observed experimentally;
- It retains the well validated *vestibular core* of the Merfeld perceptual model (Merfeld et al., 1993; Merfeld & Zupan, 2002) and predicts responses to angular velocity and linear accelerations steps, dumping, and off-vertical-axis rotation (OVAR);
- Comparison to perception data from a NASA-Ames vertical motion simulator (VMS) lunar landing simulator experiment (in collaboration with Dr. Young's NSBRI-funded lunar landing project at MIT);
- A dynamic swinging experiment (in collaboration with Drs. Rader and Merfeld at the Massachusetts Eye and Ear Infirmary);
- Linear and angular acceleration steps;
- Post-rotation tilt;
- Vertical yaw rotations (with and without vision cues);
- Somatogravic illusions (linear acceleration with and without vision cues, and fixed and variable radius centrifugation);
- Static and dynamic roll tilt;
- Large amplitude horizontal and vertical sinusoidal displacements;
- Circular vection;
- Linear vection;

- Coriolis and pseudo-Coriolis illusions; and,
- Astronaut post-flight tilt-gain and tilt-translation illusions.

Observer models are founded on human and animal experimental results, as well as anecdotal observations of specific phenomena. As such, Observer complements SDAT's less theoretical approach to assessing motions for their potential to create orientation difficulties. In contrast to SDAT's applied focus, Observer does not classify illusion types or suggest disorientation countermeasures *per se*. The two approaches are complementary and point toward the original goal of combining them to potentially detect disorientations more accurately, using Observer, and then applying appropriate countermeasures using SDAT/SOAS.

Alion's SDAT

This section first recounts the history of SDAT and then describes its enhancements due to this project.

SDAT history

Alion's Spatial Disorientation Analysis Tool (SDAT) and Spatial Orientation Aiding System (SOAS) began as a multi-sensory solution to aviation SD, funded by the Air Force Research Laboratory (AFRL). The goal was to develop a cockpit system, SOAS, to help pilots recognize when they were disoriented and to help them recover from SD events. Because of the difficulties in developing and certifying a cockpit system, Alion also pursued an intermediate step, SDAT, to help us better understand and characterize SD events. For both tools, the keys to helping dis-oriented pilots are to reliably detect such events and then to apply appropriate countermeasures to prevent the adverse consequences of SD (Figure 8). Inputs for SOAS and SDAT are the recorded parameters streaming to (for SOAS), or recorded by (for SDAT) the aircraft's flight data recorder (FDR).

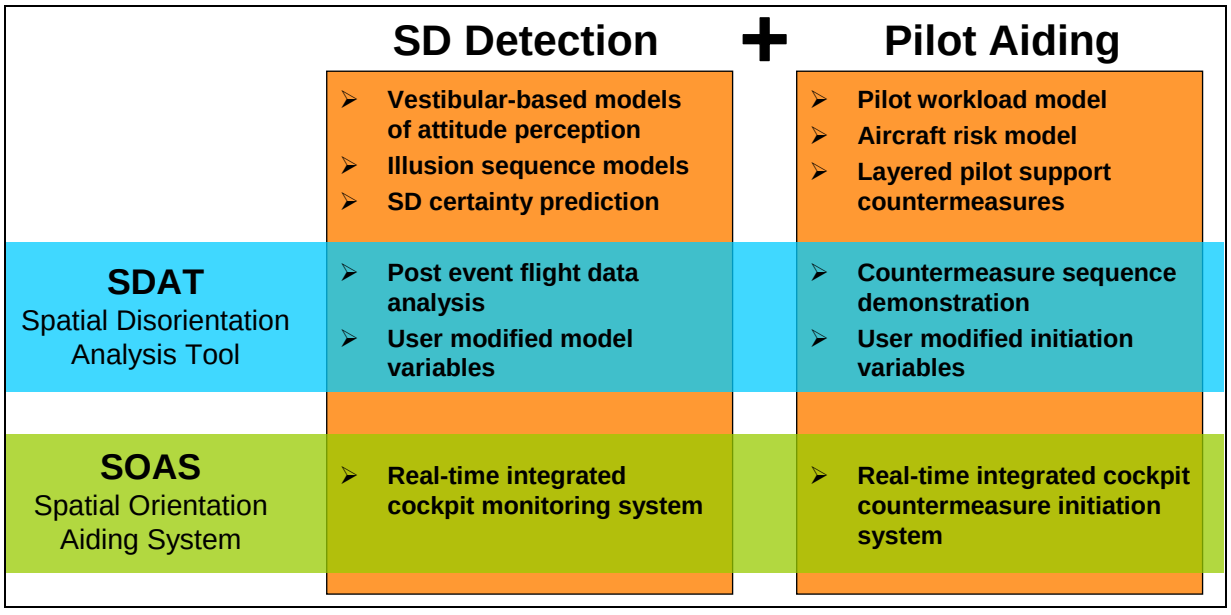

Figure 8. SDAT and SOAS philosophies and commonalities.

Our AFRL research concentrated on fixed-wing aircraft because they are much more prevalent in the Air Force, and because helicopter data sets (for in-depth analyses) were difficult to obtain at that time. Furthermore, our focus was on fixed-wing aircraft because our resident subject matter expert (SME) was a retired USAF fixed-wing pilot.

To detect SD, we focused on four conditions that relate to known susceptibilities of the human vestibular system:

1. Aircraft motions that are below the human threshold of detection. So, the aircraft attitude or direction of motion changes, but the pilot does not detect the change.
2. Sustained aircraft rotations (typically turns in the heading axis) that are no longer sensed by the pilot's vestibular system because the aircraft's angular velocity has stabilized, and the fluid in the semi-circular canals (SCCs) has returned to its original neutral position. Thus, as the aircraft continues to turn the pilot's SCCs no longer register the turn (assuming a constant-rate turn).
3. Stopping sustained turns (as when rolling-out on the desired heading) that yield erroneous sensations of turning in the opposite direction. This illusion is due to the SCCs acting as accelerometers, so that stopping a turn is a deceleration.
4. Airspeed changes that feel like pitch changes as sensed by the otoliths. The otoliths, like the SCCs, act as accelerometers. When airspeed increases, it may be misperceived as a pitch increase. When airspeed decreases, it may be misperceived as a pitch decrease. (For details about vestibular physiology in flight, the reader should consult DeHart & Davis, 2002; Young, 1984; Cheung, 2004.) We extended the otolith model during the current R&D to account for all linear accelerations and gravito-inertial forces, as described later.

In addition to modeling these four conditions, SDAT/SOAS models common aviation illusions, such as the Leans, Graveyard Spiral, Coriolis, and some new vertical landing vehicle (VLV) illusions. For details of the original research, interested readers should review the final report for our AFRL project (Small et al., 2006).

Once an SD event is reliably detected, appropriate multi-sensory countermeasures must be applied to help the pilots recover. SOAS's approach is that countermeasures should be applied in sensory channels that are available for processing critical information, and should only be applied when detection confidence is high and when the consequences of the SD event are unacceptable. These notions merit further explanation; first the multi-sensory nature of countermeasures, and then the severity of the SD event.

For multi-sensory countermeasures, SOAS provides recovery guidance in a sensory channel that is presumably not overloaded in the present circumstances (Wickens et al., 2008). For example, if the pilot is pulling a large g-load during an SD event and his/her vision is consequently narrowed, SOAS will use auditory cues to help with the recovery. Conversely, if the auditory channel is overloaded due to radio chatter, then tactile recovery cues are more appropriate. SOAS also triggers countermeasures in multiple channels to maximize the pilot's chances of noticing the cues and executing swift corrective actions. For example, auditory and tactile cues reinforce each other, as do visual and auditory cues. In some cases, all three modes (visual,

auditory, tactile) will be used, if the situation warrants. This approach was experimentally validated with Air Force F-16 pilots in a simulator (Wickens et al., 2008).
SOAS also assesses the severity of the situation while selecting countermeasures. For example, if the SD event is at high altitude and only results in minor erratic control of the aircraft, then less intrusive countermeasures (e.g., visual cues) are triggered. However, if the pilot is so disoriented that aircraft control is lost and the aircraft is hurtling toward the ground, then more intrusive countermeasures are warranted. Such countermeasures would include all three of the above (visual, auditory, and tactile), and would progress to auto-recovery (if the aircraft is so equipped), and even to auto-ejection in order to save the pilot's life if the aircraft is damaged and unable to recover.

To summarize the AFRL research, SDAT/SOAS modeled the anticipated responses of the SCCs and otoliths to detect SD events, and to enable multi-sensory countermeasures based upon the situation and the pilot's multi-channel workload to help pilots recover from SD events. To verify and validate our models, we used SD mishap data sets, we conducted pilot-in-the-loop experiments for countermeasure efficacy tests, and we analyzed data sets where an SD occurrence was unknown (to us). Early data sets and those generated by the Alion research team using desktop simulators were used to fine-tune our models. Later, data sets were used to verify and validate SDAT and SOAS (Small et al., 2006).

SDAT Enhancements

The challenges presented by the current research project were to extend SDAT and SOAS into the space domain. Toward that goal, we discussed space SD situations with domain experts, acquired actual space vehicle and simulator data sets, and enhanced SDAT/SOAS with additional illusion models, as further explained below. We also worked with our MIT colleagues to replace SDAT's SCC and otolith models with MIT's Observer model of human orientation perception.

Enhancements were to include merging MIT's Observer into SDAT and extending SDAT with SD illusion models for space vehicles. We also originally sought to include visual frame of reference transformations (FORT) in SDAT. Actual accomplishments were: improving SDAT's otolith model, combining SCC and otolith model predictions of perceived attitude angles, adding a pilot attention model (N-SEEV), designing three new SD illusion models for vertical landing vehicles (VLVs), improving SDAT's GUI, and "wrapping" the Observer.dll into SDAT. We did not incorporate FORT into SDAT, as explained in the FORT section, later. The following subsections explain the preceding accomplishments.

Otolith model enhancements

Alion enhanced SDAT with a full gravito-inertial force (GIF) calculation to replace the known deficiencies of the original otolith model which only considered airspeed changes and their effects on perceived pitch. While our original plan for this project was to replace SDAT's SCC and otolith models with Observer, that plan was only partially realized, as explained later.

The algorithms for our GIF calculation account for data sets that do not have all linear and angular acceleration parameters. In most cases, we can derive the needed accelerations from other parameters (e.g., airspeed and vertical speed). Naturally, conversions are included for data

in world frame coordinates (e.g., vertical speed) that need to be in vehicle frame coordinates. SDAT still does not account for pilot head motions as those data are rarely in actual FDR data sets. We do include the effects from moment arms where the pilot is not at the center of mass of the vehicle. However, the new algorithms do not account for vehicles that may be slipping or sliding (i.e., uncoordinated flight). Nonetheless, SDAT's otolith model is greatly improved, as shown during verification and validation tests, described later. Appendix A contains further details about our GIF calculations.

Combined pitch and roll calculations

The human vestibular system perceives attitude in two ways: through semicircular canal angular rates and otolith contributions. The individual attitude perceptions may be in perfect agreement, or may be contributing opposing effects. A method of weighting these perceptions in order to obtain a combined perceived attitude for pitch and roll angles within SDAT is needed.

The weighting method assumes a more dominating effect for a greater "neural" input from one attitude perception method compared to the other. The amount of neural input is based upon how much the perceived angle has changed in a time step. The respective deltas (i.e., differences in predicted perceived angle from one time step to the next) for the perceived angles are used for the normalized weighting scale. If no change occurs for either perception method, then the weights are both equal to 0.5. These weights are applied to the changes in perceived angles themselves. The weighted changes are then added to the previous combined perceived angles (pitch and roll) to get the new combined perceived angles.

There are two effects from this weighting method. First, if the changes in perceived angles have opposite signs, then the combined perceived change is the sum of the two opposite-sign changes. If one effect is dominant, this dominancy is apparent in the resulting sum. Second, if the changes in perceived angles have the same sign, the average is weighted by the dominancy of the respective effects. An example, below, illustrates how we calculate a combined angle (pitch and roll). The example is an excerpt from the Flash Air 604 accident FDR data set (provided to us by MIT's Dr. Larry Young) for the perceived pitch angle. The graphs (Figure 9) show the individual (otolith, SCC) and combined results for perceived pitch.

TotalChange = abs(SCCDelta) + abs(OtolithDelta)
SCCWeight = abs(SCCDelta)/TotalChange
OtolithWeight = abs(OtolithDelta)/TotalChange
Total Perceived Pitch Angle = Previous + (SCCweight * SCCDelta + OtolithWeight*OtolithDelta)

Pitch	Otolith Perceived Pitch	Otolith Delta	SCC Perceived Pitch	SCC Delta	Total Change	SCC Weight	Otolith Weight	Total Perceived Pitch Angle
0.4	10.76	-0.55	-1.05	-0.04	0.59	0.07	0.93	11.24
0.4	11.58	0.83	-1.09	-0.04	0.87	0.05	0.95	12.03
0.4	10.97	-0.61	-1.12	-0.03	0.64	0.05	0.95	11.44

As can be seen in Figure 9, combining the SCC and otolith perceived values has the desired effect of smoothing the results while accounting for the SCC model's "dominance" during significant angular rotations (pitch, in this example). The SDAT SCC model was unchanged.

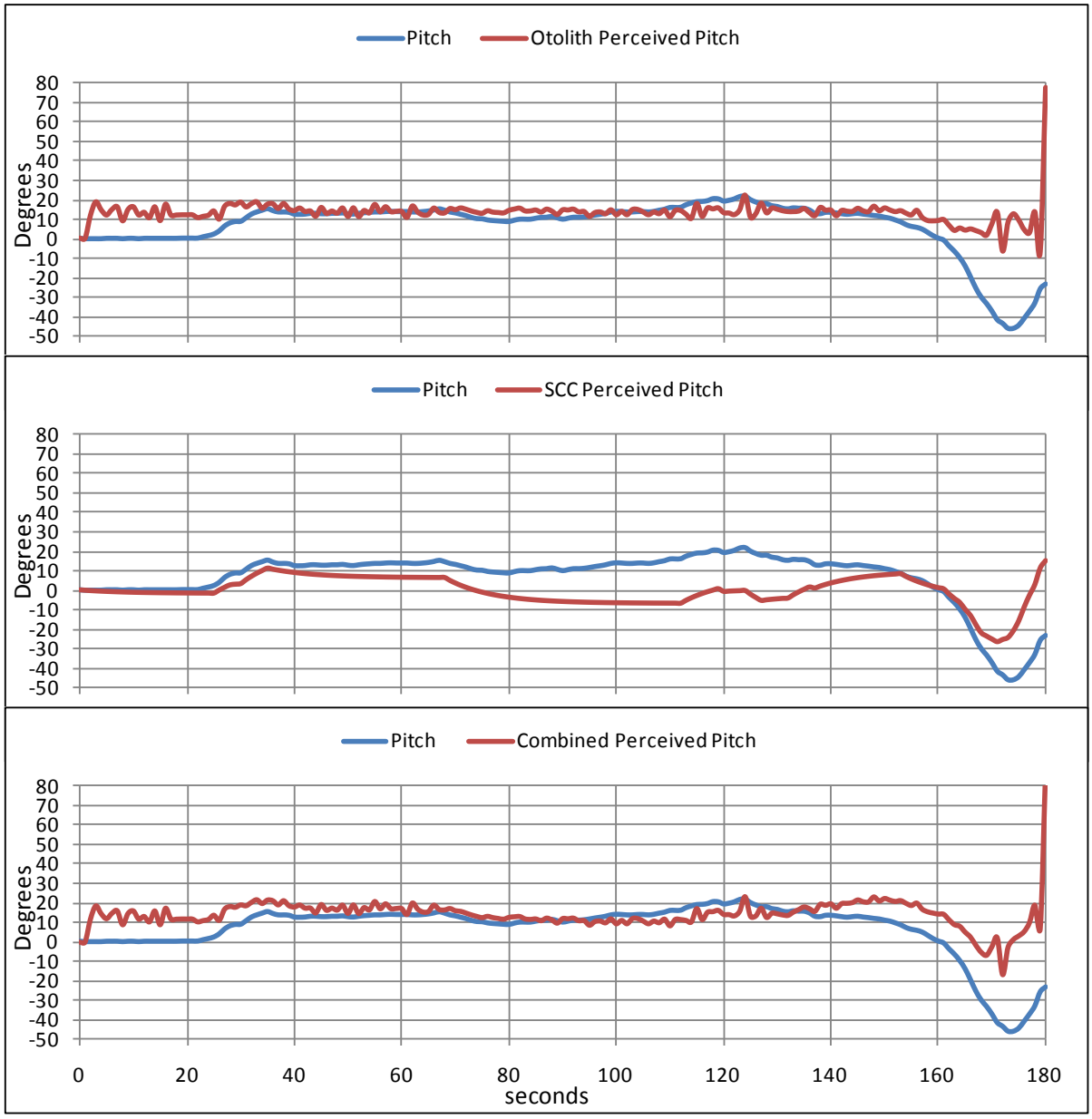

Figure 9. Perceived pitch from otolith model only (*top*), SCC only (*middle*), and combined (*bottom*).

N-SEEV enhancement

Another SDAT enhancement involved incorporating a pilot attention model into the counter-measure portion of SDAT/SOAS. The goal is to elevate the intrusiveness of countermeasures, if the attention model predicts that the pilot has not detected a less-intrusive countermeasure. The selected attention model is N-SEEV (noticing - salience, effort, expectancy, value; Wickens, Sebok et al., 2009; Wickens, Hooey et al., 2009).

The way the algorithm works is to begin processing when any low- or medium-level countermeasure first activates. A low-level countermeasure is a visual cue/command that we call the SD Icon (Wickens, Small et al., 2008). A medium-level countermeasure is an auditory or tactile alerting cue (Small et al., 2006). When SOAS triggers a low-level countermeasure, the default behavior is to wait 1.0 second to determine if the pilot noticed the low-level countermeasure (or not) based upon the N-SEEV model prediction. If the pilot did not notice, SOAS elevates the countermeasure to medium. This time, the default is 0.5 seconds. If the N-SEEV model predicts that the pilot still does not notice the countermeasure, SOAS elevates to a high-level countermeasure; i.e., an audio or tactile **command** (rather than an alert). Previously, countermeasures only increased in intrusiveness if the SD situation deteriorated. Now, with the N-SEEV model, countermeasures will become more intrusive if N-SEEV predicts that the pilot has not noticed a lower-level countermeasure within a specified time. As in the original SOAS, if the pilot recovers, all countermeasures cease.

The N-SEEV model weights salience, effort, expectancy value, and multi-channel workload to calculate a time that prior research has shown is typical for noticing such a cockpit alert. While the model is heavily focused on predicting noticing time for visual events (e.g., the low-level countermeasure described above), our efforts in this project expanded the model's predictive capabilities to auditory and tactile events.

Figure 10 shows the new SDAT GUI tab for N-SEEV. Details are in Appendix B, and Keller et al. (2011).

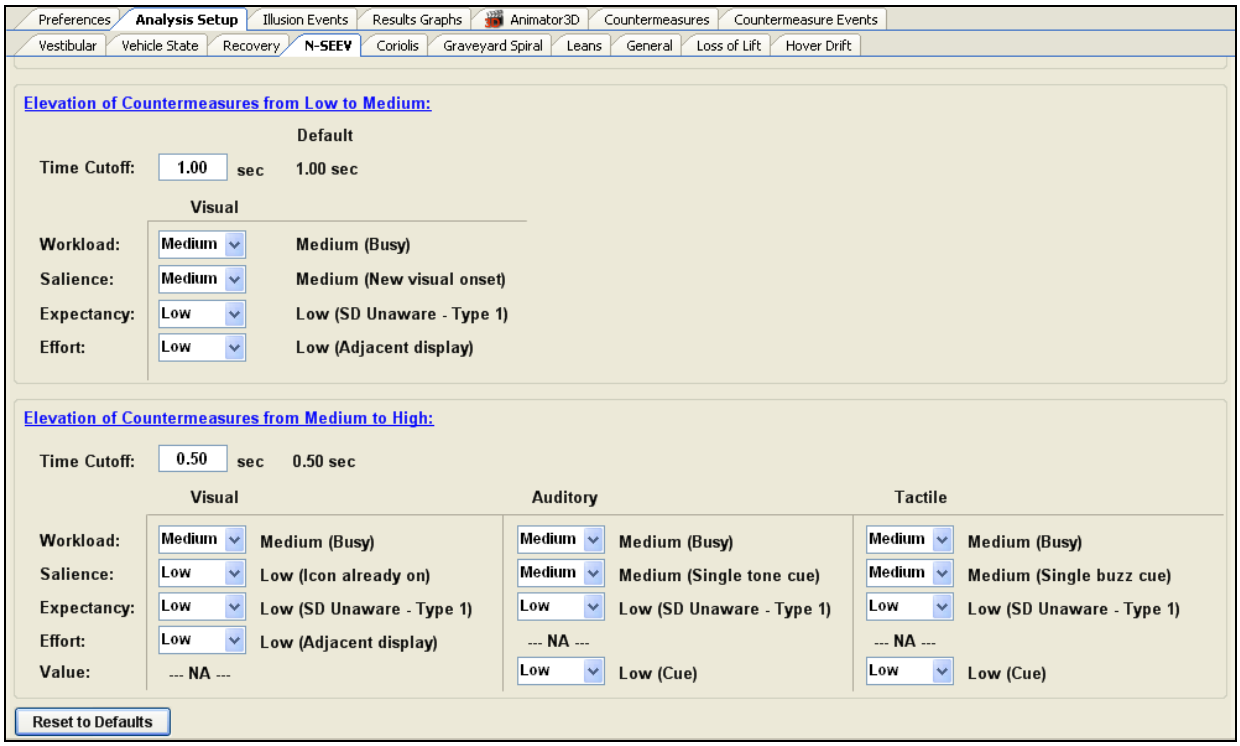

Figure 10. SDAT's N-SEEV GUI tab.

New illusion models

We designed three new illusion models for vertical landing vehicles (VLVs) and developed two of them for inclusion in SDAT. The basis for the new models was our analysis of helicopter data sets from a source that required anonymity. The data sets included self-reported SD events.

The three new models are: (1) *Undetected loss of lift* which occurs when the pilot unwittingly flies out of ground effect with insufficient thrust to maintain the new altitude, resulting in a sudden plunge toward the surface; (2) *Inadvertent drift during hover* that could result in the vehicle striking an obstacle, and (3) *Undetected drift during landing* that could cause the vehicle to tip-over. The first two are included in the newest version of SDAT; the third is not. As with other SDAT illusion models, users may tailor the new models to account for specific vehicle characteristics. Our motivation for acquiring the helicopter data sets is that helicopters are the closest analogy to space vehicles on Earth from which we could obtain usable data. (We did obtain some Space Shuttle data sets, but they were unusable. We also obtained Altair simulator data sets, but the gravity environment was 1-g, not micro-gravity, and so not as useful as the helicopter data sets.)

Undetected loss of lift

The goal of this model is to detect when a VLV increases altitude out of "ground effect" without a commensurate increase in power or thrust. In such circumstances, the VLV might plunge toward the surface. SDAT/SOAS can and should alert the pilot to a sub-threshold increase in altitude, without an increase in thrust, that might put the vehicle into an unwanted dive. Even for a lunar (or other planetary body) landing vehicle, such a situation could occur. Therefore, when flying at a fairly low altitude (in ground effect) and low speed, if an undetected climb or loss of lift occurs without the required power/thrust increase to maintain altitude, there will be a plunge toward the surface. SDAT should detect the initial conditions and a worsening situation (e.g., continued altitude increase with no power or thrust increase) to trigger the appropriate counter-measures.

Undetected drift while hovering

While in a hover near the surface, any undetected motion ("drift") could result in the vehicle striking an obstacle, causing damage to the vehicle and/or injury to the crew. Some longitudinal or lateral motion is expected, but "too much" could be dangerous. SDAT/SOAS can and should alert the pilot to sub-threshold drift that exceeds a user-specified distance (e.g., one vehicle length). This model also applies to non-terrestrial vertical take-off and landing vehicles. An assumption is that motions above the otolith threshold will be perceived and that the pilots will know that they have moved and thus know where they are. The undetected component of drift in any direction is based upon sub-threshold movements. As with other SD illusions models in SDAT, we assume that the environment is non-visual or visually compromised. This is especially true for this model as sub-threshold positioning motions will likely occur during every landing. The issue, then, is to select the appropriate distance that means "too much" undetected drift has occurred.

Undetected drift during landing

This model has been designed but not implemented. During landing, any lateral drift over a certain speed (varies by vehicle type) can result in a "trip" as the skids or wheels contact the

surface to act as a fulcrum and the vehicle tips over, causing major damage to the vehicle and injury or death to the crew and bystanders. Even in visual conditions, pilot distractions or fatigue or other factors could render lateral drift as undetected by the pilot. However, for use within SDAT we created a vestibular-based model to evaluate when the occurrence of this type of problem could be based on a vestibular illusion. For this model, the helicopter SME suggested a user-selectable cone (as shown in Appendix C) where the desired drift in any direction at touch-down is 0 knots. Some tolerances are allowed, though (as shown in the tables below the figure). To implement this SD illusion model, we will combine these values with an evaluation of a hover state (prior to landing) and a check to determine if the horizontal movements (fore, aft, left and right) are below the otolith thresholds. For the purposes of this model, if the movements are above threshold, the pilot will feel them and notice the unwanted motion. This will allow us to continue our practice of using a range of vestibular threshold settings to evaluate flight data sets.

Appendix C has details of each of these new SD illusion models. These models required an upgrade to the required data format for SDAT (from v4 to v5); new parameters include groundspeed, thrust, and surface contact (aka weight on wheels or WoW).

GUI enhancements

To accommodate all of the SDAT enhancements described in this report, we significantly changed and improved SDAT's graphical user interface (GUI). The newest user manual (v3.0; Small, 2011) describes the GUI in detail. For the purposes of this report, we list the GUI enhancements here and refer interested readers to the user manual for further details. Enhancements included those for: the new otolith model (including linear acceleration selections), and combining otolith and SCC perceptions (Figure 11); vestibular thresholds and model selections (Figure 12); N-SEEV (Figure 10); the new illusion models (Appendix C); and results graphs that now include selections for all accelerations (not shown, but described in Appendix A).

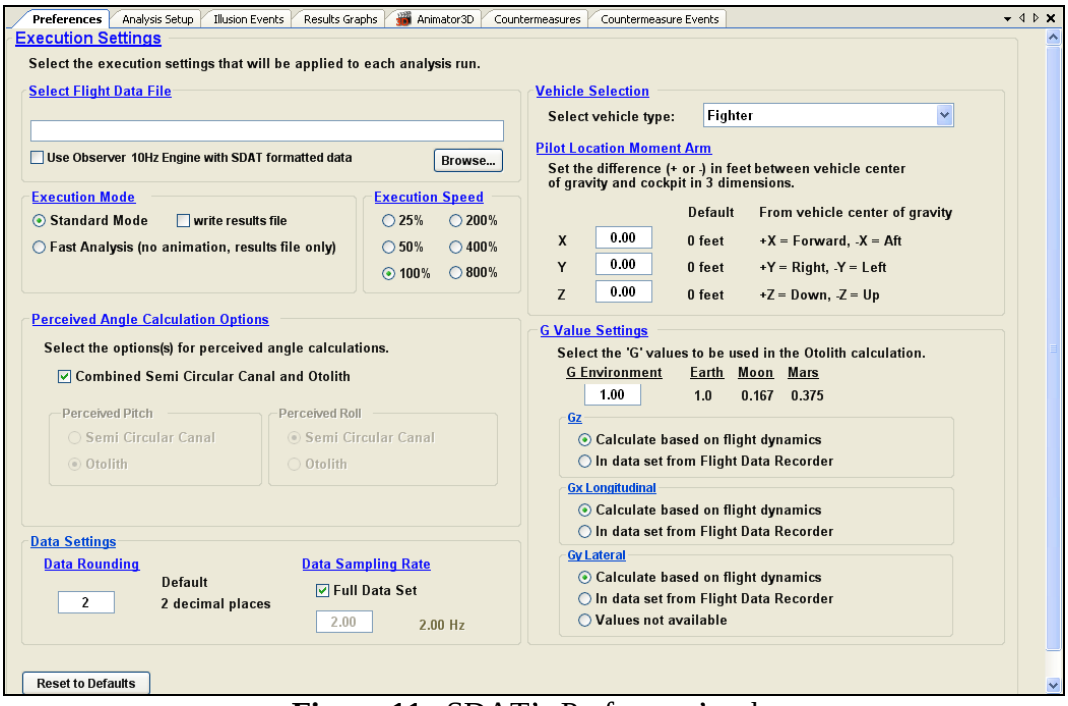

Figure 11. SDAT's Preference's tab.

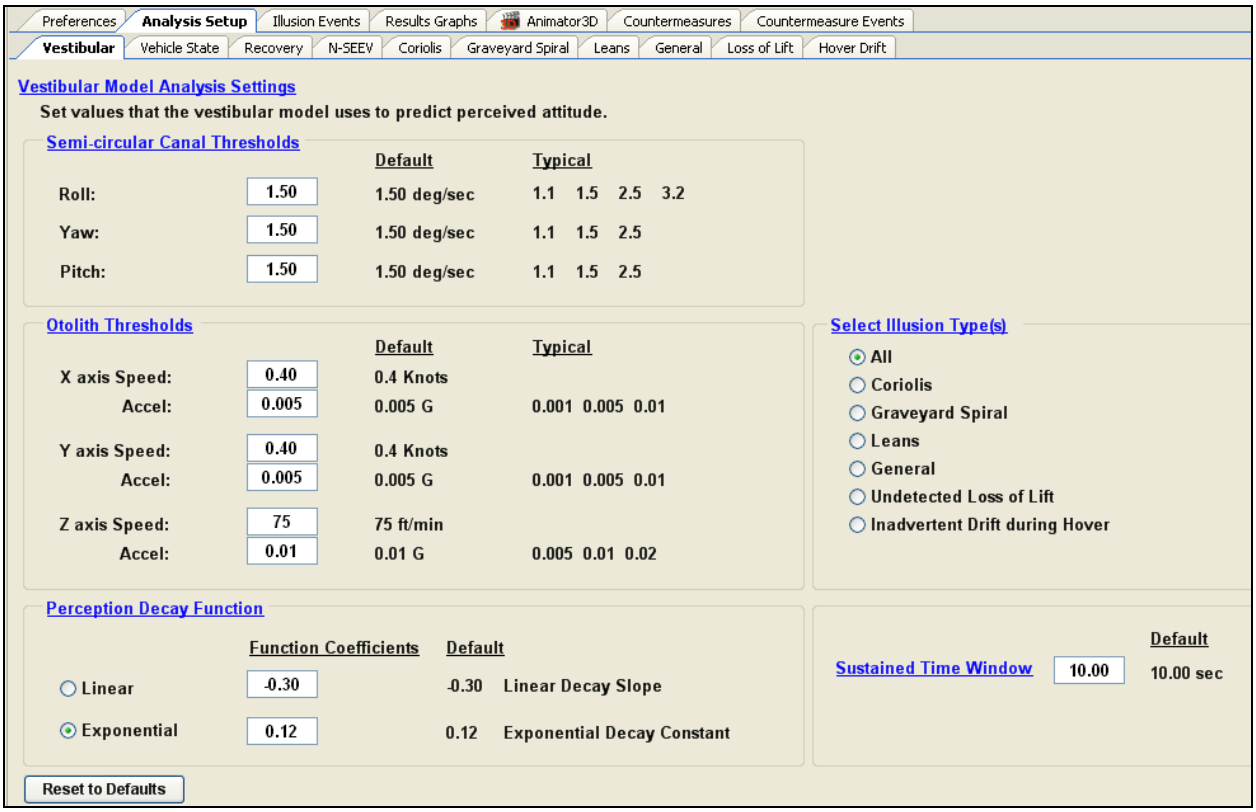

Figure 12. SDAT's Analysis Setup – Vestibular tab.

Observer.dll enhancement

In the fourth year of the project, MIT compiled Observer into a dynamically linked library (.dll) that was integrated within SDAT using a *wrapper class* to pass inputs and outputs between the Observer .dll and SDAT. The wrapper serves as a conduit within the Microsoft .NET environment for the following: Excel data set values as inputs, SDAT's illusion and countermeasure functions, and graphing outputs. Details are in Appendix D.

Consequently, SDAT users can select whether they wish to use Observer algorithms for predicted perceptions or SDAT's algorithms. Figure 13 shows the GUI for this choice.

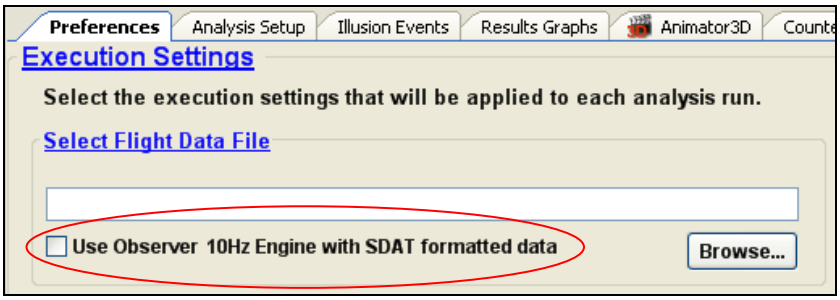

Figure 13. SDAT GUI highlighting option to use Observer for perception predictions.

The major effort to integrate Observer into SDAT is described in the next primary section (after the following summary sub-section).

Summary of SDAT Enhancements

The major accomplishments to enhance SDAT include:

- Adopting and adapting Observer techniques to suit our needs for SDAT, namely the improved otolith model;
- Adding the N-SEEV pilot attention model to SDAT to refine countermeasure triggering that accounts for the potential of a pilot not noticing lower-level countermeasures;
- Adding new illusion models for vertical landing vehicles;
- Incorporating Observer via a .dll; and,
- Updating the GUI to accommodate all of the other enhancements.

At each enhancement step, we verified that we achieved the desired processing, and we validated our results using existing and new data sets. SDAT is Alion's intellectual property, protected via registered copyright. Another validation step was to compare Observer and SDAT results when analyzing the same data set (described later). We did not undertake a laboratory or flight experiment to validate SDAT, even though that was part of the original plan four years ago. We judged that the resources would be better spent integrating SDAT and Observer (explained next) and validating other accomplishments with our existing data sets and other research results.

SDAT & Observer Integration

We made two major attempts within the four years of the project to merge Observer into SDAT. The first attempt used a compiled version of Observer embedded within SDAT and allowed the user to select this so-called *eObserver* or SDAT models for calculating perceived values (similar to the Observer.dll selection shown in Figure 13). When selecting eObserver, a user had to have an input data set in the Observer-required format. The second attempt used a compiled version of Observer as a dynamically linked library within SDAT and did not require a user to re-format a data set; it uses the current SDAT data set formatting (v5; User Manual has details). However, the SDAT data set format does not contain all of the parameters that the Observer.dll needs to fully process and calculate perceived angles and displacements.

Impediments to Observer-SDAT Integration

The difficulties with merging Observer into SDAT were due to the different intended purposes of the two distinct models. Observer is intended to be a physiologically accurate model of human orientation perception, using both vehicle motions and visual cues. Observer requires data sets to be at a high capture rate (10-100 Hz), a constant capture rate, and referenced to the human's head coordinate frame. Observer does not account for vestibular thresholds, and, although it predicts illusions, it does not attempt to classify illusion types.

In contrast, SDAT is not intended to be a physiological model; rather it is intended to predict pilot perceptions of pitch, roll and yaw angles and rates based upon vehicle motions and the impact of those motions on the pilot's vestibular system. Visual cues are assumed to be absent or ignored. Input data sets are what are typical from current flight data recorders; i.e., 1-4 Hz, irregular sample rates, in the vehicle or world reference frames. SDAT also enables users to modify common SD illusion models (e.g., Leans, Graveyard Spiral) and modify vestibular thresholds which are known to vary significantly in humans (Grabherr et al., 2008). Misperceptions

due to sub-threshold motions are critical to many SDAT illusion models (see Small et al., 2006 and the above new illusion models sub-section).

Furthermore, the vestibular inputs to Observer include head angular velocity and linear acceleration data in a head or vehicle coordinate frame. Users must perform coordinate transformations and provide the required data (although there is currently no provision within SDAT's data set format for these parameters). The vestibular models in Observer require that the input data be valid up to 2 Hz in the frequency domain. Therefore, Nyquist sampling theorem considerations require that input data should be sampled at rates of 10 Hz or above. MIT briefly considered issues related to application of the Observer model to NTSB and DoD aircraft accident investigations. Typically the pilot's visual references are not known, so only vestibular inputs can be considered. A general limitation is that terminal or approach precision radar data on aircraft position is typically sampled at 1 Hz or less. Contemporary aircraft "orange box" flight data recorders (FDRs) usually sample attitude at 1 Hz, longitudinal and lateral accelerations at 4 Hz, and normal accelerations at 8 Hz. Hence if the aircraft is making significant maneuvers, terminal and approach radar and aircraft FDR data significantly under-sample the aircraft trajectory kinematics, and thus do not fully characterize the vestibular stimulus. If the aircraft dynamics are well known, it is theoretically possible to estimate much of the missing frequency domain information, provided the position and attitude data are not very noisy. This is occasionally done by accident investigators. However, implementing the required coordinate frame transformations and Kalman estimators in SDAT for aircraft FDR data analyses was deemed beyond the scope of the current project. In NASA flight test and simulator applications, sampling rates are typically much higher (10-100Hz).

MIT's Observer model builds on decades of physiological and perceptual research. Its principal goal has been to reliably describe the relationship of angular velocity and linear acceleration cues, to the time course of eye movements and perceptions. The model predicts a variety of illusions, but was not specifically developed to detect and classify SD episodes using a traditional taxonomy. In contrast, Alion's SDAT/SOAS models have been designed and developed to use practical heuristics to estimate the probability of an SD episode based on aircraft trajectory data, and to classify the type of illusion experienced. The ultimate goal of SOAS/SDAT is to then determine the severity of the SD event and trigger appropriate countermeasures. If an SD event is fairly benign, then less intrusive countermeasures are warranted; for severe SD events (i.e., surface collision imminent), SOAS/SDAT triggers more intrusive countermeasures.

So, the two approaches are different and, not surprisingly, the resulting perception models, as instantiated within the tools called Observer and SDAT, are different. Merging the two models proved to be impossible during this project. However, lessons from each approach were applied to each tool. For example, Observer now has a graphical user interface that aids users in selecting parameters for data analyses. And, SDAT now has gravito-inertial force calculations that replace the old 1-D otolith model of pitch perception changes.

Observer & SDAT Analysis Comparisons

As part of our verification and validation efforts, we compared the analytical results of SDAT and Observer whenever the opportunity arose to do so for common data sets. This section describes our results comparisons over the project's four years.

While working to improve our respective models, the Alion and MIT teams compared analyses of common data sets with Observer and SDAT, respectively, to compare and contrast the models. The differences between the two approaches are significant, and to be expected, given their respective derivations, emphases and developments (as already articulated).

We compared the analytical results from SDAT and Observer with three actual data sets – one from the NTSB (NTSB, 2003), another from the U.S. Navy, and the third from the Flash Airlines 604 accident in 2004 (Egyptian Ministry of Civil Aviation). These data sets are from accidents in which SD was suspected. Results of analyses using Observer and SDAT compare favorably with those of the accident investigators.

Each of the following sets of graphs contains the analytical results from Observer and SDAT. In each graph, the blue line represents the actual aircraft flight dynamics from the data set. The red line represents the perceived value calculated by either Observer or SDAT. The yellow line (where shown) is the difference between the actual flight data and the calculated perceived values (i.e., the absolute value of the difference between the blue and red values at each moment in time). In the MIT graphs the red line data is labeled "Estimated" while, in the SDAT graphs, the red line is labeled "Perceived." In all graphs, the horizontal axis is elapsed time in seconds and the vertical axis is angular rate (roll or heading) in degrees per second, or angle in degrees, as noted. Positive values are rightward motions from the pilot's perspective; negative values represent leftward motions.

Figures 14-17 compare results before the most recent enhancements to SDAT. Figures 18 and 19 compare results after the enhancements described earlier.

The first two graphs (Figure 14, a & b) show the roll velocity data as analyzed by the two tools for the NTSB (Strasburg accident) data set in which a small twin-engine aircraft's pilot experienced a graveyard spiral while flying in clouds and crashed into the ground killing all aboard. For the first three quarters of the time period the two tools show similarly small, but not identical, delta values (yellow line) between the actual roll velocity and the perceived roll velocity calculated by the tools. During this time period, the majority of the roll actions are relatively small. However, for the last quarter of the time period, the deltas diverge dramatically. During this later time period, the aircraft is experiencing very high roll velocities when the pilot presumably lost control of the aircraft. Based on the fact that these large roll rates are well above the SCC detection thresholds, SDAT shows that the delta between actual and perceived roll velocity would be quite low. In contrast, Observer calculates very high roll rate deltas between the actual and the estimated values.

The next set of graphs (Figure 15) compares the yaw velocity calculations for the same accident data set (NTSB Strasburg). The graphs show that the aircraft slowly increased its rate of heading change (a graveyard spiral) until the apparent loss of control near the end. The MIT and SDAT

models calculate very similar perceived yaw velocity values and associated deltas for most of the time period. Late in the data set, during the apparent loss of control, the values calculated by the two tools again diverge. SDAT (Figure 15b) shows that the above threshold yaw velocities are all perceived but maintain the accrued yaw velocity error delta. For this same time period, the MIT model (Figure 15a) shows large variations in the perception delta.

Both tools lead to the conclusion of a somatogyral illusion.

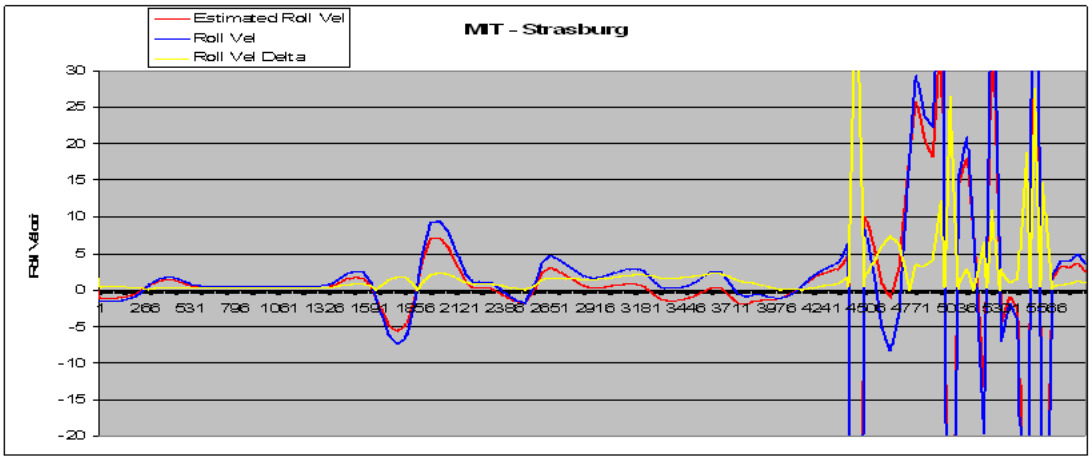

a. Observer roll velocity for Strasburg (NTSB) accident data set.

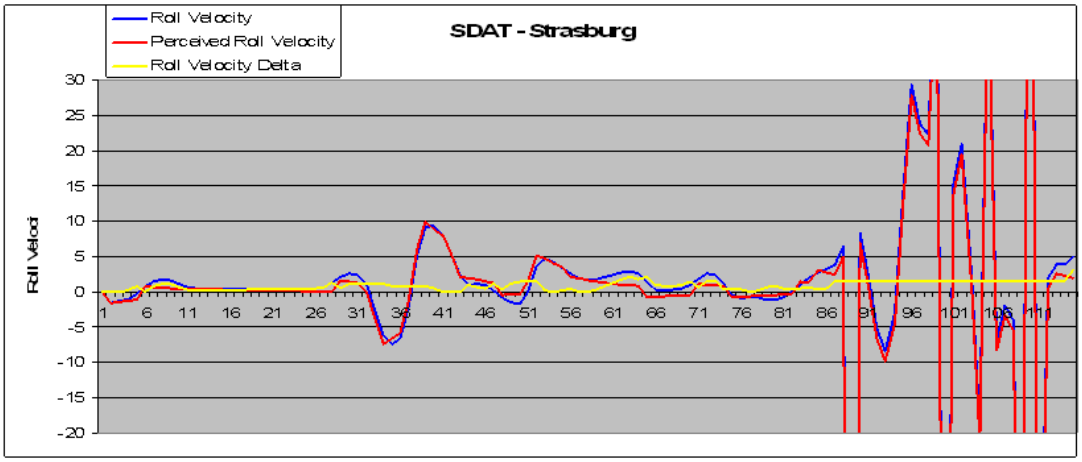

b. SDAT roll velocity for Strasburg (NTSB) accident data set.

Figure 14. Comparison of Observer (MIT) and SDAT roll velocity for NTSB data set.

Next, we compared the two tools' analyses of a Navy mishap data set in which a sustained turn in the airfield traffic pattern was followed by a sudden dive into the ground. The first set of graphs (Figure 16) show the roll velocity results. The Observer results indicate that the estimated roll velocity is generally much lower than the actual roll velocity. The SDAT model predicts that the perceived roll velocity more closely matches the actual values. While the magnitude of the calculated deltas differs, it is interesting to note that the general shape of the yellow delta lines are similar (meaning that the peaks and valleys mostly correspond), indicating

some level of agreement about the general character of the perception deltas and the conclusion of a somatogyral illusion.

Figure 17 shows the graphs for the yaw velocity of the Navy data set. The MIT model estimates that a small amount of the yaw velocity is perceived, with a maximum delta approaching 4 deg/sec. SDAT allows analyses using a range of threshold values; the first SDAT graph (Figure 17b) shows that, at the default yaw threshold of 1.1 deg/sec, almost none of the yaw velocity would have been perceived. Figure 17c shows that, in order to obtain perception values similar to the MIT model, SDAT uses a 0 deg/sec threshold value. Since Observer does not use thresholds in its estimation of yaw velocity perception, the contrast between SDAT and Observer results is not surprising.

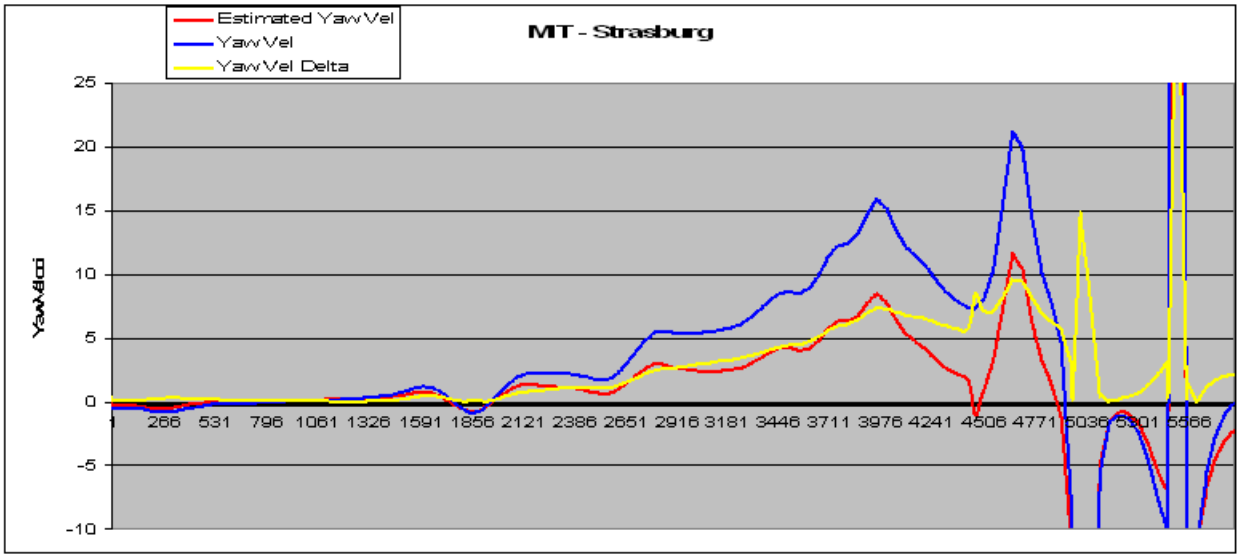

a. Observer yaw velocity for Strasburg (NTSB) accident data set.

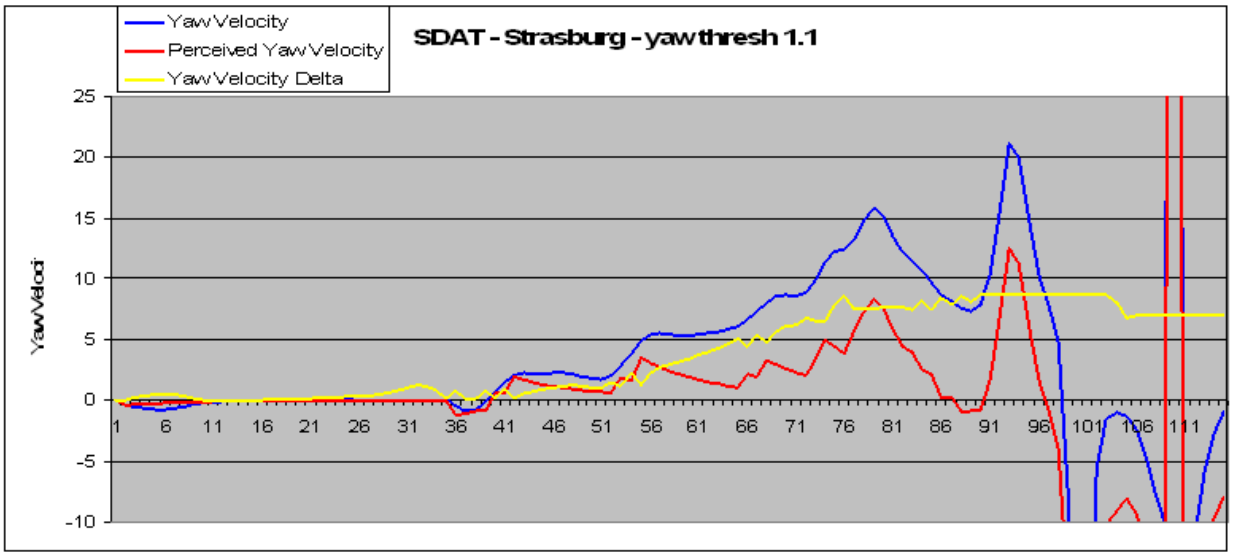

b. SDAT yaw velocity for Strasburg (NTSB) accident data set.

Figure 15. Comparison of Observer (MIT) and SDAT yaw velocity for NTSB data set.

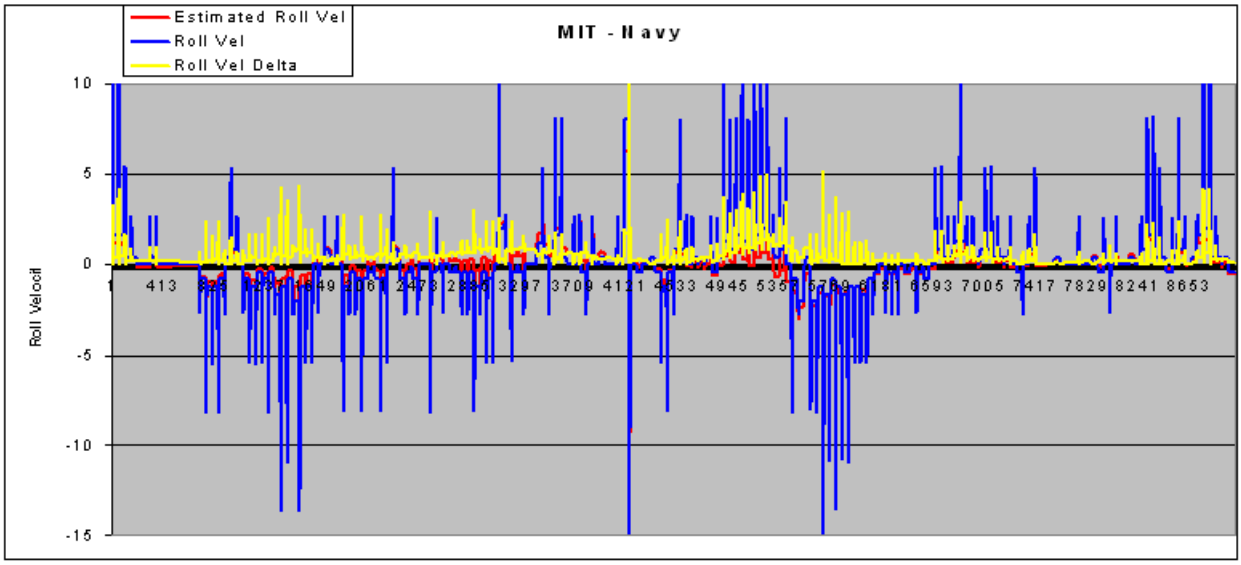

a. Observer roll velocity for Navy accident data set.

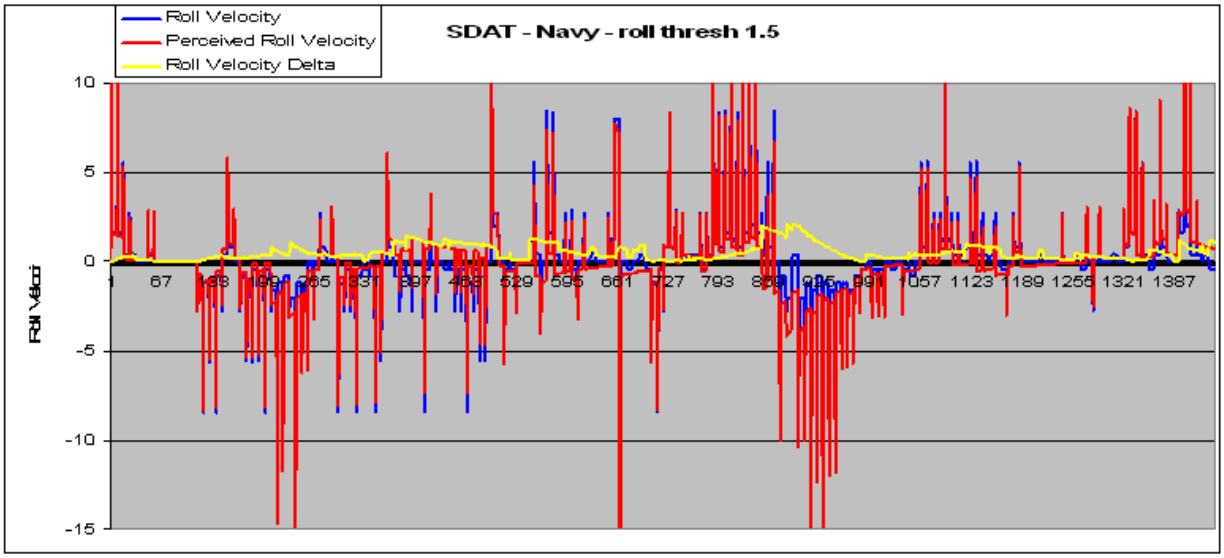

b. SDAT roll velocity for Navy accident data set.

Figure 16. Comparison of Observer (MIT) and SDAT roll velocity for Navy data set.

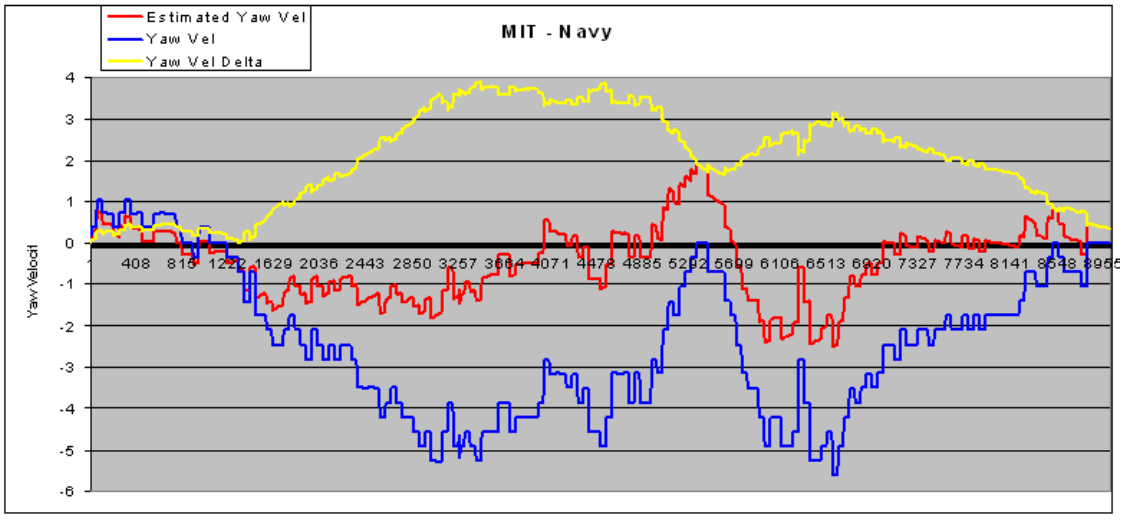

a. Observer yaw velocity for Navy accident data set.

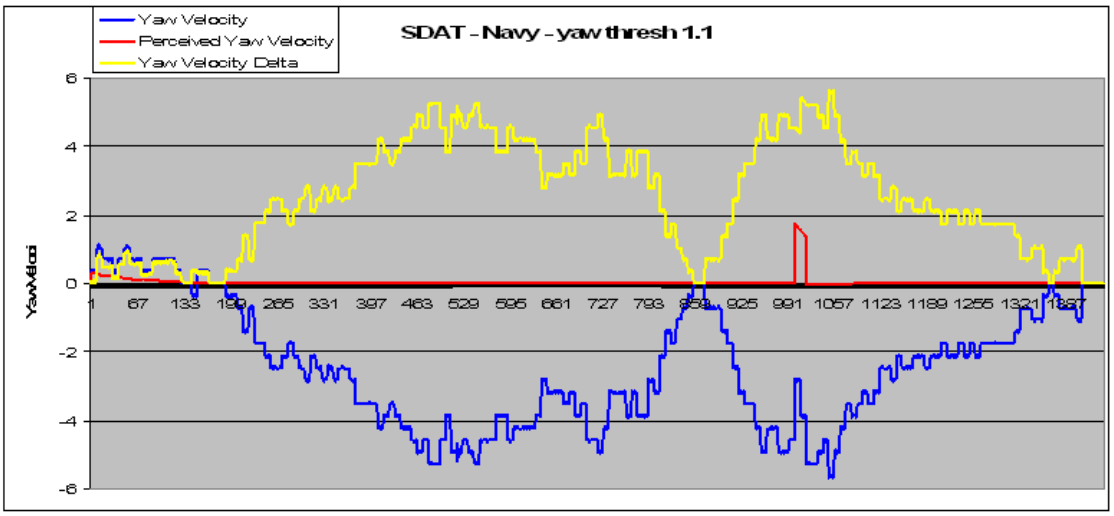

b. SDAT yaw velocity for Navy data set at default 1.1 deg/sec threshold setting.

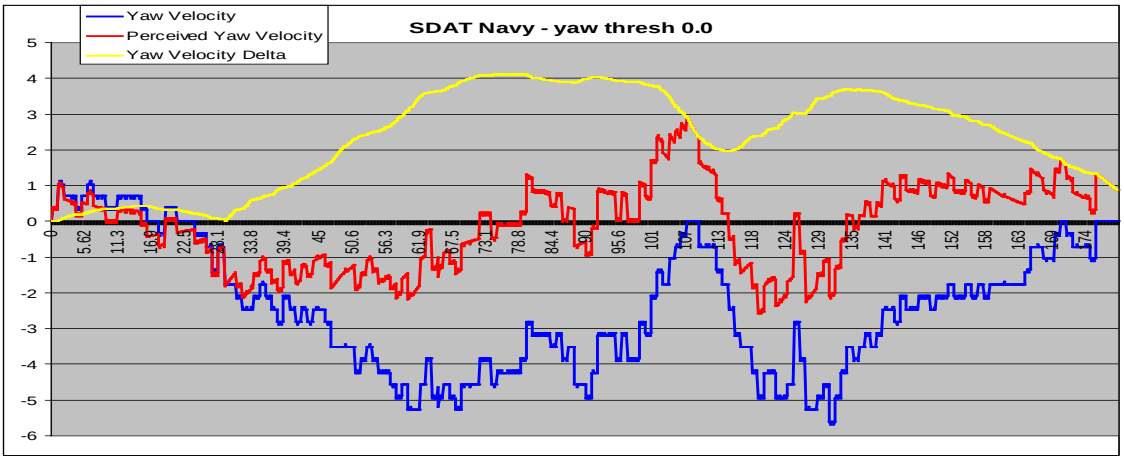

c. SDAT yaw velocity set at 0.0 deg/sec threshold for direct comparison to Observer.

Figure 17. Comparison of Observer (MIT) and SDAT yaw velocity for Navy data set.

The last set of comparisons is from the Flash Air accident. Results from Observer and SDAT both show somatogyral and somatogravic illusions. In these graphs (Figures 18 & 19), the green line is the actual pitch or roll. The Observer results (top graphs in both figures) show perceived angles (pitch or roll, respectively) from two variations of Observer (Merfeld and NAMRL), as well as the GIF time series graph. The SDAT graphs (bottom in both figures) show the combined perceived pitch or roll angles with red lines.

The bottom (SDAT) graphs are offset to the right to align time scales because the SDAT analysis used a data set that truncated the time to 30 seconds before the pilots began their takeoff acceleration.

The vertical axes are in degrees with the same scale (-30 to +30 degrees) in all four graphs shown in Figures 18 and 19.

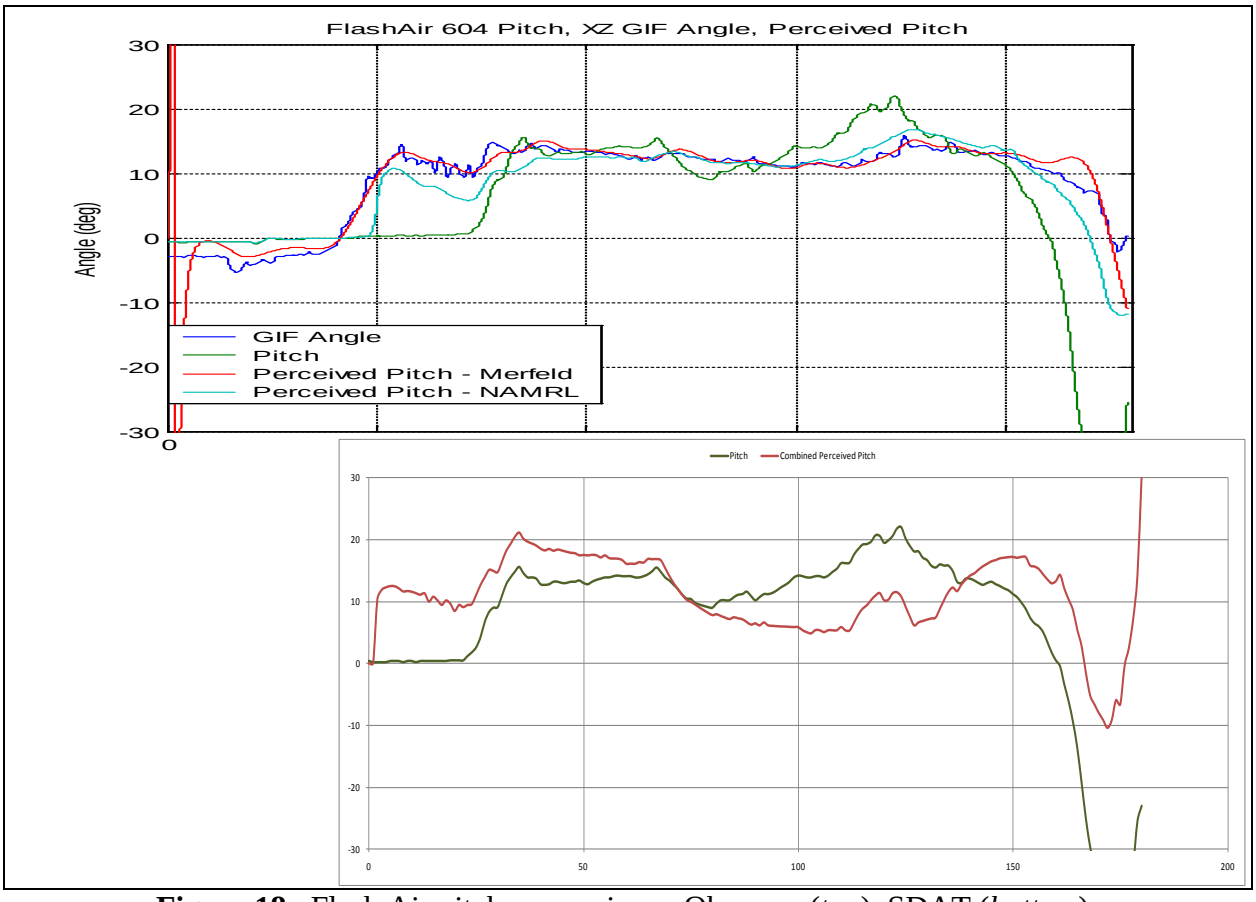

Figure 18. Flash Air pitch comparison. Observer (*top*), SDAT (*bottom*).

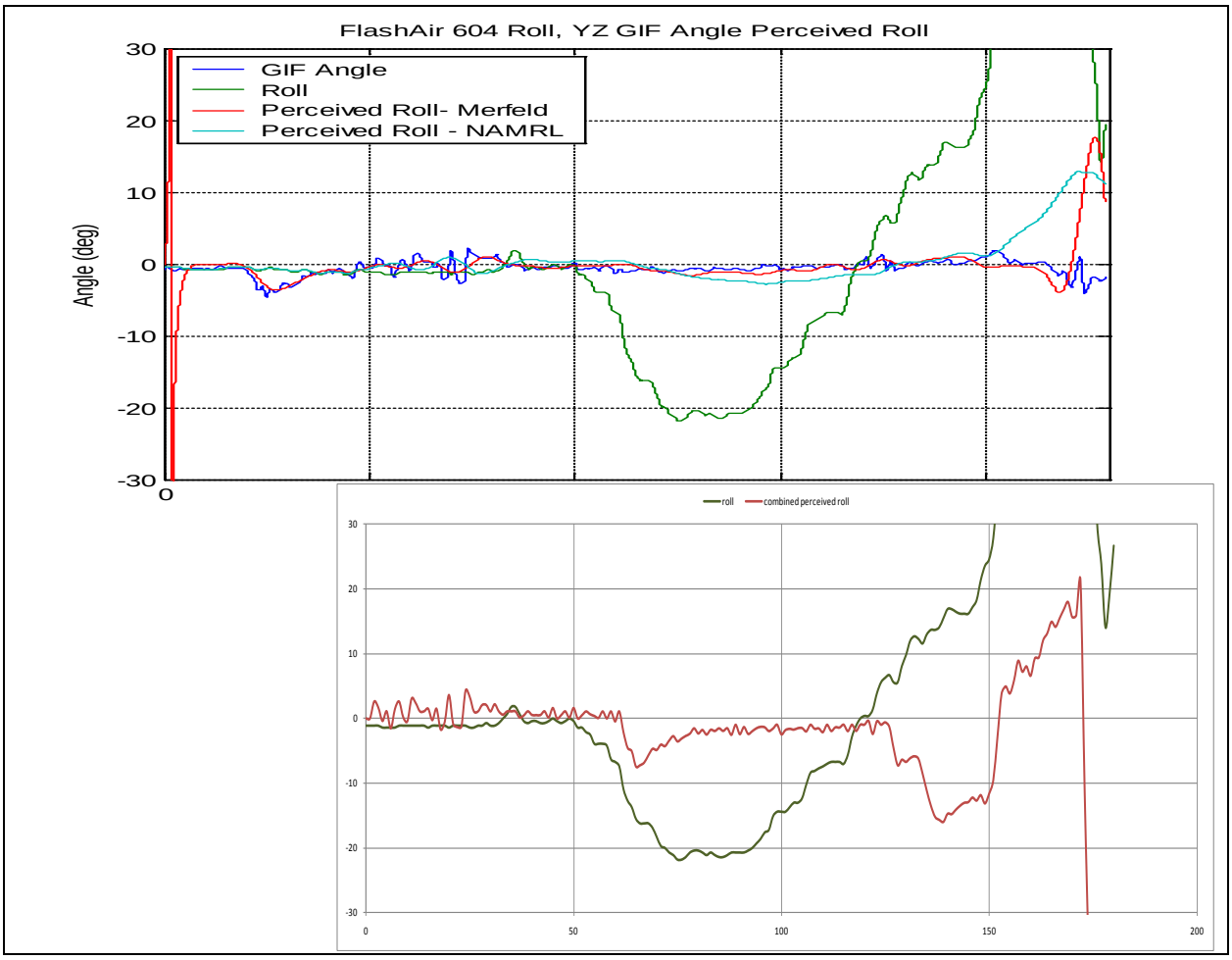

Figure 19. Flash Air pitch comparison. Observer (*top*), SDAT (*bottom*).

In Figure 19, the SDAT roll threshold was set to 3.2 deg/sec for the results shown.

While there are some differences from the two tools, Figures 18-19 show a closer match than 14-17. This closer match is likely due to SDAT's new GIF calculation (Appendix A), since that is also a basis for Observer's perceived angle calculations. Because each tool's GIF vector was independently derived, the Flash Air results are a form of "cross validation."

Ancillary Accomplishments

There are two other major accomplishments from this project to describe: Development and validation of the frame of reference transformation (FORT) tool, and our survey of Space Shuttle flight crew members that was intended to capture the subjective recollections of illusory sensations experienced by this population of astronauts during their Shuttle missions. A secondary objective of the survey was to capture these data for historical purposes before the Shuttle was retired earlier this year.

FORT Tool

The FORT tool is our response to an initial objective to examine alternative visual reference frames (see Aim #3 in the executive summary). Because SDAT does not have visual inputs, it does not make sense to integrate FORT into SDAT. It may make sense to merge FORT into Observer, since Observer does take visual cues as inputs. However, the R&D reported here did not attempt to integrate FORT into either SDAT or Observer. The FORT tool is a stand-alone deliverable to NSBRI.

To set the context for the FORT model, we suggest a scenario in which a crew is 200 miles above Earth as a Shuttle steadily approaches the ISS for docking. The commander, using reaction control jets, moves his translational hand controller (THC) to carefully align the space-craft with the docking port, while viewing the error of alignment at an off angle – because the status and position display is oriented 90 degrees from the axis of control and of the approach as shown in Figure 20. At the last moment, just before contact, the commander moves the THC in the wrong direction from that intended. The Shuttle's docking ring fails to engage the docking receptacle, rebounds, and is damaged by the off-axis impact.

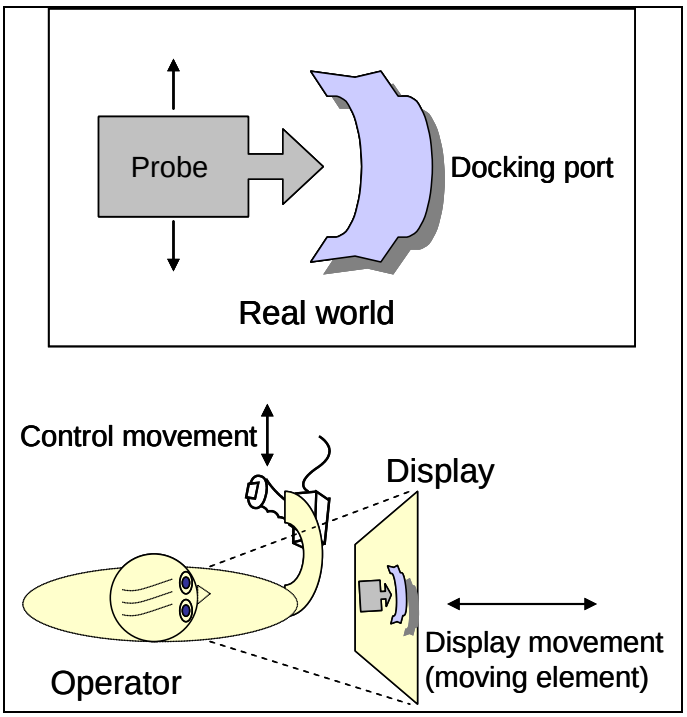

Figure 20. Docking task: reality vs. display-control alignments.

It is quite likely that such a hypothetical but plausible error could have been due to a form of spatial disorientation not previously discussed here, since the axis of control did not correspond to the axis along which the error was perceived. The human operator was required to make a frame-of-reference transformation. FORT theory is designed to understand the nature and cause of such errors. Below, we describe the theory and our efforts to translate this into a usable computational model.

Our FORT tool is designed to predict the response time or speed, the error likelihood (including both discrete and continuous errors), and the mental workload imposed in any circumstance in which a human needs to translate from one frame of reference to another. FORT theory, and the FORT model described below, can be applied to two general classifications of tasks: (1) **image comparison** tasks, such as those when the astronaut examines a diagram or map and tries to establish how items on the diagram or map correspond to those in the real world; and (2) **control** tasks, for example the continuous alignment task illustrated in Figure 20. Furthermore, these two tasks can be carried out in any of the following three situations:

1. Self orientation: either out of vehicle (EVA) or in vehicle (IVA). In the former case, astronauts may be navigating to a particular landmark on the spacecraft. In the latter, they may be deciding which exit to take to go from one ISS node to another.
2. Vehicle navigation and control: for example (a) rendezvous with another vehicle from a distance, (b) docking with another vehicle, or (c) guiding and landing a vehicle on a planetary surface.
3. Robotics control.

We also note three important uses of the FORT model, designed to predict astronaut performance in these environments:

1. Using a task analysis, we can identify "red flags" or particularly challenging control-display configurations with specific tasks, which will invite errors. In some circumstances we will be able to predict the time required to perform certain FORT maneuvers, a critical prediction in certain time-critical, time-limited situations (e.g., approaching a landing or docking; executing emergency procedures).

2. Embedded within FORT theory are costs associated with transformations. Given this, it should be straightforward to use the model to identify various countermeasures when such red flags appear; countermeasures that may vary in their feasibility and degree of success. In the case of the misaligned display cited at the outset (Figure 20), it may be that a full repositioning, so that the error is viewed straight on, is impossible because of other physical constraints. But, relocating the display 20 degrees toward the operator's trunk alignment and axis of control movement in Figure 20 will mitigate some control-display confusion problems.

3. FORT can be used as a retrospective mishap analysis tool, analogous to the manner in which SDAT is employed, so long as certain key data are available, regarding the interface design and a time record of actual control activity and system state.

FORT tool operation

The FORT model interface is shown in Figure 21. In the left panel (step A), the operator is positioned at a workspace, manipulating a **control element** positioned in front of the body, as shown. On the cube in front of the operator are represented the six degrees of freedom with which this control element can be moved. The user selects one of these, with the direction of movement designated by the arrow. For example, the driver steering a vehicle would select the clockwise vertical rotation (CVR).

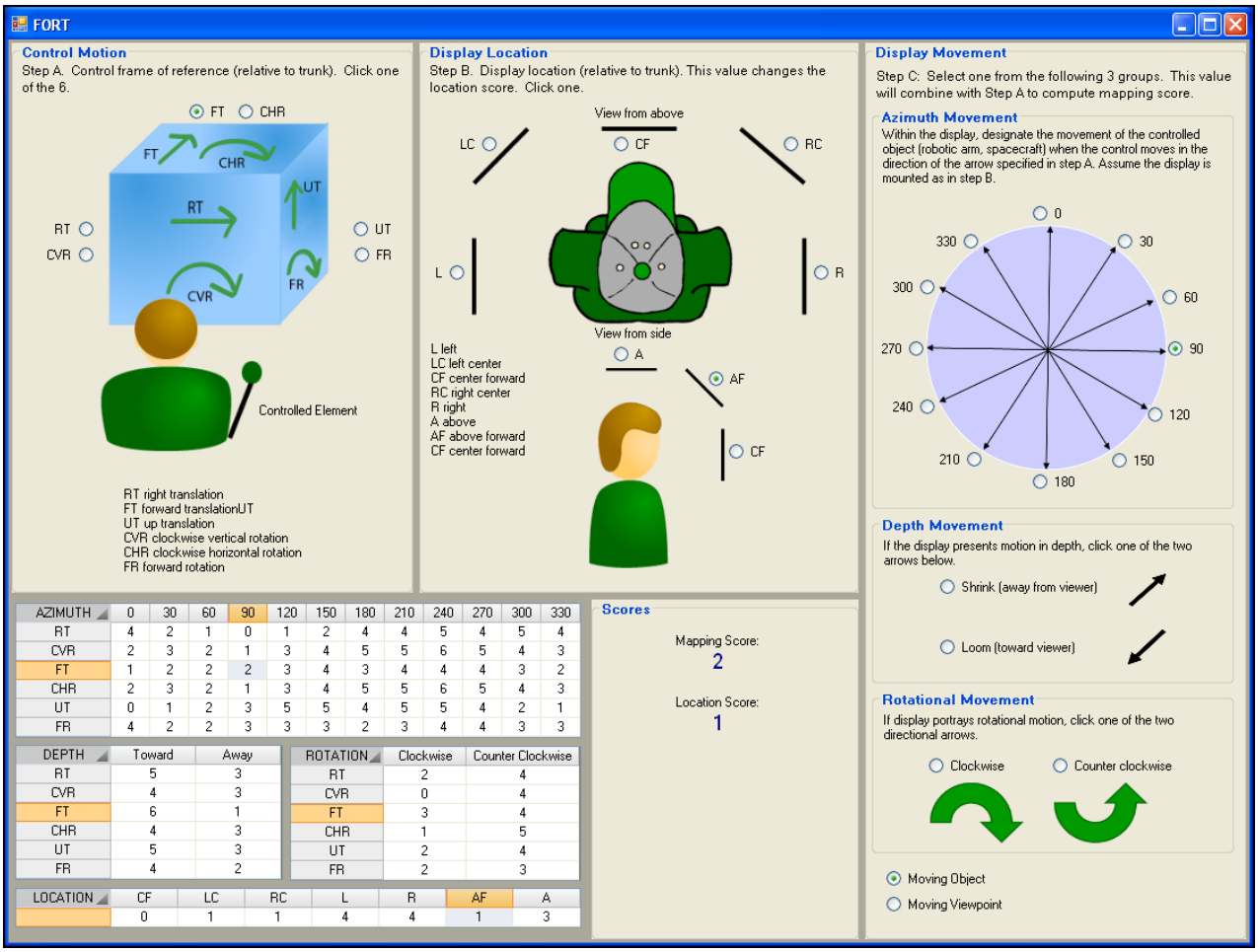

Figure 21. FORT tool interface.

In the middle panel (Step B), the user selects the second design feature of the workspace, the **display position** relative to this forward view. While typically in work station design this will be 'center forward' (CF), in many space applications the display could be displaced sideways and/or upward. The term 'display' is used to represent either a computer generated display or camera view, or a direct visual input, as when looking out a window. In this version of the FORT tool, the designer must select one option from either the top view (labeled 'view from above') or the side view. Because the center-front choice is located in both the above and side views, either can be clicked to represent that typical display location.

In the right panel (Step C), the operator designates the motion of the **moving element on the display** when the control moves in the direction and orientation specified in Step A. If the displayed element translates linearly parallel to the display's surface, a direction of movement is selected from the top panel of azimuth movement or compass headings. If the moving element translates in depth toward (looming) or away (shrinking) from the operator, one of the two arrows in the middle panel is selected. If the moving element on the display rotates (e.g., the horizon line on an aircraft attitude indicator), one of the two direction-of-rotation options in the bottom panel is selected. Only one of the three movement panels (azimuth, depth, rotation) can be selected for each control motion and display movement situation.

Finally, the user specifies whether the control movement affects an object location (movement) against a stable background (or display frame), or controls the viewpoint with which the user sees the display. An example of the first case is if a camera were mounted to the vehicle in which an operator was controlling a robotic arm. Here the operator would see the arm receding, as the arm approached the target object at some distance from the vehicle. An example in the second case would be the image conveyed by a camera mounted to the robotic arm. If the arm moved forward, the display viewer would see the target getting closer (looming). In every case where there is direct viewing of the outside world through a viewport of a controlled vehicle (e.g., looking through the cockpit window), the motion frame of reference (FOR) is a controlled viewpoint, corresponding to what researchers in aviation have termed an "inside-out" display (Roscoe, 1968).

Once the user completes these steps, the model automatically computes two penalty scores, one for the control and display movement relationship as specified by panels A and C, and one for display positioning (panel B). These penalties are shown in the bottom panel. For a multi-axis control or for multiple display locations, the designer will run the model repeatedly, once for each combination of control axis, display location, and display movement.

The score is based upon the matrix shown in the bottom left of the tool interface (Figure 21). The penalties for mapping within each cell are derived from consideration of the collective empirical data reviewed in Small et al. (2008) and are imposed by linearly combining different components of a control-display mapping as further described in Appendix E.

Further FORT tool development

Currently there are only two frames of reference to be matched, with mismatch between these defined by the 3-component rotational vector represented in Figure 21. It is possible that effective control may require three frames: control frame, display frame, and end-effector frame (e.g., robot arm). This need for three frames will occur when the display depicts motion relative to the human trunk that is in a different vector from the actual end effector motion. For example, a display of forward motion mounted at a 45-degree offset from forward, or viewing the end effector (i.e., the controlled element; e.g., a robot arm) through a head-mounted display while looking off-bore-sight. With three such frames, we may want to sum or average the vectors of mismatch between each pair of frames (where each vector itself contains the three-axis components).

In a separate project, we are also extending FORT to accommodate additional spatial awareness biases, which can create visual illusions for astronauts in landing approaches or in lunar surface navigation (Wickens, 2002). These biases include estimating velocity, biases in global optic flow, surface slant overestimation, display size, or 3-D display compression. Most of these biases can be expressed within the framework of the FORT tool, to the extent that all 18 transformations are considered.

Another key collaboration is that the FORT model is a module within a larger computational model of an astronaut robotics controller for a NASA project that is identifying functional allocation strategies between humans and automation (*MIDAS FAST*, contract # NNX09AM81G, technical customer is Dr. Barbara Woolford; Sebok et al., 2011).

FORT tool summary

A frame of reference transformation (FORT) tool was designed and developed as part of this research effort. We have presented the theory and its embodiment in our FORT tool at professional conferences (see Wickens, Keller & Small, 2010, 2011) and have submitted a manuscript to the journal *Human Factors* that describes the theory and tool. We have validated predictions of the FORT model for azimuth transformations against data of other researchers and have found correlations between predicted and obtained movement times or tracking error in the range between r=0.714 and r=0.85). The model's history, detailed theoretical foundation, tool details and exercises, and validation steps are in Appendix E. It is protected as Alion intellectual property via registered copyright.

Understanding Space Operations SD via a Shuttle Survey

In pursuit of an original goal to better understand and quantify space operations SD, we developed a Shuttle orientation survey (Appendix F) to capture relevant historical information from Shuttle commanders and pilots before the Shuttle was retired. The survey package received approvals from the MIT and JSC IRBs.

We received 40 usable survey responses, analyzed the data from the 71 missions in the responses, and submitted a draft article to the journal *Aviation, Space and Environmental Medicine* reporting our methods and results; following is the abstract from the article:

> *A survey was distributed to 77 Space Shuttle flight crew members; 40 responded covering 71 missions. The goal was to capture historical information before Shuttle retirement and to better understand subjective experiences of illusory sensations due to the transition from 1-g to 0-g and back. We analyzed the response data to answer four questions: (1) Do older astronauts suffer more from illusory sensations than younger astronaut? We conclude that they do not. (2) Do trial head motions during re-entry in an effort to hasten re-adaptation to 1-g really help? Apparently not. (3) Do symptoms decrease as flight experience increases? Yes, although there are individual exceptions. (4) Do longer duration missions lead to more illusory sensations and re-adaptation difficulties than shorter duration missions? Yes. Based upon our results, long-duration missions may induce orientation problems that could have significant mission impacts.*

Table 2 gives the basic response data to the main questions in the survey (Appendix F).

Table 2. Basic data tabulated by question.

Q	Question Topic	Most recent missions only	All missions
		Total (40 max), yes (%), no (%)	***Total (71 max), yes (%), no (%)***
1	MECO spontaneous	40, 8 (20.0%), 32 (80.0%)	56, 16 (28.6%), 40 (71.4%)
2	MECO head motion	40, 5 (12.5%), 35 (87.5%)	47, 7 (14.9%), 40 (85.1%)
4	Head motion illusions	37, 16 (43.2%), 21 (56.8%)	46, 21 (45.7%), 25 (54.3%)
6	TAEM illusions	40, 4 (10.0%), 36 (90.0%)	47, 5 (10.6%), 42 (89.4%)
7	Auto to manual flt. illusions	40, 1 (2.50%), 39 (97.5%)	45, 1 (2.2%). 44 (97.8%)
8	HAC turn illusions	38, 6 (15.8%), 32 (84.2%)	48, 9 (18.8%), 39 (81.3%)
9	Deceleration illusions	40, 5 (12.5%), 35 (87.5%)	45, 5 (11.1%), 40 (88.9%)
10	Landing flare illusions	40, 4 (10.0%), 36 (90.0%)	45, 4 (8.9%), 41 (91.1%)
11	De-rotation illusions	40, 3 (7.50%), 37 (92.5%)	45, 3 (6.7%), 42 (93.3%)
12	After stop head motions	39, 20 (51.3%), 19 (48.7%)	48, 23 (47.9%), 25 (52.1%)
13	Entry no head motions	40, 4 (10.0%), 36 (90.0%)	41, 4 (9.8%), 37 (90.2%)
14	Manual flight, no head motions	39, 6 (15.4%), 25 (64.1%), n/a 8 (20.5%)	45, 9 (20.0%), 28 (62.2%), n/a 8 (17.8%)
18	Walk-around illusions	39, 24 (61.5%), 15 (38.5%)	46, 27 (58.7%), 19 (41.3%)
19	<= 2 hrs head motions	39, 25 (64.1%), 14 (35.9%)	48, 28 (58.3%), 20 (41.7%)
20	2-24 hrs head motions	40, 19 (47.5%), 21 (52.5%)	46, 22 (47.8%), 24 (52.2%)
21	<= 24 hrs balance	40, 30 (75.0%), 10 (25.0%)	51, 34 (66.7%), 17 (33.3%)
22	> 24 hrs head motions	40, 4 (10.0%), 36 (90.0%)	49, 7 (14.3%), 42 (85.7%)
23	> 24 hrs balance	40, 5 (12.5%), 35 (87.5%)	49, 8 (16.3%), 41 (83.7%)
	TOTALS for illusory sensations	189 yes (26.6%), 514 no (72.3%), 8 n/a (1%)	233 yes (27.5%), 606 no (71.5%), 8 n/a (1%)

TAEM is terminal area energy management. HAC is heading alignment circle.

Response data about answers to questions not in the above table were:

Q3: *During re-entry did you make any <u>deliberate</u> head movements to see how they felt?* There were 39 most recent mission responses: 22 Yes's (56.4%) and 17 No's (43.6%). Of the 52 other missions, there were 28 Yes's (53.8%) and 24 No's (46.2%).

Q5: *Were there any phases of flight or maneuvers where you deliberately <u>avoided</u> moving your head?* We received 26 No responses (56.5%) and 20 Yes responses (43.4%). The maneuvers where Yes respondents avoided moving their heads were: HAC turn (15), Intercepting the inner glide slope (13), Landing flare (12), Rotation to nose-wheel touchdown (9), Rollout (9), and TAEM turns (6).

Q15 & 16: *If you experienced illusions while flying manually, how difficult was it to "fly through" and which technique(s) did you use if you did have any difficulty?* Ten respondents reported that they did not fly manually; they selected "N/A". Twenty-six reported no problems; two indicated it was "very easy," two "easy," four "moderate," and one "difficult." No one selected "very difficult" or "impossible." Of those who reported any level of difficulty, 8 responses indicated that focusing on the head-up display (HUD) or other flight instruments helped them to "fly through" those difficulties.

Q17 & 24: Recommendations for helping to maintain orientation in future Shuttle missions (Q17) or future vehicles (Q24) included: head-mounted display, laser horizon, and wider HUD. Seventeen respondents emphasized the importance of the HUD.

Q25: Other free form comments included:

> *The only unusual thing for me is that each flight I experienced more spatial discomfort/illusions/issues than the previous (unlike zero g adaptation, which got better each time). In other words, coming back into g got harder every time.*
>
> *I contribute the fact that I had no sensations while flying was due to concentrating on the task at hand and due to the large amount of Shuttle approach and landing training that was done. It should also be noted that the minor sensations I had got less and less with each flight and were basically non-existent on my 4th flight.*
>
> *[Commander] had told me repeatedly during training to minimize my head movements post MECO. I did and experienced no difficulties. Reentry was same. As noted, my 'problems' (minor) were post homecoming. The Jack Daniels could have been partly to blame!!*

We also sent de-identified data to our customer, NASA-JSC's Dr. Jacob Bloomberg, and will make the full set of de-identified data available to anyone who wishes it.

Recommendations

For future enhancements to Observer, we want to develop additional input routines to accommodate different input sources and sampling rates. For example, users who have 5 Hz head linear acceleration data in a head frame, instead of 1 Hz head position data in a world frame, should also be able to input their data into Observer. A second goal is to incorporate threshold phenomena into the model. A third is to develop quantitative model-based metrics of spatial disorientation. Currently the model provides quantitative metrics of perceived vs. actual orientation, and also perceived vs. actual velocity, position, etc. How should these different dimensions of spatial orientation be combined for purposes of, for example, SD illusion prediction, SD accident investigation or flight simulator washout optimization applications, or to trigger countermeasures? These are research questions that we hope to address in future efforts.

Future enhancements to SDAT should include the following:

- A cubic spline interpolation routine for filling blank data set cells. This Excel macro would also be useful for up-sampling 1 Hz data sets to 10 Hz for analyses using Observer.
- Verify and validate the new SD illusion models; complete the "undetected drift while landing" model. Improve all illusion models to include "unusual attitude" as an event within each model.
- Design and develop a "batch mode" for accident investigators who need to quickly try a range of vestibular thresholds as they test for possible somatogyral or somatogravic illusions within an accident data set
- Add embedded Help to explain SDAT's features and functions in a more user-friendly way.

- Design and develop a method to enhance SDAT GIF calculations for uncoordinated flight (e.g., slips and slides).

Even though it is inappropriate to integrate the FORT tool into SDAT, it may make sense to integrate it with Observer. SDAT has no visual processing because no actual vehicle data sets (of which we are aware) have vision or visibility parameters. However, Observer does now have visual information represented, and so it may make sense to integrate FORT theory and penalty calculations into Observer.

Conclusions

Merging Observer into SDAT proved to be much more difficult than originally envisioned, which impacted all other plans for this research project. The difficulty was primarily due to the fundamentally different approaches of the two models of human orientation perception. Observer is a physiologically-based representation of the vestibular and visual systems that models how the central nervous system (CNS) disambiguates gravity from linear accelerations using a combination of SCC, otolith and visual cues. It operates best with data sampled at a high rate. SDAT, on the other hand, does not attempt to represent physiology; rather it models perceptual responses to motion (with no vision cues) as captured within low frequency noisy FDR data sets. Observer is the product of academic researchers seeking to model quantitative data from laboratory experiments in order to understand how motion cues determine orientation perception. SDAT is the product of a human performance and applied research engineering company that seeks to mitigate the adverse consequences of spatial disorientation.

Despite these differences in the MIT and Alion models and approaches, each tool (Observer and SDAT) has been improved as a result of this collaboration. Observer has a much improved and more usable GUI. SDAT has a vastly improved otolith model and a novel method for combining the results from the otolith and SCC models within SDAT to predict total perceived pitch and roll. Each has other improvements as noted in their respective sections.

Even though we did not completely accomplish a primary goal, we have three additional research products that were not in our original plan: (1) A FORT tool useful to complex system designers and human factors or human-system integration professionals. (2) Our collaboration led to capturing important historical information about Space Shuttle illusory sensations via a written survey of flight crews and submission of a draft manuscript to ASEM. (3) We added a pilot attention model (N-SEEV) to SDAT

NSBRI benefitted from this collaboration because both Observer and SDAT were improved and delivered to the customer. A separate FORT tool was also delivered. And, the project team produced 20 publications, as listed in the Bibliography for the years 2007-2011 for the primary authors of Donaldson (1), Keller (1), Newman (3), Oman (2), Selva (2), Small (8), Venkatesan (1), and Wickens (3).

Bibliography

Alexander, A., C.D. Wickens, & T.J. Hardy (2005). Synthetic vision systems: The effects of guidance symbology, display size, and field of view. *Human Factors, 47*, 693-707.

Andre, A.D., & C.D. Wickens (1992). Compatibility and consistency in display-control systems: Implications for aircraft decision aid design. *Human Factors, 34*(6), 639-653.

Aoki, H., C.M. Oman, & A. Natapoff (2007). Virtual-reality-based 3D navigation training for emergency egress from spacecraft. *Aviation, Space, & Environmental Medicine, 78*(8), 774-83.

Aoki, H., C.M. Oman, A. Natapoff, & A. Liu (2006). The effect of the configuration, frame of reference, and spatial ability on spatial orientation during virtual 3-dimentional navigation training. In *7th Symposium on the Role of the Vestibular Organs in Space Exploration*. Noordwijk, the Netherlands: European Space Agency, European Space Technology Centre (ESTEC).

Aretz (1991). The design of electronic map displays. *Human Factors, 33*, 85-101.

Aretz, A.J. & C.D. Wickens (1992). The mental rotation of map displays. *Human Performance, 5*, 303-328.

Bainbridge, L. (1999). Processes underlying human performance. In *Handbook of Aviation Human Factors*, D.J. Garland, J.A. Wise, and V.D. Hopkin, Editors. Mahwah, NJ: Earlbaum, 107-171.

Beckman, PA (2002). Concordance between task and interface rotational and translational control improves ground vehicle performance. *Human Factors, 44*(4), 644-653.

Benson, A.J., Spencer, M.B., & J.R. Stott (1986). Thresholds for the detection of the direction of whole-body, linear movement in the horizontal plane. *Aviation, Space and Environmental Medicine, 57*(11), 1088-96.

Bilien, V. (1993). *Modeling human spatial orientation perception in a centrifuge using estimation theory* (Masters thesis). Cambridge, MA: MIT Department of Aeronautics and Astronautics.

Boeckman, K.J., & Wickens, C.D. (2001). The resolution and performance effects of three-dimensional display rotation on local guidance and spatial awareness measures (Technical Report ARL-01-4/NASA-01-3). Savoy, IL: University of Illinois, Aviation Research Lab.

Borah, J., & L.R. Young (1983). *Spatial orientation and motion cue environment study in the total in-flight simulator* (AFHRL-TP-82-28 under contract F33615-78-C-0062). Williams AFB, AZ: AFHRL.

Borah, J., & L.R. Young (1982). Orientation perception during aircraft coordinated turns. In *Proceedings of the AIAA 20th Aerospace Sciences Meeting* (AIAA-82-0258). NY: AIAA.

Borah, J., Young, L.R., & R.E. Curry (1988). Optimal estimator model for human spatial orientation. *Annals of the New York Academy of Sciences, 545*, 1-73.

Borah, J., L. Young, & R.E. Curry (1979). Optimal estimator model for human spatial orientation. *IEEE Transactions on Systems, Man and Cybernetics*, 800-805.

Borah, J., Young, L.R. & Curry, R.E. (1978). *Sensory mechanism modeling* (AFHRL-TR-78-83, Final Report July 20, 1977-October 30, 1978). Wright-Patterson AFB, OH: AFHRL.

Borah, J., Young, L.R., Curry, R.E., Albery, W.B. & Fiore, M.D. (1978). Motion and orientation sensory mechanism modeling. In *Proceedings of National Electronics Conference*, Chicago, October.

Borel, L., B. Le Goff, O. Charade, & A. Berthoz (1994). Gaze strategies during linear motion in head-free humans. *Journal of Neurophysiology, 72*, 2451-2466.

Bos, J.E. & W. Bles (2002). Theoretical considerations on canal-otolith interaction and an observer model. *Biological Cybernetics, 86*, 191-2007.

Burrough, B. (1998). *Dragonfly: NASA and the crisis aboard Mir*. New York: Harper Collins.

Chan, A., & Hoffman, E. (2010). Movement compatibility for frontal controls with displays located in four cardinal directions. *Ergonomics, 53*, 1403-1419.

Cheung, B. (2004). Nonvisual spatial orientation mechanisms. In Previc, F.H. & W.R. Ercoline, editors, *Spatial disorientation in aviation*. Reston, VA: American Institute of Aeronautics and Astronautics, 37-94.

Cizaire, C. (2007). *Effect of 2 module docked spacecraft configurations on spatial orientation* (Master's thesis). Cambridge, MA: MIT.

Cizaire, C., C.M. Oman, D.A. Buckland, A. Natapoff, H. Aoki, & A. Liu (2007). Effect of two-module docked spacecraft configurations on spatial orientation (abstract). *16th IAA Humans in Space Symposium*. Beijing, China.

Clark, T.K. (2010). *Human spatial orientation perceptions during simulated lunar landing* (SM thesis). Cambridge, MA: Department of Aeronautics and Astronautics, Massachusetts Institute of Technology.

Cooper, H.S.F., Jr. (1976). *A House In Space.* New York: Holt, Rhinehart, and Winston.

DeHart, R.L., & J.R. Davis, Editors (2002). *Fundamentals of aerospace medicine, 3rd ed.* (ISBN 0-7817-2898-3). New York, NY: Lippincott Williams & Wilkins.

DeLucia, P. & Griswald, J. (2011). How should surgeons view surgical sites in minimally-invasive surgery? Effects of camera design on perceptual-motor performance. *Journal of Experimental Psychology: Applied, 17.*

Donaldson, A., & CM Oman (2011, April 6). *Application of MIT Observer Spatial Disorientation Model to Aircraft Accident Investigations*, Research presentation to the FAA Joint University Program, Princeton, NJ (paper 4011).

Egyptian Ministry of Civil Aviation (2004). *Final report of the accident investigation of Flash Airlines flight 604*. Retrieved from: http://www.bea.aero/docspa/2004/su-f040103a/pdf/su-f040103a.pdf.

Ellis, S.R. (2000). Collision in space. *Ergonomics in Design* (winter), 4-9.

Fernandez, C. & J. Goldberg (1972). Physiology of peripheral neurons innervating the semicircular canals of the squirrel monkey. *International Journal of Neurophysiology, 34*, 661-675.

Francisco, D.R. & J.V. Meck (2006). *Small Assessment Team (SAT) Report - Final*. Houston, TX: NASA Johnson Space Center, 28.

Franklin, N., & B. Tversky (1990). Searching imagined environments. *Journal of Experimental Psychology: General, 119*, 63-76.

Fulgham, D., & K. Gillingham (1989). Inflight assessment of motion sensation thresholds and disorienting maneuvers. In *Proceedings of the Annual Aerospace Association Meeting*.

Geiselman, E.E. (1999). Development of a non-distributed flight reference symbology for helmet-mounted display use during off boresight viewing. In *Proceedings of the 4th Annual situational awareness in the tactical air environment conference*. Piney Point, MD, 118-127.

Gillingham, K.K. & F.H. Previc (1996). Spatial orientation in flight. In *Fundamentals of Aerospace Medicine, 3rd ed*. R.L. DeHart, Editor. Baltimore, MD: Williams and Wilkins, 309-397.

Gillingham, K.K. & J.W. Wolfe (1986). Spatial orientation in flight. In R.L. DeHart, Editor, *Fundamentals of Aerospace Medicine, 2nd ed*. Philadelphia, PA: Lea and Febiger, 299-381.

Grabherr, L., K. Nicoucar, F.W. Mast, & D.M. Merfeld (2008). Vestibular thresholds for yaw rotation about an earth-vertical axis as a function of frequency. *Experimental Brain Research, 186,* 677-681.

Groen, E.L., M.H. Smaili, T. Haslwanter, R. Jaeger, S. Mayr, & M. Fetter (2000). Three-dimensional eye-movement responses to off-vertical axis rotations in humans. *Experimental Brain Research, 134*, 96-106.

Groen, E.L., M.H. Smaili, & R.J.A.W. Hosman (2007). Perception model analysis of flight simulator motion for a decrab maneuver. *AIAA Journal of Aircraft 44*(2), 427-435.

Gugerty, L., & J. Brooks (2004). Reference frame misalignment and cardinal direction judgments: Group differences and strategies. *Journal of Experimental Psychology: Applied, 10*, 75-88.

Guedry, F.E. (1974). Psychophysics of vestibular sensation Chapter 1. In H.H. Kornhuber, Editor, *Handbook of Sensory Physiology, Vol. 6*. Berlin: Springer-Verlag, 3-154.

Gundry, A.J. (1979). Thresholds of perception for periodic linear motion. *Aviation, Space, & Environmental Medicine, 49*, 679-686.

Harm, D.L., M.F. Reschke, & D.E. Parker (1999). Visual-Vestibular Integration Motion Perception Reporting. In *Extended Duration Orbiter Medical Project Final Report*, C.F. Sawin, G.R. Taylor, and W.L. Smith, Editors, 5.2.1-5.2.12.

Harris, L., R. Dyde, C.M. Oman, & M. Jenkin (2006). Visual cues to the direction of the floor (abstract). In *7th Symposium on the Role of the Vestibular Organs in Space Exploration*. Noordwijk, the Netherlands: European Space Agency, European Space Technology Centre (ESTEC).

Haslwanter, T., R. Jaeger, S. Mayr and M. Fetter (2000). Three-dimensional eye-movement responses to off-vertical axis rotations in humans. *Experimental Brain Research (134),* 96-106.

Hickox, J.C., & C.D. Wickens (1999). Effects of elevation angle disparity, complexity, and feature type on relating out-of-cockpit field of view to an electronic cartographic map. *Journal of Experimental Psychology: Applied, 5*(3), 284-301.

Hofer, E.F., & C.D. Wickens (1997). Part-mission simulation evaluation of issues associated with electronic approach chart displays. *Proceedings of the 9th International Symposium on Aviation Psychology*. Columbus, OH: Ohio State University.

Holmes, S.R., A. Bunting, D.L. Brown, K.L. Hiatt, M.G. Braithwaite, & M.J. Harrigan (2003). Survey of spatial disorientation in military pilots and navigators. *Aviation, Space, and Environmental Medicine, 74*(9), 957-965.

Howard, I.P. and G. Hu (2000). Visually induced reorientation illusions. *Perception, 30*(5), 583-600.

Hu, G., I.P. Howard, & S. Palmisano (1999). The role of intrinsic and extrinsic polarity in generating reorientation illusions. *Investigative Ophthalmology and Visual Science, 40*, S801.

Jenkin, H.L., J.E. Zacher, M.R. Jenkin, C.M. Oman, & L.R. Harris (2007). Effect of field of view on the levitation illusion. *Journal of Vestibular Research, 17*, 271-277.

Johnson, S., & S. Roscoe (1972). What moves? The airplane or the world. *Human Factors, 14*, 107-129.

Jones, T.D. (2006). *Skywalking: An astronaut's memoir*. New York, NY: HarperCollins.

Kanas, N. & D. Manzey (2008). *Space Psychology and Psychiatry, 2nd ed.* El Segundo CA: Microcosm Press.

Keller, Wickens, Small (2011). N-SEEV in SOAS: Predicting Time to Notice for Multi-Modal Cockpit Alerting Events. *Proceedings of the HFES Annual Meeting*. Santa Monica, CA: HFES.

Kingma, H. (2005, Jun 22). Thresholds for perception of direction of linear acceleration as a possible evaluation of the otolith function. *BMC Ear Nose Throat Disorders, 5*(1), 5.

Kovalenko, P.A. (1991). Psychological aspects of pilot spatial orientation. *ICASO Journal, 46*, 18-23.

Kozhevnikov, M. & M. Hegarty (2001). A dissociation between object manipulation spatial ability and spatial orientation abilities. *Memory and Cognition, 29*, 745-756.

Leone, G. (1998). The effect of gravity on human recognition of disoriented objects. *Brain Research Reviews, 28*, 203-214.

Linenger, J. (2000). *Off the Planet*. New York: McGraw Hill.

Liu, P (2008). *Mental Rotation in 3-Dimensional Environments* (unpublished PhD dissertation). Singapore: Nanyang Technical University.

Longnecker, D. & M. Molins (2005). *Bioastronautics Roadmap: A Risk Reduction Strategy for Human Exploration of Space*. Washington, D.C.: National Research Council, Committee on Review of NASA's Bioastronautics Roadmap, 142.

Lu, E. (2003). *Ed Lu's Journal Entry #12: Which Way is Up?* (http://www.edlu.com/whichWay.pdf). Houston, TX: NASA Johnson Space Center.

Luenberger, D.G. (1971). An introduction to observers. *IEEE Transactions on Automatic Control, 16*, 596-602.

Macedo, J., Kaber, D., Endsley, M., Powanusorn, P., & S. Myung (1998). The effect of automated compensation for incongruent axes on teleoperator performance. *Human Factors, 40*, 541-553.

Malcolm, R., & G. Melvill Jones (1974). Erroneous perception of vertical motion by humans seated in the upright position. *Acta Otolaryngolica, 77*, 274-283.

McGreevy, M., & Ellis, S. (1986). The effect of perspective geometry on judged direction in spatial information instruments. *Human Factors, 28*, 439-456.

McRuer, D.T. (1992). Human dynamics and pilot induced oscillations (Minta Martin lecture series). Cambridge, MA: MIT Dept. of Aeronautics and Astronautics.

Melvill Jones, G. & L.R. Young (1978). Subjective detection of vertical acceleration: a velocity dependent response? *Acta Otolaryngolica, 85*, 45-53.

Menchaca-Brandan, M., Liu, A., Oman, C., & Natapoff, A. (2007). Influence of perspective taking and mental rotation abilities in space teleoperation. *Proceedings, HRI 07*. Association for Computing Machinery: Washington DC.

Merfeld, D.M. (2003). Rotation otolith tilt-translation reinterpretation (ROTTR) hypothesis: A new hypothesis to explain neurovestibular spaceflight adaptation. *Journal of Vestibular Research*, 13, 309-320.

Merfeld, D., S. Park, C. Gianna-Poulin, F.O. Black, & S. Wood (2005). Vestibular perception and action employ qualitatively different mechanisms, II: VOR and perceptual responses during combined tilt & translation. *Journal of Neurophysiology, 94*, 199-205.

Merfeld, D.M., L.R. Young, C.M. Oman, & M.J. Shelhamer (1993). A multidimensional model of the effect of gravity on the spatial orientation of the monkey. *Journal of Vestibular Research, 3*(2), 141-161.

Merfeld, D.M., & L.H. Zupan (2002). Neural processing of gravitoinertial cues in humans, III: Modelling tilt and translation responses. *Journal of Neurophysiology, 87*, 819-33.

Mindell, D.A. (2008). *Digital Apollo: Human and Machine in Spaceflight* (ISBN 978-0-262-13497-2). Cambridge, MA: MIT Press.

Mittelstaedt, H. (1996). Inflight and postflight results on the causation of inversion illusions and space sickness. In *Scientific Results of the German Spacelab Mission D1*. Norderney & Koln, Germany: Wissenshaftliche Projecktfuhrung D1/DFVLR.

Mittelstaedt, H. (1983). A new solution to the problem of subjective vertical. *Naturwissenschaften, 70*, 272-281.

NASA (2005). *Bioastronautics Roadmap*. Houston, TX: NASA Johnson Space Center, p. 164.

Newman, M.C. (2009). *A multisensory Observer model for human spatial orientation perception* (SM thesis). Cambridge, MA: Department of Aeronautics and Astronautics, Massachusetts Institute of Technology.

Newman, M.C., & C.M. Oman (2009). Observer model for spatial orientation research and accident investigation (abstract & poster). *Aviation, Space and Environmental Medicine, 80*(3), 208.

Newman, M.C., CM Oman, TK Clark, J Mateus, & JD Kaderka (2011). Pseudo-Coriolis effect: A 3-D angular velocity storage phenomenon described by a left-hand rule. Presented at the Vestibular Symposium of the International Academy of Astronautics. Houston, TX: IAA. Abstract in special edition of the *Journal of Vestibular Research, 21*(2).

NTSB (2003). *Aircraft accident report: In-flight electrical system failure and loss of control, Jet Express Services, Raytheon (Beechcraft) Super King Air 200, N81PF near Strasburg, Colorado January 27, 2001* (NTSB/AAR-03/01, PB2003-910401, Notation 7358A, Adopted January 15, 2003). Washington, DC: Author.

Olmos, O., C.-C. Liang, & C.D. Wickens (1997). Electronic map evaluation in simulated visual meteorological conditions. *International Journal of Aviation Psychology, 7*(1), 37-66.

Olmos, O., C.D. Wickens, & A. Chudy (2000). Tactical displays for combat awareness: An examination of dimensionality and frame of reference concepts and the application of cognitive engineering. *International Journal of Aviation Psychology, 10*(3), 247-271.

Oman, C.M. *Aircraft Accident Investigation Applications for MIT Observer Spatial Orientation Model.* Presentation to Boeing Corporation, Commercial Airplane Division, Renton, WA, August 23, 2010.

Oman, C.M. (2007). Spatial orientation and navigation in microgravity. In F.W. Mast & L. Jancke, Editors, *Spatial Processing in Navigation, Imagery and Perception*. New York: Springer Verlag.

Oman, C. M. (2003). Human visual orientation in weightlessness. In L. Harris & M. Jenkin, Editors, *Levels of Perception*. New York, NY: Springer Verlag, 375-398.

Oman, C. M. (1991). Sensory conflict in motion sickness: an observer theory approach. In S. Ellis, Editor, *Pictorial communication in real and virtual environments*. London: Taylor and Francis, 362-367.

Oman, C. M. (1990). Motion sickness: A synthesis and evaluation of the sensory conflict theory. *Canadian Journal of Physiological Pharmacology, 68*, 294-303.

Oman, C.M. (1987). The role of static visual orientation cues in the etiology of space motion sickness. In *Symposium on vestibular organs and altered force environment.* Houston, TX: NASA-Space Biomedical Research Institute.

Oman, C.M. (1986). Symptoms and signs of space motion sickness on Spacelabs 1 and D1 (abstract). In *7th IAA Man in Space Symposium: Physiologic Adaptation of Man In Space.* Houston, TX.

Oman, C.M. (1982). A heuristic mathematical model for dynamics of sensory conflict and motion sickness. *Acta Otolaryngolica (Stockholm), 392 (Supplement)*, 1-44.

Oman, C.M., D. Benveniste, D.A. Buckland, H. Aoki, A. Liu, & A. Natapoff (2006). Spacecraft module visual verticals and training affect spatial task performance. *Habitation, 10*(3-4), 202-203.

Oman, C.M., & J.J. Bloomberg (2003). *Neurovestibular Adaptation Strategic Plan*. Houston, TX: National Space Biomedical Research Institute, 34.

Oman, C.M., B.K. Lichtenberg, & K.E. Money (1990). Space motion sickness monitoring experiment: Spacelab 1. In G.H. Crampton, Editor, *Motion and Space Sickness*. Boca Raton, FL: CRC Press, 217-246.

Oman, C.M., B.K. Lichtenberg, K.E. Money, & R.K. McCoy (1986). MIT/Canadian vestibular experiments on the Spacelab-1 mission: 4. Space motion sickness: symptoms, stimuli, and predictability. *Experimental Brain Research, 64*, 316-334.

Oman, C.M., E.N. Marcus, & I.S. Curthoys (1987). The influence of semicircular canal morphology on endolymph flow dynamics: An anatomically descriptive mathematical model. *Acta Otolaryngolica, 103*(1-2), 1-13.

Oman, C.M., & M.C. Newman (2009). Observer model for spatial orientation research and accident investigation. *Aviation, Space and Environmental Medicine, 80*(3), 208. (Also, paper 41 at 80th Annual Scientific Meeting of the Aerospace Medical Association, Los Angeles, CA.)

Parker, D.E., M.F. Reschke, A.P. Arrott, J.L. Homick, & B.K. Lichtenberg (1985). Otolith tilt-translation reinterpretation following prolonged weightlessness: Implications for preflight training. *Aviation, Space, and Environmental Medicine, 56*, 601-606.

Previc, F.H., & Ercoline, W.R. (Eds.) (2004). *Spatial disorientation in aviation* (ISBN 1-56347-654-1). Reston, VA: American Institute of Aeronautics and Astronautics, Inc.

Previc, F., & W. Ercoline (1999). The "outside in" attitude display concept revisited. *International Journal of Aviation Psychology, 9*, 377-401.

Prinzel, L.J.I., J.R. Comstock, Jr., L.J. Glaab, L.J. Kramer, J.J. Arthur, & J.S. Barry (2004). The efficacy of head-down and head-up synthetic vision display concepts for retro- and forward-fit of commercial aircraft. *International Journal of Aviation Psychology, 14*(1), 53-77.

Raphan, T., V. Matsuo, & B. Cohen (1979). Velocity storage in the vestibulo-ocular reflex arc (VOR). *Experimental Brain Research, 35*, 229-248.

Reason, J.T. (1978). Motion sickness adaptation: a neural mismatch model. *Journal of the Royal Society of Medicine, 71*, 819-829.

Repperger, D.W., & W.B. Albery (1992). *Spatial disorientation detector* (patent number 5,629,848). US Patent & Trademark Office (www.uspto.gov).

Reschke, M.F., J.J. Bloomberg, D.L. Harm, W.H. Paloski, and D.E. Parker (1994). Neurophysiological aspects: Sensory and sensory-motor function. In A.E. Nicogossian, Editor, *Space Physiology and Medicine*. Philadelphia, PA: Lea and Febiger.

Reschke, M.F., & D.E. Parker (1987). Effects of prolonged weightlessness on self-motion perception and eye movements evoked by roll and pitch. *Aviation, Space, and Environmental Medicine, 58*(9), A153-A157.

Robinson, D.A. (1981). The use of control systems analysis in the neurophysiology of eye movements. *Annual Review of Neuroscience, 4*, 463-503.

Roscoe, S. (2002). Ergavionics: Designing the job of flying an airplane. *International Journal of Aviation Psychology, 12*, 331-339.

Roscoe, S. (1968). Airborne displays for flight navigation. *Human Factors, 10*, 321-332.

Sarter, N. & B. Schroeder (2002). Supporting decision-making and action selection under time pressure and uncertainty: The case of inflight icing. *Human Factors, 43*(4), 573-583.

Schaub, H., and Junkins, J. L. (2009). *Analytical Mechanics of Space Systems*, 2nd ed. Reston, VA: American Institute of Aeronautics and Astronautics, Chap. 3.

Schreiber, B.T., C.D. Wickens, G.J. Renner, J. Alton, & J.C. Hickox (1998). Navigational checking using 3D maps: The influence of elevation angle, azimuth, and foreshortening. *Human Factors, 40*(2), 209-223.

Sebok, A., C. Wickens, AM Gacy (2011). Automation for human-robotic interaction: Modeling and predicting operator performance. *Proceedings of the International Symposium on Aviation Psychology*. Dayton, OH: Wright State University.

Selva, P, & Oman, CM (2011, April 8). Relationships between Observer and Kalman Filter Models for Human Dynamic Spatial Orientation (abstract, paper 3010). *8th Symposium on the Role of the Vestibular Organs in Space Exploration*, Houston, TX.

Selva, P., & C.M. Oman (2011, submitted). Relationships between Observer and Kalman filter models for human dynamic spatial orientation. *Journal of Vestibular Research*.

Shepard, R., & Cooper, L. (1982). *Mental images and their transformations*. Cambridge, MA: MIT press.

Shepard, R., & S. Hurwitz (1984). Upward direction, mental rotation and discrimination of left and right turns in maps. *Cognition, 18*, 161-193.

Shepard, R., & Metzler, D. (1971). Mental rotation of 3 dimensional objects. *Science, 171*, 701-703.

Small, R.L. (2011). *SDAT Version 3.0 User Manual*. Boulder, CO: Alion Science and Technology Corp.

Small, R.L., Fisher, A.M., Keller, J.W., & Wickens, C.D. (2005). A pilot spatial orientation aiding system (AIAA paper 2005-7431). In *Proceedings of the AIAA 5th ATIO and 16th Lighter-Than-Air Sys Tech. and Balloon Systems Conference*. Arlington, VA: AIAA.

Small, R.L., Fisher, A.M., Keller, J.W., & Wickens, C.D. (2005). A pilot spatial disorientation aiding system. In V. Ponomarenko (Ed.), *International Academy of Human's Problems in Aviation and Cosmonautics Bulletin, 1*(17), pp. 26-45 & *2*(18), pp. 28-38.

Small, R., Fisher, A., Keller, J. & Wickens, C. (2004). Multisensory integration for pilot spatial orientation. In *Proceedings of the WinterSim Conference 2004*. Washington, D.C.: ACM.

Small, R.L., J.W. Keller, A.M. Fisher, & C.D. Wickens (2005). *Method for spatial disorientation identification, countermeasures, and analysis*. US Patent Application. Boulder, CO: Micro Analysis and Design, Inc.

Small, Keller, & Wickens (2011). Analyzing spatial disorientation events. *Proceedings of the 82nd annual meeting of the Aerospace Medical Association* (AsMA). Anchorage, AK: AsMA.

Small, Keller, Wickens, Oman, & Jones (2011). *Modeling and mitigating spatial disorientation in low g environments: A progress report* {emphasis on Shuttle survey}. Presented at the Vestibular Symposium of the International Academy of Astronautics. Houston, TX: IAA.

Small, Keller, Wickens, Oman, & Jones (2010). *Modeling and mitigating spatial disorientation in low g environments: Year 3 report* (NASA-NSBRI NCC 9-58-511, SA01302). Boulder, CO: Alion Science & Technology Corp. Also online at: http://www.faa.gov/library/online_libraries/aerospace_medicine/sd/advancedtech/

Small, R.L., J.W. Keller, C.D. Wickens, C.M. Oman, M. Newman, L.R. Young, T.D. Jones, & M. Brehon (2010). *Modeling and mitigating spatial disorientation in low g environments: Year 2 report* (under NASA contract NCC 9-58-511, NSBRI project # SA01302, Alion project # 4658). Boulder, CO: Alion Science & Technology Corp. [Available from the first author at rsmall@alionscience.com.]

Small, R.L., J.W. Keller, C.D. Wickens, C. Socash, A.M. Ronan, & A.M. Fisher (2006). *Multisensory integration for pilot spatial orientation* (final report under AFRL contract FA8650-04-C-6457). Boulder, CO: Alion Science and Technology Corp., MA&D Operation.

Small, Oman, TD Jones (submitted). Space Shuttle Flight Crew Spatial Orientation Survey Results. *Aviation, Space and Environmental Medicine*

Small, R., Oster, A., Keller, J. & Wickens, C. (2004). Multisensory integration for pilot spatial orientation. In *Proceedings of the International Conference on Human-Computer Interaction in Aeronautics (HCI-Aero 2004)*. Toulouse: Eurisco International.

Small, RL, & Wickens, CD (2011, August 4). *Alion's Spatial Disorientation Analysis Tool*. Presentation and discussion at Boeing Commercial Airplanes, Everett, WA.

Small, R.L., C.D. Wickens, J.W. Keller, C.M. Oman, L.R. Young, T.D. Jones, M. Newman, & M. Brehon (2008). *Modeling and mitigating spatial disorientation in low g environments: Year 1 report* (under NASA contract NCC 9-58-511, NSBRI project # SA01302, Alion project # 4658). Boulder, CO: Alion Science & Technology Corp. [Available from the first author at rsmall@alionscience.com.]

Small, R.L., Wickens, C.D., Oster, A.M., Keller, J.W., & French, J.W. (2004). *Multisensory integration for pilot spatial orientation* (AFRL contract F33615-03-M-6360; AFRL Technical Report AFRL-HE-WP-TR-2004-0035). Boulder, CO: Micro Analysis & Design. Also online at: http://www.faa.gov/library/online_libraries/aerospace_medicine/sd/advancedtech/

Sundstrom, J.N. (2004). *Flight Conditions Leading to Class A Spatial Disorientation Mishaps in U.S. Air Force Fighter Operations: FY93-02* (Masters of Public Health Thesis). Washington, D.C.: The Department of Preventive Medicine and Biometrics of the Uniformed Services University of the Health Sciences.

Stelzer, E.M., & C.D. Wickens (2006). Pilots strategically compensate for display enlargements in surveillance and flight control tasks. *Human Factors, 48*(1), 166-181.

Taube, J., R. Stackman, J. Calton, & C.M. Oman (2004). Rat head direction cell responses in zero-gravity parabolic flight. *Journal of Neurophysiology, 92*, 2887-2997.

Tokumaru, O., Kaida, K., Ashida, H., Mizumoto, C., & J. Tatsuno (1998). Visual influence on the magnitude of somatogravic illusion evoked on advanced spatial disorientation demonstrator. *Aviation, Space and Environmental Medicine, 69*, 111-116.

Venkatesan, R.H. (2010). *Multisensory models for human spatial orientation including threshold effects* (SM thesis). Cambridge, MA: Department of Aeronautics and Astronautics, Massachusetts Institute of Technology.

Veronneau, S.J.H., & R.H. Evans (2004). Spatial disorientation mishap classification, data, and investigation. In F.H. Previc & W.R. Ercoline, Editors, *Spatial Disorientation in Aviation.* Reston, VA: AIAA, 197-241.

Vingerhoets, R.A.A., Medendorp, W.P., & J.A.M. Van Ginsbergen (2006). Time course and magnitude of illusory translation perception during off-vertical axis rotation. *Journal of Neurophysiology, 95*, 1571-1587.

Vingerhoets, R.A.A., J.A.M. Van Ginsbergen, & W.P. Medendorp (2007). Verticality perception during off-vertical axis rotation. *Journal of Neurophysiology, 97*, 3256-3268.

Wickens, C.D. (2003). Aviation displays. In P.S. Tsang & M.A. Vidulich, Editors, *Principles and practice of aviation psychology*. Mahwah, NJ: Lawrence Erlbaum, 147-199.

Wickens, C.D. (2002). *Spatial awareness biases* (Technical Report ARL-02-6/NASA-02-4). Savoy, IL: University of Illinois, Aviation Research Laboratory.

Wickens, C.D. (2000a). Human factors in vector map design: The importance of task-display dependence. *Journal of Navigation, 53*(1), 54-67.

Wickens, C.D. (2000b). The when and how of using 2-D and 3-D displays for operational tasks. In *Proceedings of the IEA2000/HFES2000 Congress*. Santa Monica, CA: Human Factors and Ergonomics Society.

Wickens, C.D. (1999). Frames of reference for navigation. In D. Gopher & A. Koriat, Editors, *Attention and performance, Vol. 17: Cognitive regulation for performance: Interaction of theory and application.* Cambridge, MA: Bradford Book, 113-144.

Wickens, C.D. & J. Hollands (2000). *Engineering Psychology and Human Performance*. Prentice Hall.

Wickens, C.D., B.L. Hooey, B.F. Gore, A. Sebok, & C.S. Koenicke (2009). Identifying black swans in NextGen: Predicting human performance in off-nominal conditions. *Human Factors, 51*(5), 638-651.

Wickens, Keller, Small (submitted). Development and validation of the frame of reference transformation (FORT) tool. *Human Factors*.

Wickens, Keller, Small (2011). A frame of reference transformation (FORT) model of 3D control-display relationships. *Proceedings of the 82nd annual meeting of the Aerospace Medical Association* (AsMA). Anchorage, AK: AsMA.

Wickens, C.D., J.W. Keller, & R.L. Small (2010). Left. No, right! Development of the frame of reference transformation tool (FORT). *Proceedings of the HFES Annual Meeting* in San Francisco. Santa Monica, CA: HFES.

Wickens, C.D., C.-C. Liang, T. Prevett, & O. Olmos (1996). Electronic maps for terminal area navigation: Effects of frame of reference and dimensionality. *International Journal of Aviation Psychology, 6*(3), 241-271.

Wickens, C.D., A. Sebok, J. Bzostek, K. Steelman-Allen, J. McCarley, & N. Sarter (2009). NT-SEEV: A model of attention capture and noticing on the flight deck. In *Proceedings of the 15th International Symposium on Aviation Psychology*. Dayton, OH: Wright State University.

Wickens, C.D., B.P. Self, T.S. Andre, T.J. Reynolds, R.L. Small (2007). Unusual attitude recoveries with a spatial disorientation icon. *International Journal of Aviation Psychology, 17*(2), 153-165.

Wickens, C.D., B.P. Self, R.L. Small, C.B. Williams, C.L. Burrows, B.R. Levinthal, & J.W. Keller (2006). Rotation rate and duration effects on the somatogyral illusion. *Aviation, Space and Environmental Medicine, 77*(12), 1244-51.

Wickens, C., R. Small, T. Andre, T. Bagnall, and C. Brenaman (2008). Multi-sensory enhancement of command displays for unusual attitude recovery. *International Journal of Aviation Psychology*, 18(3), 255-267.

Wickens, C.D., Vincow, M., & M. Yeh (2005). Design applications of visual spatial thinking: The importance of frame of reference. In A. Miyaki & P. Shah (Eds.), *Handbook of visual spatial thinking*. Oxford, UK: Oxford University Press.

Wiegmann D., T. Faaborg, A. Boquet, C. Detwiler et al. (2005). Human error and general aviation accidents: A comprehensive fine-grained analysis using HFACS (Report No. AM-05/24). Washington DC: Federal Aviation Administration.

Williams, H., S. Hutchinson, & C.D. Wickens (1996). A comparison of methods for promoting geographic knowledge in simulated aircraft navigation. *Human Factors, 38*(1), 50-64.

Worringham, C., & Beringer, D. (1989). Operator orientation and compatibility in visual-motor task performance. *Ergonomics, 32,* 387-399.

Young, L.R. (2003). Spatial orientation. In P.S. Tsang & M.A. Vidulich, Editors, *Principles and practice of aviation psychology*. Mahwah, NJ: Earlbaum, 69-144.

Young, L.R. (1984). Perception of the body in space: Mechanisms. In I.D. Smith, Editor, *Handbook of Physiology - The Nervous System III*. Bethesda, MD: American Physiological Society, 1023-1066.

Young, L.R., & J.L. Meiry (1968). A revised dynamic otolith model. *Aerospace Medicine, 39,* 606-608.

Young, L.R., Meiry, J.L., & Y.T. Li (1966, Jan 25-27). Control engineering approaches to human dynamic spatial orientation. *2nd Symposium on the Vestibular Organs in Space Exploration* (NASA SP-115). Sunnyvale, CA: NASA Ames Research Center, 217-227.

Young, L.R., & C.M. Oman (1969). Model for vestibular adaptation to horizontal rotation. *Aerospace Medicine 40*(10), 1076-80.

Young, L.R., C.M. Oman, D.G. Watt, K.E. Money, & B.K. Lichtenberg (1984). Spatial orientation in weightlessness and readaptation to earth's gravity. *Science, 225*(4658), 205-8.

Young, L.R., C.M. Oman, D.G. Watt, K.E. Money, B.K. Lichtenberg, R.V. Kenyon, & A.P. Arrott (1986). MIT/Canadian vestibular experiments on the Spacelab-1 mission: 1. Sensory adaptation to weightlessness and readaptation to one-g: an overview. *Experimental Brain Research, 64*(2), 291-8.

Zhang, L., & Cao, C. (2010). The effect of image orientation on a dynamic laparoscopic task. *Proceedings of the 54th annual meeting Human Factors Society*. Santa Monica, CA: HFES.

Appendix A. SDAT's New Otolith Model

This appendix explains the derivation of the algorithms for calculating the GIF vector based upon vehicle attitude and motions. It also includes source code. Its author is Brian Curtis, an aeronautical engineering master's degree student at the University of Colorado; he was a summer intern at Alion in 2011.

Nomenclature

bx	=	inertial acceleration of aircraft in the body frame *x* direction (g's)
by	=	inertial acceleration of aircraft in the body frame *y* direction (g's)
bz	=	inertial acceleration of aircraft in the body frame *z* direction (g's)
gx	=	linear acceleration of aircraft in the body frame *x* direction (g's)
gy	=	linear acceleration of aircraft in the body frame *y* direction (g's)
gz	=	linear acceleration of aircraft in the body frame *z* direction (g's)
Gz	=	environmental gravity (g's)
r	=	FDR accelerations to pilot position vector (feet)
α	=	angular acceleration of body frame (deg/s^2)
ω	=	angular velocity of body frame (deg/s)
ψ	=	yaw (degrees)
θ	=	pitch (degrees)
φ	=	roll (degrees)

Introduction

The strain on a pilot's otolith organs, combined with the tactile perception of up or down, provides neural input to the vestibular system. This input is directly dependent on the inertial accelerations that the pilot experiences. For analysis, the inertial accelerations are combined to form a gravito-inertial force (GIF) vector. This vector yields the perceived "down" for the pilot, and thus the pilot's perceived vehicle orientation.

Depending upon the completeness of the data provided, several steps of calculations may need to be taken in order to derive the most accurate inertial accelerations of the pilot. FDR accelerations are ideal and require just one transformation in order to obtain these inertial accelerations. However, many data sets do not include a complete set of FDR accelerations (in the X, Y, Z axes), and so the missing data must be derived from the known dynamics of the aircraft. The following calculations step through a complete derivation of the required accelerations, assuming a minimal amount of data is provided. Once the accelerations are calculated, the pilot's perceived otolith pitch and roll attitude is resolved using the GIF in the CalculateBlindPerceivedPitch/Roll function.

Airspeed, Lateral Speed, and Vertical Speed Derived Accelerations

1) Fixed-wing Aircraft

For fixed-wing aircraft, a no-slip condition is implemented. This condition assumes that the aircraft moves in the direction it is pointed. Therefore, the only speed that becomes relevant in the acceleration calculations is airspeed. The linear acceleration *gx* is derived directly from airspeed. The accelerations *gy* and *gz* are derived from the centripetal accelerations of an aircraft in a turn, as presented in Section B.

2) Rotary-wing and Vertical Lander Vehicles

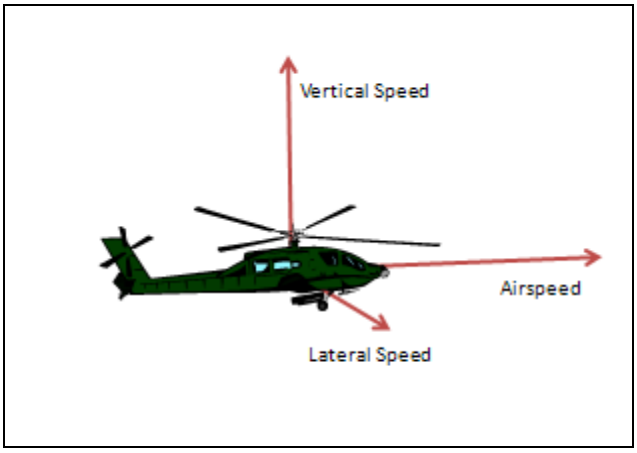

Rotary-wing and Vertical Lander Vehicles are different from fixed-wing aircraft in that they do not always translate in the direction that they are pointed. A significant amount of slip usually occurs for these vehicles during normal flight operations. Therefore, the linear accelerations, *gx* and *gy*, are derived from airspeed and lateral speed (assuming that airspeed and lateral speed are both given in the body-fixed frame). The *gz* acceleration is derived from Vertical Speed, which is given in the world coordinate frame. The Direction Cosine Matrix (DCM) for 3-2-1 Euler angles is used to calculate the component of the vertical acceleration (derived from vertical speed) that lies in the body-fixed *z* direction, as illustrated in the following figure.

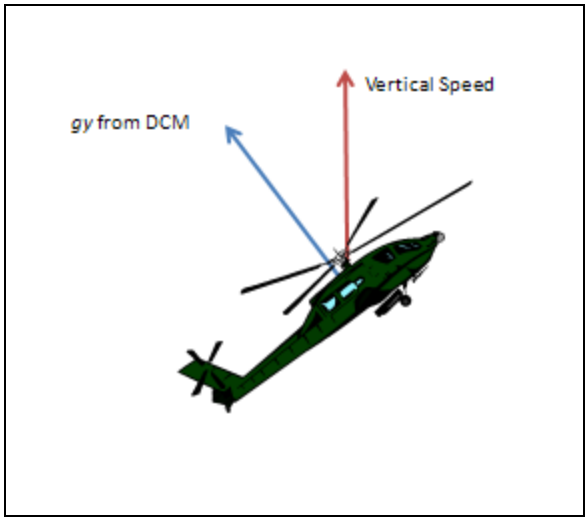

One situation of note may arise when *gy* needs to be calculated and no lateral speed information is provided. Some information for *gy* can still be gleaned from vertical speed, given certain orientations of the aircraft. Information for *gy* is lost, however, if the vehicle is in level

flight. Again, the DCM is used to find the component of global vertical acceleration in the body-fixed *y* direction for this scenario (e.g., an aircraft rolled 90 degrees and falling). See Appendix A-1, below, for the DCM rotation formulae.

Caveat: If large jumps are present in the vertical speed data, combined with small time steps, erroneous derived accelerations may result. For example, a vertical speed jump from -720fpm to -1440fpm in one time step is equivalent to a jump of -12fps in the same time step. If that time step is very small, 0.125 seconds, then the jump is equivalent to about -3g. This erroneous jump would lead to a false perceived inversion for level flight.

General Centripetal Acceleration

These calculations are used to determine the *gy* and *gz* accelerations for fixed-wing aircraft. The instantaneous centripetal accelerations in the *y* and *z* directions (for an aircraft in a turn or loop) are calculated using airspeed and the angular velocity of the body frame about the *z* and *y* axes, respectively. An example is illustrated below for an aircraft in a pure yaw turn (angular velocity about the *z* axis). See Appendix A-2 for calculations and code.

No calculations have been implemented for an aircraft that is only rolling. For the case of rolling, the magnitude of the centripetal acceleration is dependent upon lateral speed. Lateral speed information is usually non-existent for fixed-wing aircraft, and, as such, this calculation was not implemented.

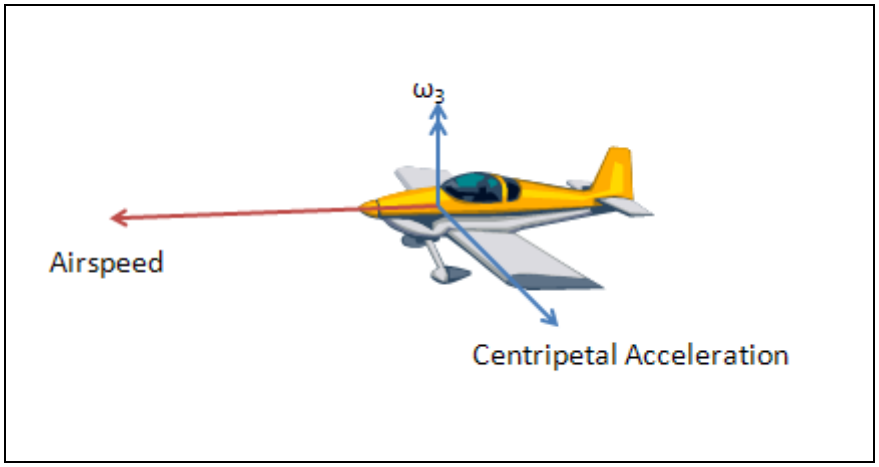

Caveat: These calculations assume that no slipping occurs during the aircraft maneuver. This assumption should only be used for fixed-wing aircraft and would not hold true for VLVs. An adaptation of these calculations for rotary-wing vehicles, which may or may not have significant slip, has not yet been devised. The current implementation assumes that rotary-wing and space vehicles only slip, and that fixed-wing aircraft do not slip at all.

Calculate Body Frame Forces

The purpose of this function is to determine the inertial forces acting on the accelerometers of the FDR (*bx*, *by*, and *bz*). First, the function uses the known orientation of the aircraft to rotate *Gz* into the body frame. This rotation is accomplished using the DCM for 3-2-1 Euler angles. For example, an aircraft pitched up at 45 degrees would have the components of *Gz* mapped into the *bx* and *bz* directions as shown in the figure below. Then, the accelerations of the aircraft (*gx*, *gy*, and *gz*) are combined with the accelerations due to *Gz* in order to yield the inertial forces for the FDR. This function is presented in Appendix A-3.

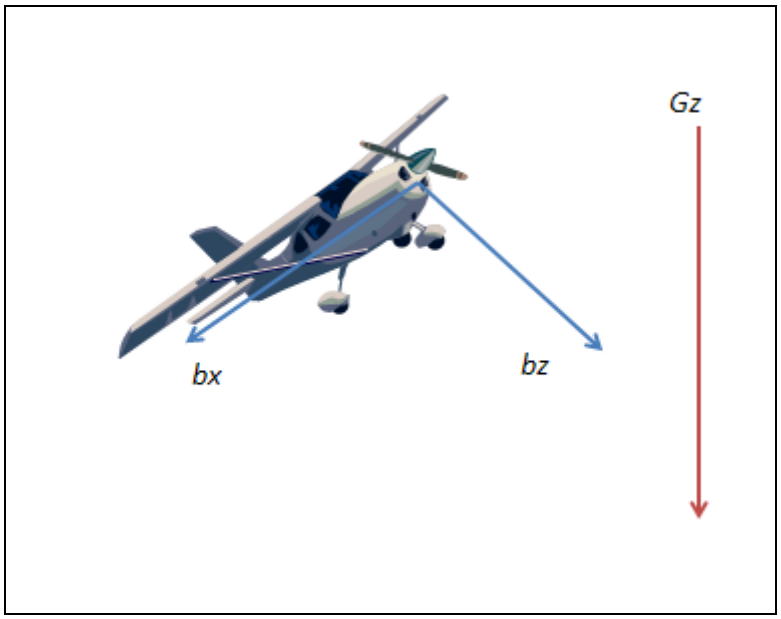

Previously, SDAT calculated otolith perceived pitch and roll separately. However, pitch orientation affects the *by* vector, for example, and therefore also affects one's perception of roll. This function now allows for perceived pitch and roll to be calculated simultaneously for any arbitrary pitch and roll combination.

Calculate Moment Arm Forces

This function transforms the inertial forces (*bx, by,* and *bz*) from the FDR location to the location of the pilot, given the moment arm *r*. Two additional forces arise from this moment arm calculation. The first is the centrifugal force given by the $-\omega\times(\omega\times r)$ term. The second is the tangential force given by the angular acceleration of the aircraft. See Appendix A-4 for the derivation of these forces.

Calculate Blind Perceived Pitch and Roll

This function calculates the perceived pitch and roll due to otolith perception and tactile cues assuming a non-visual environment. The function is labeled "blind" for this reason and only uses the body-frame inertial forces and thresholds as arguments. No aircraft orientation data is passed to this function. For the same forces, the same stresses on the otoliths result, and the same angles are returned regardless of actual aircraft orientation.

By utilizing an arctangent function (atan2) with a built-in quadrant check, this function allows for large rotation angles to be perceived. Furthermore, using the GIF vector to resolve otolith perception with tactile cues, inversions can be sensed even if there is no force on the otoliths (e.g., 180-degree roll or inverted). This function is therefore robust when handling large rotations or purely tactile cues.

The GIF alone does not resolve otolith perception correctly for hypogravity or hypergravity. If the GIF were used to resolve the perception angle in these scenarios, no difference would result for any orientation in hypogravity or hypergravity. However, it is known that less of an angle will be perceived in hypogravity and more of an angle in hypergravity, due to differences in strain on the otolith hairs (Previc & Ercoline, 2004). Therefore, three separate scenarios were created to accurately capture these effects.

1) The Earth-analog scenario uses the GIF to resolve perceived angles. This is the default scenario. An example is an aircraft accelerating at 2g for takeoff.

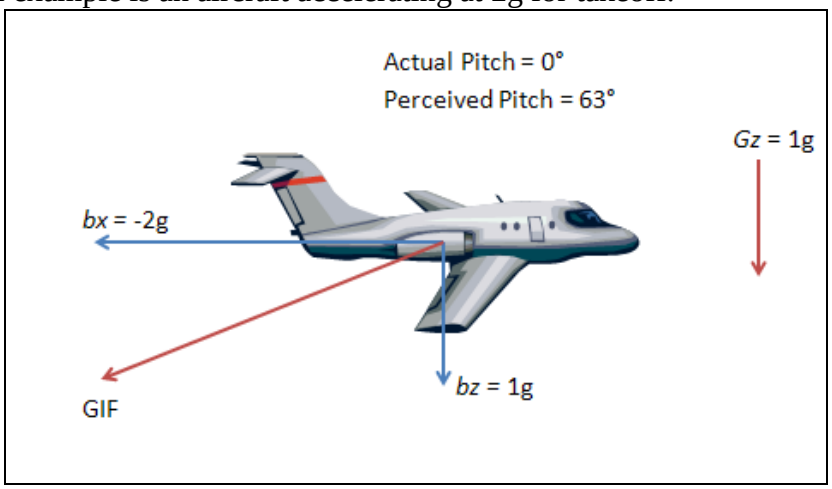

2) The hypogravity scenario occurs when the total magnitude of all forces acting on the body is less than 1g. The numerator of the arctangent function is scaled in this scenario by the total magnitude of the forces acting on the body. Less of an angle is perceived in this hypogravity environment, and this angle is dependent upon the magnitude of the hypogravity environment itself.

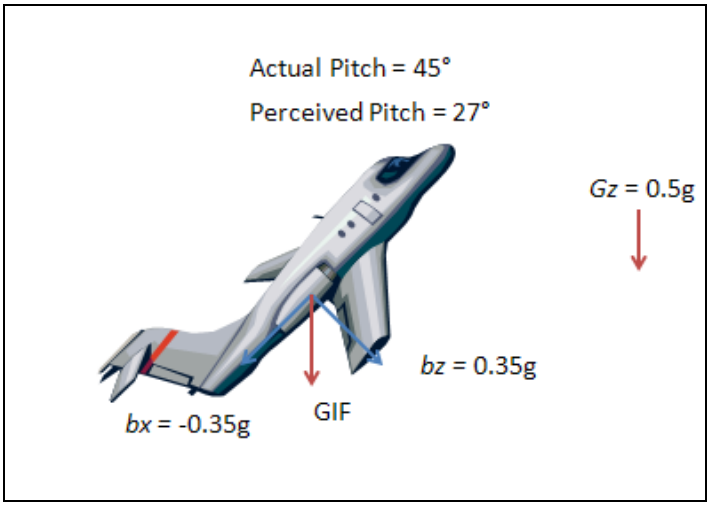

3) The hypergravity scenario occurs when the magnitude of the down vector (*bz* combined with *by*) is greater than 1g. In the case of pitch for example, if the denominator of the

arctangent function is still set to the magnitude of the down vector, then the GIF resolves exactly the same angle. However, we need the GIF to resolve a greater angle in the hypergravity environment. Therefore, the denominator of the arctangent function is set to be Earth gravity so that the higher *bx* in this scenario will yield a larger angle, scaled by the *bx* magnitude. For Roll, the angle is scaled by *by*.

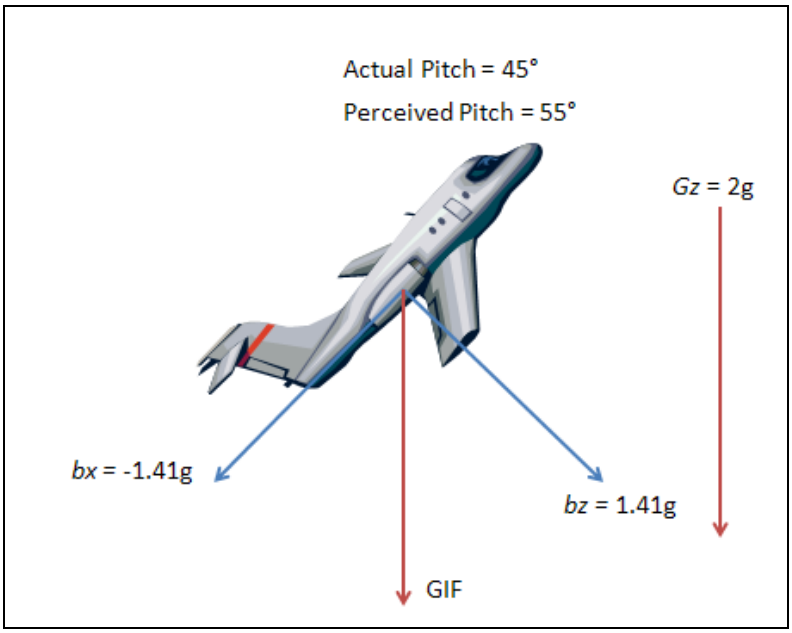

Although this function is divided into three different scenarios, the perceived angles are continuous when transitioning among all three scenarios. This result is consistent with experimental data, as indicated in the G-Excess effect, Chapter 6, Previc and Ercoline (2004). The function is presented in Appendix A-5.

Appendix A-1

(3-2-1) Direction Cosine Matrix

The (3-2-1) Direction Cosine Matrix is given below. The numbers (3-2-1) correspond to a rotation first about the 3rd axis, then the 2nd, then the 1st. The (3-2-1) rotation corresponds to Euler Angles ψ (yaw), θ (pitch), and φ (roll). This matrix is used to transform vectors from the world coordinate frame to the local/vehicle coordinate frame.

$$[C] = \begin{pmatrix} \cos\theta\cos\psi & \cos\theta\sin\psi & -\sin\theta \\ \sin\phi\sin\theta\cos\psi - \cos\phi\sin\psi & \sin\phi\sin\theta\sin\psi + \cos\phi\cos\psi & \sin\phi\cos\theta \\ \cos\phi\sin\theta\cos\psi + \sin\phi\sin\psi & \cos\phi\sin\theta\sin\psi - \sin\phi\cos\psi & \cos\phi\cos\theta \end{pmatrix}$$

The rotation of the vertical acceleration vector from the world frame to the body frame is accomplished through the matrix multiplication below.

$$\begin{pmatrix} gx \\ gy \\ gz \end{pmatrix} = [C] \begin{pmatrix} 0 \\ 0 \\ VerticalAcceleration \end{pmatrix}$$

Appendix A-2
General Centripetal Acceleration

The angular velocity is first rotated into the body frame. This rotation is described in detail in Appendix A-4. Currently ω_1, for the case of roll, is not used in the general centripetal acceleration calculation. The calculation for ω_1 is provided for completeness of the angular velocity vector.

```
//double omega1 = psidot * (-Math.Sin(theta * (Math.PI / 180))) + phidot;
double omega2 = psidot * (Math.Sin(phi * (Math.PI / 180)) * Math.Cos(theta * (Math.PI /
180))) + thetadot*(Math.Cos(phi* (Math.PI / 180)));
double omega3 = psidot * (Math.Cos(phi * (Math.PI / 180)) * Math.Cos(theta * (Math.PI /
180))) - thetadot * Math.Sin(phi * (Math.PI / 180));
```

The centripetal accelerations are combined with the previous calculated accelerations. For calculation of the *gz* centripetal acceleration, the angular velocity ω_2 is used. The centripetal acceleration for the *z* component is then given by ω_2 multiplied by airspeed.

```
if (aircraft.FixedWing)
{
    gz -= ((aircraft.Airspeed * 0.5144444) * (omega2 * (Math.PI / 180))) / 9.80665;
}
```

For combination with the *gy* acceleration, the angular velocity ω_3 is used. The centripetal acceleration for the *y* component is then given by ω_3 multiplied by airspeed.

```
if (aircraft.FixedWing)
{
    gy += ((aircraft.Airspeed * 0.5144444) * (omega3 * (Math.PI / 180))) / 9.80665;
}
```

Appendix A-3
Calculate Body Frame Forces

```
protected Vector3 CalculateBodyFrameForces(double Gz, double gx, double gy, double gz, double psi, double
theta, double phi)
        {
            //Function CalculateBodyFrameForces
            //Return Value:
            //Body Frame Inertial Forces (b vector)
            //Parameters:
            //Gz: Acceleration in g's in global axis (Gravity)
            //gx,gy,gz: Linear acceleration of A/C (not FDR inertial)
            ////3-2-1 (yaw, pitch, then roll) euler angles (in degrees)
            //psi: Yaw of aircraft in degrees
            //theta: Pitch of aircraft in degrees
```

```
        //phi: Roll of aircraft in degrees

        Vector3 ret = new Vector3();

        double torad = Math.PI / 180; //for conversion from degrees to radians

        //convert to radians
        psi = psi * torad;
        theta = theta * torad;
        phi = phi * torad;

        //create Direction Cosine Matrix (DCM)
        double[,] C = new double[3, 3];
        C[0, 0] = Math.Cos(theta) * Math.Cos(psi);
        C[0, 1] = Math.Cos(theta) * Math.Sin(psi);
        C[0, 2] = -Math.Sin(theta);
        C[1, 0] = Math.Sin(phi) * Math.Sin(theta) * Math.Cos(psi) - Math.Cos(phi) * Math.Sin(psi);
        C[1, 1] = Math.Sin(phi) * Math.Sin(theta) * Math.Sin(psi) + Math.Cos(phi) * Math.Cos(psi);
        C[1, 2] = Math.Sin(phi) * Math.Cos(theta);
        C[2, 0] = Math.Cos(phi) * Math.Sin(theta) * Math.Cos(psi) + Math.Sin(phi) * Math.Sin(psi);
        C[2, 1] = Math.Cos(phi) * Math.Sin(theta) * Math.Sin(psi) - Math.Sin(phi) * Math.Cos(psi);
        C[2, 2] = Math.Cos(phi) * Math.Cos(theta);

        /////*Rotate global acceleration to local using DCM
        double px, py, pz; //acceleration due to orientation of A/C
        px = C[0, 2] * Gz;
        py = C[1, 2] * Gz;
        pz = C[2, 2] * Gz;

        //////Find FDR inertial acceleration
        double bx, by, bz; //declare acc. that FDR feels (inertial acc.)

        //inertial acceleration due to linear acceleration(g) plus orientation of A/C (p)
        bx = -gx + px;
        by = -gy + py;
        bz = -gz + pz;

        System.Diagnostics.Debug.WriteLine("The body-fixed g load vector is:\n");
        System.Diagnostics.Debug.WriteLine(string.Format("bx = {0}\n", bx));
        System.Diagnostics.Debug.WriteLine(string.Format("by = {0}\n", by));
        System.Diagnostics.Debug.WriteLine(string.Format("bz = {0}\n", bz));

        ret[0] = bx;
        ret[1] = by;
        ret[2] = bz;

        return ret;
    }
```

Appendix A-4
Moment Arm Acceleration Derivation

This derivation follows that outlined in Schaub and Junkins (2009).

The angular velocity vector ω, given as,

$$\vec{\omega} = \omega_1 \hat{b}_1 + \omega_2 \hat{b}_2 + \omega_3 \hat{b}_3$$

must first be found in terms of the Euler Angle rates shown below, where *n* is the world coordinate frame and *b* is the body frame. The term *b'* refers to the intermediate axis before the third rotation.

$$\vec{\omega} = \dot{\psi}\hat{n}_3 + \dot{\theta}\hat{b}'_2 + \dot{\phi}\hat{b}_3$$

The world axis, via the DCM, and intermediate coordinate axis can be expressed, respectively, as

$$\hat{n}_3 = -\sin\theta\hat{b}_1 + \sin\phi\cos\theta\hat{b}_2 + \cos\phi\cos\theta\hat{b}_3$$

$$\hat{b}_2' = \cos\phi\hat{b}_2 - \sin\phi\hat{b}_3$$

Substituting, the angular velocity is now given as

$$\vec{\omega} = \begin{pmatrix} -\sin\theta & 0 & 1 \\ \sin\phi\cos\theta & \cos\phi & 0 \\ \cos\phi\cos\theta & -\sin\phi & 0 \end{pmatrix} \begin{pmatrix} \dot{\psi} \\ \dot{\theta} \\ \dot{\phi} \end{pmatrix}$$

An identical transformation is used for the angular acceleration α.

$$\vec{\alpha} = \begin{pmatrix} -\sin\theta & 0 & 1 \\ \sin\phi\cos\theta & \cos\phi & 0 \\ \cos\phi\cos\theta & -\sin\phi & 0 \end{pmatrix} \begin{pmatrix} \ddot{\psi} \\ \ddot{\theta} \\ \ddot{\phi} \end{pmatrix}$$

The moment-arm *r* is written as

$$\vec{r} = r_1\hat{i} + r_2\hat{j} + r_3\hat{k}$$

and its derivative taken, where the time derivative of *r* in the body frame is zero (*r* does not change length), and the component due to the rotation is shown below.

$$\dot{\vec{r}} = \vec{\omega} \times \vec{r}$$

Taking the second derivative yields the following steps

$$\ddot{\vec{r}} = \frac{d\dot{\vec{r}}}{dt} + \vec{\omega} \times \dot{\vec{r}}$$

$$\ddot{\vec{r}} = \frac{d\vec{\omega}}{dt} \times \vec{r} + \vec{\omega} \times (\vec{\omega} \times \dot{\vec{r}})$$

$$\ddot{\vec{r}} = \vec{\alpha} \times \vec{r} + \vec{\omega} \times (\vec{\omega} \times \dot{\vec{r}})$$

The cross products are carried out and codified as shown in the function below:

```
protected Vector3 CalculateMomentArmForces(double phi, double theta, double psi,
            double phidot, double thetadot, double psidot,
            double phidoubledot, double thetadoubledot, double psidoubledot,
            double rx, double ry, double rz)
        {
```

```
    //Function CalculateMomentArmForces
    //Return Value: Moment Arm Inertial Acceleration Vector
    //Parameters:
    //   phidot: Roll Rate in deg/s
    //   thetadot: Pitch Rate in deg/s
    //   psidot: Yaw Rate in deg/s
    //   phidoubledot: Roll Acceleration in deg/s^2
    //   thetadoubledot: Pitch Acceleration in deg/s^2
    //   psidoubledot: Yaw Acceleration in deg/s^2
    //   rx: offset from cg to pilot in x direction in ft
    //   ry: offset from cg to pilot in y direction in ft
    //   rz: offset from cg to pilot in z direction in ft

    #region declare accelerations
    double ax;
    double ay;
    double az;
    #endregion

    #region Convert to radians
    phidot = phidot * StateTableBase.convertDegreeToRadian;
    thetadot = thetadot * StateTableBase.convertDegreeToRadian;
    psidot = psidot * StateTableBase.convertDegreeToRadian;
    phidoubledot = phidoubledot * StateTableBase.convertDegreeToRadian;
    thetadoubledot = thetadoubledot * StateTableBase.convertDegreeToRadian;
    psidoubledot = psidoubledot * StateTableBase.convertDegreeToRadian;
    #endregion

    //Transform from Global to Local coordinate frame
    double omega1 = psidot * (-Math.Sin(theta * (Math.PI / 180))) + phidot;
    double omega2 = psidot * (Math.Sin(phi * (Math.PI / 180)) * Math.Cos(theta * (Math.PI /
    180))) + thetadot * (Math.Cos(phi * (Math.PI / 180)));
    double omega3 = psidot * (Math.Cos(phi * (Math.PI / 180)) * Math.Cos(theta * (Math.PI / 180)))
    - thetadot * Math.Sin(phi * (Math.PI / 180));

    double alpha1 = psidoubledot * (-Math.Sin(theta * (Math.PI / 180))) + phidoubledot;
    double alpha2 = psidoubledot * (Math.Sin(phi * (Math.PI / 180)) * Math.Cos(theta * (Math.PI /
    180))) + thetadoubledot * (Math.Cos(phi * (Math.PI / 180)));
    double alpha3 = psidoubledot * (Math.Cos(phi * (Math.PI / 180)) * Math.Cos(theta * (Math.PI /
    180))) - thetadoubledot * Math.Sin(phi * (Math.PI / 180));

    //Calculate radial and tangential accelerations
    ax = alpha2 * rz - alpha3 * ry - (omega2 * omega2 + omega3 * omega3) * rx + omega2 * omega1 *
    ry + omega3 * omega1 * rz;
    ay = alpha3 * rx - alpha1 * rz - (omega3 * omega3 + omega1 * omega1) * ry + omega3 * omega2 *
    rz + omega1 * omega2 * rz;
    az = alpha1 * ry - alpha2 * rx - (omega1 * omega1 + omega2 * omega2) * rz + omega1 * omega3 *
    rx + omega2 * omega3 * ry;

    //Convert accelerations from ft/s^2 to g's and make forces inertial(negative sign).
    ax = -ax * 0.03108095;
    ay = -ay * 0.03108095;
    az = -az * 0.03108095;

    //Save as a vector
    Vector3 MAAVector = new Vector3(ax, ay, az);
    return MAAVector;
}
```

These accelerations are then added to the FDR accelerations, completing the acceleration transformation from the FDR to the pilot.

Appendix A-5
Calculate Blind Perceived Pitch and Roll

```
protected double CalculateBlindPerceivedRoll(double bx, double by, double bz, double byThreshold)
        {
            //Function CalculateBlindPerceivedRoll
            //Return Value:
            //Perceived roll in degrees
            //Parameters:
            //bx,by,bz: Body Frame Inertial Forces
            //byThreshold: Otolith bx direction threshold

            double torad = Math.PI / 180; //for conversion from degrees to radians

            //Check threshold
            double absby = Math.Abs(by);
            if (absby < byThreshold)
            {
                by = 0;
            }


            double magdown = Math.Sqrt((bz * bz) + (bx * bx));  //find magnitude of bz and by
            double totalmag = Math.Sqrt((bz * bz) + (by * by) + (bx * bx));

            //find signs of bz and bx
            int signbz = 1;
            if (bz < 0)
            {
                signbz = 1;
            }

            int signbx = 1;

            //Find perceived pitch in the body frame
            double RollInBody = 0;

            if (magdown <= 1)
            {
                RollInBody = Math.Atan2(by, Math.Sqrt((bz * bz) + (bx * bx)) * signbx * signbz);
            }

            if (totalmag < 1)
            {
                RollInBody = Math.Atan2(by * totalmag, Math.Sqrt((bz * bz) + (bx * bx)) * signbx *
                 signbz);
            }

            if (magdown > 1)
            {
                RollInBody = Math.Atan2(by, signbx * signbz);
            }

            RollInBody = RollInBody / torad;

            System.Diagnostics.Debug.WriteLine(string.Format("The perceived body roll angle is: {0}\n",
            RollInBody));

            return RollInBody;

        }


protected double CalculateBlindPerceivedPitch(double bx, double by, double bz, double bxThreshold)
        {
            //Function CalculateBlindPerceivedPitch
            //Return Value:
            //Perceived pitch in degrees
```

```
        //Parameters:
        //bx,by,bz: Body Frame Inertial Forces
        //bxThreshold: Otolith bx direction threshold

        double torad = Math.PI / 180; //for conversion from degrees to radians
        double absbx = Math.Abs(bx);
        if (absbx < bxThreshold)
        {
            bx = 0;
        }


        double magdown = Math.Sqrt((bz * bz) + (by * by));  //find magnitude of bz and by down
        double totalmag = Math.Sqrt((bz * bz) + (by * by) + (bx * bx));

        //find signs of bz and by
        int signbz = 1;
        if (bz < 0)
        {
            signbz = -1;
        }
        int signby = 1;

        //Find perceived pitch in the body frame
        double PitchInBody = 0;

        if (magdown <= 1)
        {
            PitchInBody = Math.Atan2(-bx, Math.Sqrt((bz * bz) + (by * by)) * signbz * signby);
        }
        if (totalmag < 1)
        {
            PitchInBody = Math.Atan2(-bx * totalmag, Math.Sqrt((bz * bz) + (by * by)) * signbz *
         signby);
        }
        if (magdown > 1)
        {
            PitchInBody = Math.Atan2(-bx, signbz * signby);
        }
        PitchInBody = PitchInBody / torad;

        System.Diagnostics.Debug.WriteLine(string.Format("The perceived body pitch angle is: {0}\n",
        PitchInBody));

        return PitchInBody;
    }
```

Appendix A-6
Get Quaternion

The algorithm for the following function is found in Schaub and Junkins (2009). Currently, this function is not being used in SDAT. It was coded for integration with Observer, in the case that SDAT needed to compute the quaternion.

```
protected double[] GetQuaternion(double psi, double theta, double phi)
        {
            double torad = Math.PI / 180; //for conversion from degrees to radians
            //convert to radians
            psi = psi * torad;
            theta = theta * torad;
            phi = phi * torad;
            //create Direction Cosine Matrix (DCM)
            double[,] C = new double[3, 3];
            C[0, 0] = Math.Cos(theta) * Math.Cos(psi);
            C[0, 1] = Math.Cos(theta) * Math.Sin(psi);
            C[0, 2] = -Math.Sin(theta);
            C[1, 0] = Math.Sin(phi) * Math.Sin(theta) * Math.Cos(psi) - Math.Cos(phi) * Math.Sin(psi);
            C[1, 1] = Math.Sin(phi) * Math.Sin(theta) * Math.Sin(psi) + Math.Cos(phi) * Math.Cos(psi);
            C[1, 2] = Math.Sin(phi) * Math.Cos(theta);
            C[2, 0] = Math.Cos(phi) * Math.Sin(theta) * Math.Cos(psi) + Math.Sin(phi) * Math.Sin(psi);
            C[2, 1] = Math.Cos(phi) * Math.Sin(theta) * Math.Sin(psi) - Math.Sin(phi) * Math.Cos(psi);
            C[2, 2] = Math.Cos(phi) * Math.Cos(theta);
            //find quaternion based on trace function
            double trace = C[0, 0] + C[1, 1] + C[2, 2];
            double[] Bsq = new double[4];
            Bsq[0] = .25 * (1 + trace);
            Bsq[1] = .25 * (1 + 2 * C[0, 0] - trace);
            Bsq[2] = .25 * (1 + 2 * C[1, 1] - trace);
            Bsq[3] = .25 * (1 + 2 * C[2, 2] - trace);

            int flag = 0;
            if (Bsq[0] > Bsq[1] && Bsq[0] > Bsq[2] && Bsq[0] > Bsq[3])
            {
                flag = 0;
            }
            if (Bsq[1] > Bsq[0] && Bsq[1] > Bsq[2] && Bsq[1] > Bsq[3])
            {
                flag = 1;
            }
            if (Bsq[2] > Bsq[1] && Bsq[2] > Bsq[0] && Bsq[2] > Bsq[3])
            {
                flag = 2;
            }
            if (Bsq[3] > Bsq[1] && Bsq[3] > Bsq[2] && Bsq[3] > Bsq[0])
            {
                flag = 3;
            }
            double B0 = 0, B1 = 0, B2 = 0, B3 = 0;
            if (flag == 0)
            {
                B0 = Math.Sqrt(Bsq[0]);
                B1 = (C[1, 2] - C[2, 1]) / (4 * B0);
                B2 = (C[2, 0] - C[0, 2]) / (4 * B0);
                B3 = (C[0, 1] - C[1, 0]) / (4 * B0);
            }
            if (flag == 1)
            {
                B1 = Math.Sqrt(Bsq[1]);
                B0 = (C[1, 2] - C[2, 1]) / (4 * B1);
                B2 = (C[0, 1] + C[1, 0]) / (4 * B1);
                B3 = (C[2, 0] + C[0, 2]) / (4 * B1);
            }
            if (flag == 2)
```

```
        {
            B2 = Math.Sqrt(Bsq[2]);
            B1 = (C[0, 1] + C[1, 0]) / (4 * B2);
            B0 = (C[2, 0] - C[0, 2]) / (4 * B2);
            B3 = (C[1, 2] + C[2, 1]) / (4 * B2);
        }
        if (flag == 3)
        {
            B3 = Math.Sqrt(Bsq[3]);
            B1 = (C[2, 0] + C[0, 2]) / (4 * B3);
            B0 = (C[0, 1] - C[1, 0]) / (4 * B3);
            B2 = (C[1, 2] + C[2, 1]) / (4 * B3);
        }

        //print results
        System.Diagnostics.Debug.WriteLine(string.Format("The quaternion vector is:  {0}, {1}, {2},
        {3}", B0, B1, B2, B3));

        double[] B = new double[4] { B0, B1, B2, B3 };

        return B;
    }
```

Appendix B. N-SEEV Pilot Attention Model

We use N-SEEV to modify the compensatory action initiation process. Once the first compensatory action has been initiated, N-SEEV provides a time-to-notice value for the channel of the compensatory action. This update includes tactile and auditory channels and uses look-up tables for the time-to-notice values. The user may select the individual settings described in the table below. The settings will be used to select a single value from one of the tables.

	Values	Default	Notes
Visual			
Workload	L, M, H	M	
Salience	L, M, H (0, .5, 1)	M	Text or small change to existing display; New visual onset; Flashing
Expectancy	L, M (.1, .5)	L	SD Unaware – Type 1; SD Aware – Type 2
Effort	L, M	L	Adjacent display; 20deg display separation
Value	NA		No difference to the type of information presented
Auditory			
Workload	L, M, H	M	
Salience	L, M, H	M	Very soft single tone; single moderate tone; repeating tone
Expectancy	L, M (.1, .5)	L	SD Unaware – Type 1; SD Aware – Type 2
Effort	NA		
Value	(2 levels)		Cue; Command (two different levels of information)
Tactile			
Workload	L, M, H	M	
Salience	L, M, H	M	Very soft single buzz; single moderate buzz; repeating buzzes
Expectancy	L, M (.1, .5)	L	SD Unaware – Type 1; SD Aware – Type 2
Effort	NA		
Value	(2 levels)		Cue; Command (two different levels of information)

With this information, the N-SEEV model predicts the probability of noticing a cockpit alert and the potential delay in noticing.

Interface

- Select N-SEEV values for Visual, Auditory & Tactile
- Make selections for both Level 1 and Level 2
- Make selections for cut-off times for both Level 1 & Level 2

Level 1

- SD Icon – Use Visual settings 1
- Cut-off time 1

Level 2

- SD Icon – Use Visual settings 2
  - May not be a Visual onset (Salience M) if the SD Icon was already running from Level 1
    - If the SD Icon was already running then the Visual Salience = L
  - If Level 2 was initiated at the same time as Level 1
    - then the SD Icon would be an onset; Visual Salience = M
- Tactile Cue – Use Tactile settings 2
- Auditory Cue – Use Auditory settings 2

- Cut-off time 2
- Timing choice options (waiting for Chris to determine)
  - Average
  - Shortest of the three
  - Some other mechanism

Visual				Auditory & Tactile			
Expectancy = Medium (SD Aware)							
Effort = Low (Adjacent AOIs)				Value = Medium (Alarm)			
	Salience				Salience		
Workload	Low	Med	High	Workload	Low	Med	High
Low	1.27	0.8	0.57	Low	0.59	0.37	0.26
Med	1.35	0.9	0.57	Med	0.63	0.42	0.26
High	1.48	0.91	0.61	High	0.69	0.42	0.28
Effort = Medium (Separated AOIs)				Value = Low (Notification)			
	Salience				Salience		
Workload	Low	Med	High	Workload	Low	Med	High
Low	1.6	0.86	0.61	Low	1.02	0.64	0.46
Med	2.1	0.96	0.66	Med	1.08	0.72	0.46
High	3.07	1.04	0.68	High	1.18	0.73	0.49
Expectancy = Low (SD Unaware)							
Effort = Low (Adjacent AOIs)				Value = Medium (Alarm)			
	Salience				Salience		
Workload	Low	Med	High	Workload	Low	Med	High
Low	1.53	1	0.61	Low	0.71	0.46	0.28
Med	1.64	0.94	0.69	Med	0.76	0.44	0.32
High	1.71	0.94	0.7	High	0.79	0.44	0.32
Effort = Medium (Separated AOIs)				Value = Low (Notification)			
	Salience				Salience		
Workload	Low	Med	High	Workload	Low	Med	High
Low	1.88	1.02	0.69	Low	1.22	0.80	0.49
Med	2.34	1.28	0.76	Med	1.31	0.75	0.55
High	2.64	1.56	1.1	High	1.37	0.75	0.56

The outputs from this enhancement to SDAT/SOAS are below.

Outputs & Status Display

No values were added to SDAT's output file. The Countermeasure Events screen uses color to indicate which trigger initiated the compensatory action – black for normal SOAS elevation, blue for N-SEEV-triggered elevation of countermeasures, as shown below.

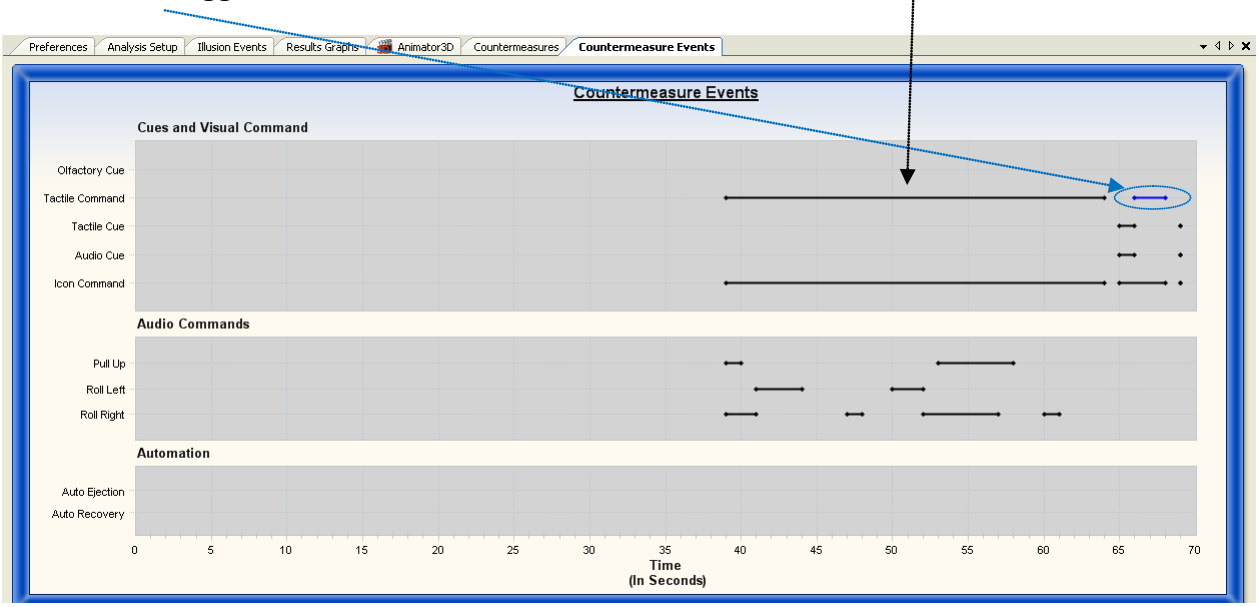

When integrating SOAS into an actual vehicle's cockpit, N-SEEV values should be updated to reflect the vehicle's geometry and capabilities; for example, display locations and offsets from the pilot's forward view, and whether or not tactile cues are available.

Appendix C. Three New SDAT Illusion Models

This appendix provides details of the three new SD illusion models designed for SDAT during this NSBRI project. Due to time constraints, only the first two models were actually developed and added to SDAT.

Undetected Loss of Lift

Intent – When flying at a fairly low altitude (in ground effect) and low speed, if an undetected climb or loss of lift occurs without the required power/thrust increase to maintain altitude, there will be a plunge toward the surface. SDAT should detect the initial conditions and a worsening situation (e.g., continued altitude increase with no power/thrust increase) to trigger the appropriate countermeasures.

1. Airspeed and groundspeed slow (less than 20 knots), and AGL altitude is "out of ground effect" (defined as the rotor radius, which varies for each vehicle. For small helicopters, the radius could be 10'; for a medium helo, use about 25'; for a large helo, use about 35'). [No countermeasures.]
2. An increase in altitude at or below the vertical otolith threshold for about 50 feet of altitude gain (i.e., more than some noise level or minimal amount that might be caused by turbulence) which will take about 10 seconds AND engine speed/thrust during the altitude increase is at or below 90% (default; user selectable) the whole time. [Low countermeasures; problem is just developing.]
3. Altitude gain with low power (<=90%) continues for another 5 seconds. [Medium countermeasures as situation evolves.]
4. Rapid drop in altitude with insufficient power to arrest the plunge (i.e., engine speed/thrust less than 98%). [High countermeasures as the consequences of the SD occur.]
    a. Rapid drop defined as -1000 fpm or greater vertical speed.

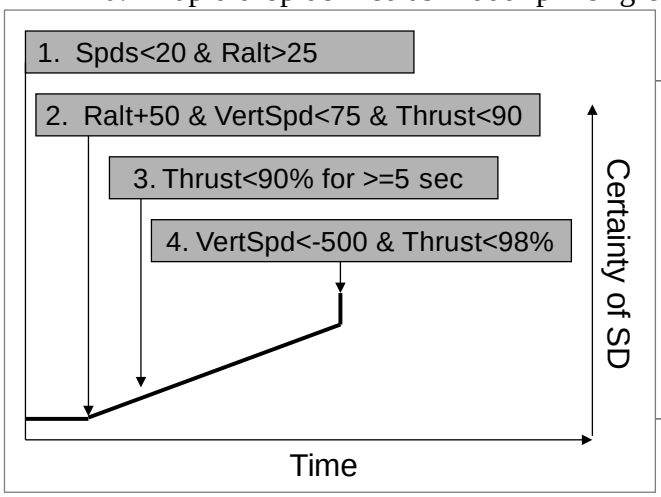

1. Almost hover out of "ground effect": Airspeed & groundspeed < 20 knots; AGL > 25'.
2. Sub-threshold altitude increase with low thrust: VertSpd < 75 fpm; alt gain of 50'; thrust < 90%.
3. Continues: Thrust < 90% for 5 more sec.
4. Plunge toward surface with insufficient thrust to recover: VertSpd < -500 fpm; thrust < 98%.

Trigger appropriate countermeasures:

    b. Low (visual cue) – "Check power."
    c. Medium – auditory and tactile cues added to visual cue.
    d. High – continue visual; add auditory & tactile commands to "Check power" and "Pull up."
    e. Auto-recovery when surface impact is impending (2 seconds or less; user selectable).

Here is this model's GUI tab:

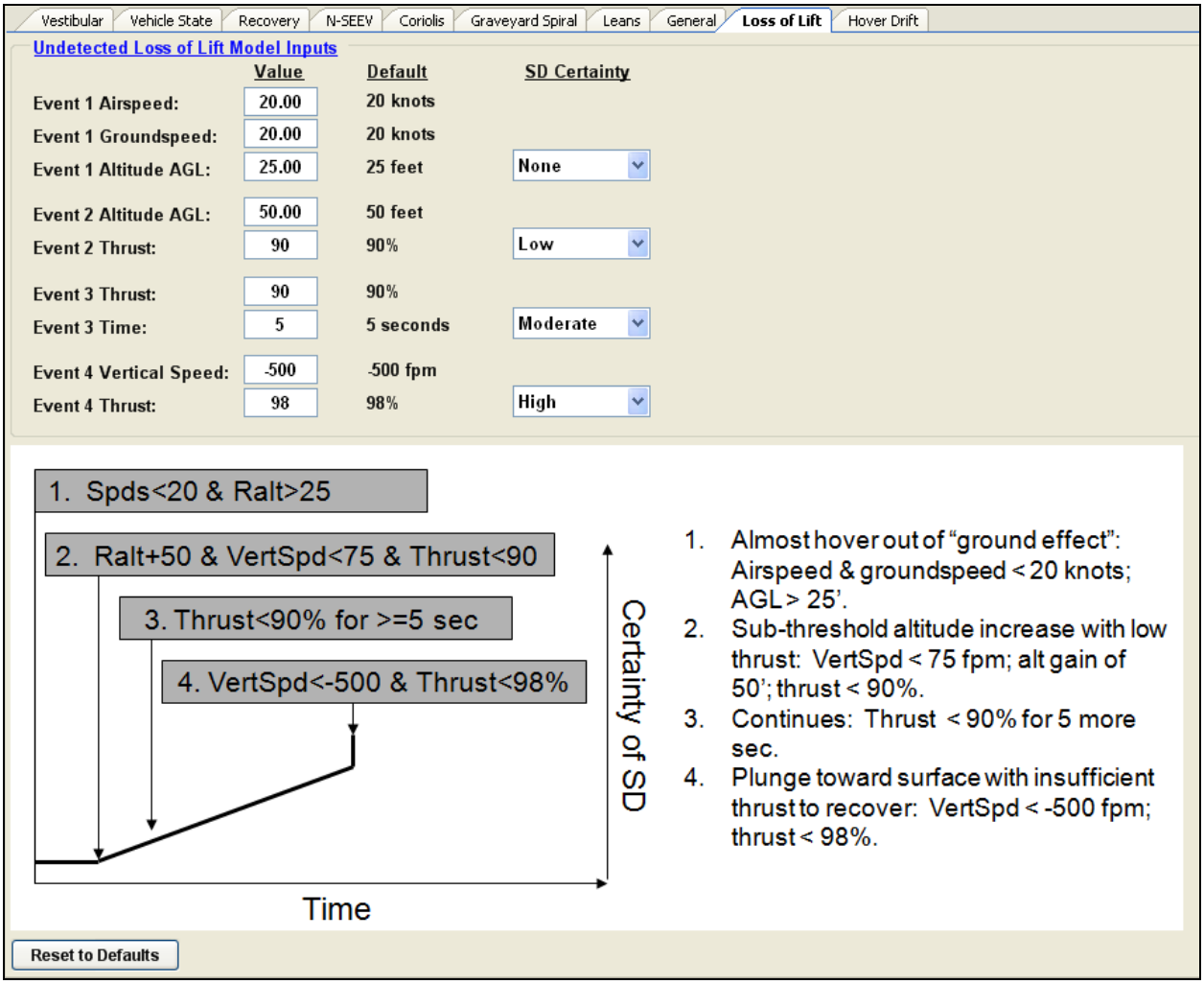

Inadvertent Drift during Hover Illusion Model

While in a hover near the surface, any undetected motion ("drift") could result in the vehicle striking an obstacle, causing damage to the vehicle and/or injury to the crew. Some longitudinal or lateral motion is expected, but "too much" could be dangerous. The model should also apply to a non-terrestrial vertical take-off and landing vehicle.

The assumption is that motions above the otolith threshold will be perceived and that the pilots will know that they have moved and thus know where they are. The 'inadvertent' component of drift in any direction is based on sub-threshold movements. As with other SD illusions models in SDAT, we assume that the environment is non-visual or somehow visually compromised. This is especially true for this model as sub-threshold positioning motions will likely occur during every landing.

SME comments (in red font throughout):
Sometimes the pilot has to maneuver while in a hover – relative to a moving surface object or even when the intent is an otherwise geostationary hover. But, for unintended motion, the SME would halve the radii and definitely weight rearward drift more heavily as being undesirable.

The model begins with determining if the vehicle has reached the 'hover' criteria. While the hover criteria are maintained, the model keeps a running calculation of the difference between current actual location and current perceived location. The various levels of disorientation are purely based on the delta between actual and perceived location. For each time period, ground speed and lateral speed are used to determine change in position in an X/Y coordinate system. All motions are used in Actual Position. Only above-threshold movements are used in Perceived Position. For each time period, the current X/Y values for Actual and Perceived position are used to determine the perception delta.

We have not yet added a weighting factor for rearward drift.

Model Stages

1. When in a hover for at least 2 seconds, where hover is defined as a low radio altitude and low groundspeed
    a. where low altitude is 50' or less AGL, and
    b. where low groundspeed is < 10 knots
        i. SME comments{20 knots would be better, otherwise hover definition is good and applicable to just about any helo}
    c. This version of the hover may also work for some conditions in which the vehicle is holding station over a moving object. While this would likely be a visual environment, there may still be cases of distraction where inadvertent drift is a consideration.
2. Sub-threshold horizontal motions resulting in a location perception delta of >=10 feet
    a. Low level of SD.
    b. 5 feet.
3. Sub-threshold horizontal motions resulting in a location perception delta of >=20 feet
    a. Medium level of SD.
    b. 10 feet.
4. Sub-threshold horizontal motions resulting in a location perception delta of >=30 feet
    a. High level of SD.
    b. 15 feet.

<u>Questions for subject matter experts (SMEs):</u>

- Are the numeric values above reasonable? Please especially examine distance and time assumptions. Yes, they seem reasonable, but could be half for distances; timing seems OK.
- Instead of displacement in feet, should we use a vehicle length metric? No, pilots think in terms of feet, not helo lengths. For example, one vehicle length of below-threshold drift is Low; two vehicle lengths is Medium, and three lengths is High.

- Is the severity of the situation appropriately captured by the Low, Medium, and High assessments? Yes.

Units

The user-entered values for distances and speeds versus the data input values are in mixed units and must be resolved. 'Feet' is useful for the drift criterion and knots is a well known speed value. In some cases we've seen data sets where the ground speed is given in km/hr and some given as knots and lateral is actually a 'G' value rather than a speed. Our current decision is to keep all speeds as 'knots' for the incoming data. As such, to meet SDAT version 5 format, any speeds in other units will have to be converted and any accelerations will have to be converted to speeds. This will most likely occur for ground speed and lateral speed values.

- Knots: ground speed, lateral speed, otolith thresholds
- Feet: user entered drift criteria

The otolith threshold speed values are also given as knots. However, the time units for the data sets are seconds. So at some point we'll have to convert from knots to some distance unit per second. Likewise we'll have to convert either the X/Y coordinate positions or the perceived delta to feet. The easiest approach was to convert everything to feet and feet/second.

User Entered Values

We'll use the values provided by the SME. The interface will support changes to hover values and drift criteria.

Event 1: Hover
- Time: 2 seconds
- Altitude: 50 feet AGL (radio alt)
- Speed: 20 knots (ground speed)

Event 2: Low SD
- Actual vs. Perceived position delta: 5 feet

Event 3: Medium SD
- Actual vs. Perceived position delta: 10 feet

Event 4: High SD
- Actual vs. Perceived position delta: 15 feet

Model Pseudo-Code

For each time period:
IF Event 1 = FALSE
    Determine if Hover criteria are met
    Event 1: Hover
        If Altitude <=50ft AND Groundspeed <=20 knots
        AND both conditions are sustained for 2 seconds
        Then illusion event 1 = TRUE
IF Event 1 = TRUE
    Check to see that altitude and groundspeed criteria are still met
    IF Alt > 50ft OR Speed > 20 knots
    Then reset entire illusion (no longer in hover)

IF Event 1 still TRUE
Calculate Actual & Perceived Location on X/Y coordinate
Calculate distance delta between Actual & Perceived Location

The code determines how much forward/backward distance has been traveled and adds that to the current X position. Then determines how much left/right distance has been traveled and adds that to the current Y position. The same is done for perceived but only for speed values above threshold (where threshold is set by the user on the Vestibular tab).

Actual Location X = Actual Location X + (Ground speed * time step)
Actual Location Y = Actual Location Y + (Lateral speed * time step)

(For perceived locations)
IF Ground Speed > Otolith Threshold
THEN Perceived Location X = Perceived Location X + (Ground speed * time step)
ELSE Perceived Location X is unchanged
(same code for Lateral speed & perceived Y location)

Delta between Actual & Perceived = (standard X/Y coordinate distance calc)
Sqrt ((x2 – x1)^2 + (y2 – y1)^2)

Event 2: Low SD
IF Absolute Value of Delta between Actual & Perceived >= 5 & < 10 feet (user input value)
THEN Event 2 = TRUE

Event 3: Medium SD
IF Absolute Value of Delta between Actual & Perceived >= 10 & < 15 feet (user input value)
THEN Event 3 = TRUE

Event 4: High SD
IF Absolute Value of Delta between Actual & Perceived >= 15 feet (user input value)
THEN Event 4 = TRUE

Backing Down the Sequence

This model is slightly different than the others that involve more dependent step sequences. In this case, the subsequent events are dependent on Event 1 but not on each other in order. So the process for 'backing down' the sequence focuses primarily on Event 1.

For each time step, if either the altitude or speed values are outside of the hover criteria then the model will be completely reset. Movement across the other events is simply an evaluation of the current movement delta state (provided hover is maintained) and does not require determining the status of any event except Event 1.

Illusion Sequence Graph

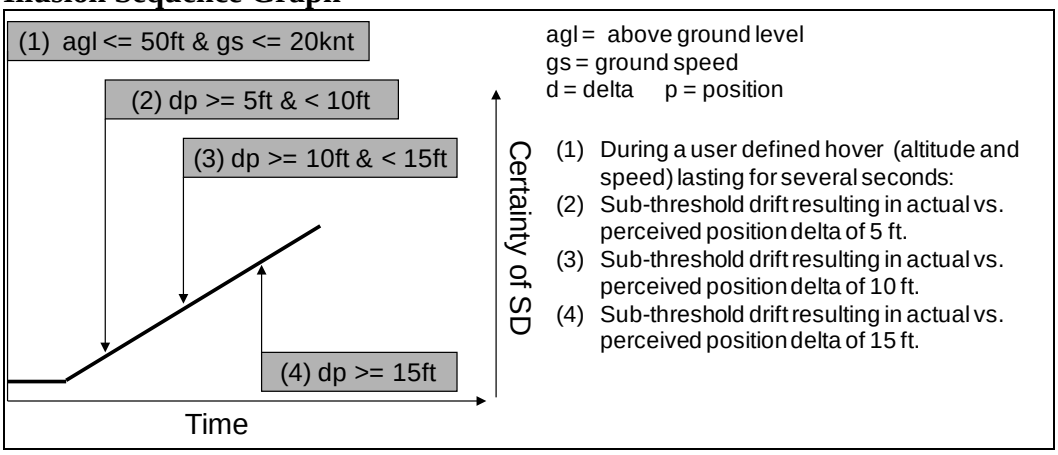

Illusion Event Sequence Display

Since the model isn't built as a full sequence of events like most others, it was decided that the illusion event sequence display would represent the event sequence differently. Only Event 1 will be displayed along with one of the other events (when active) rather than showing, for example, Event 2 and Event 3 in active sequence if Event 4 is active. Rather, Events 2-4 will only show when individually active, as shown below.

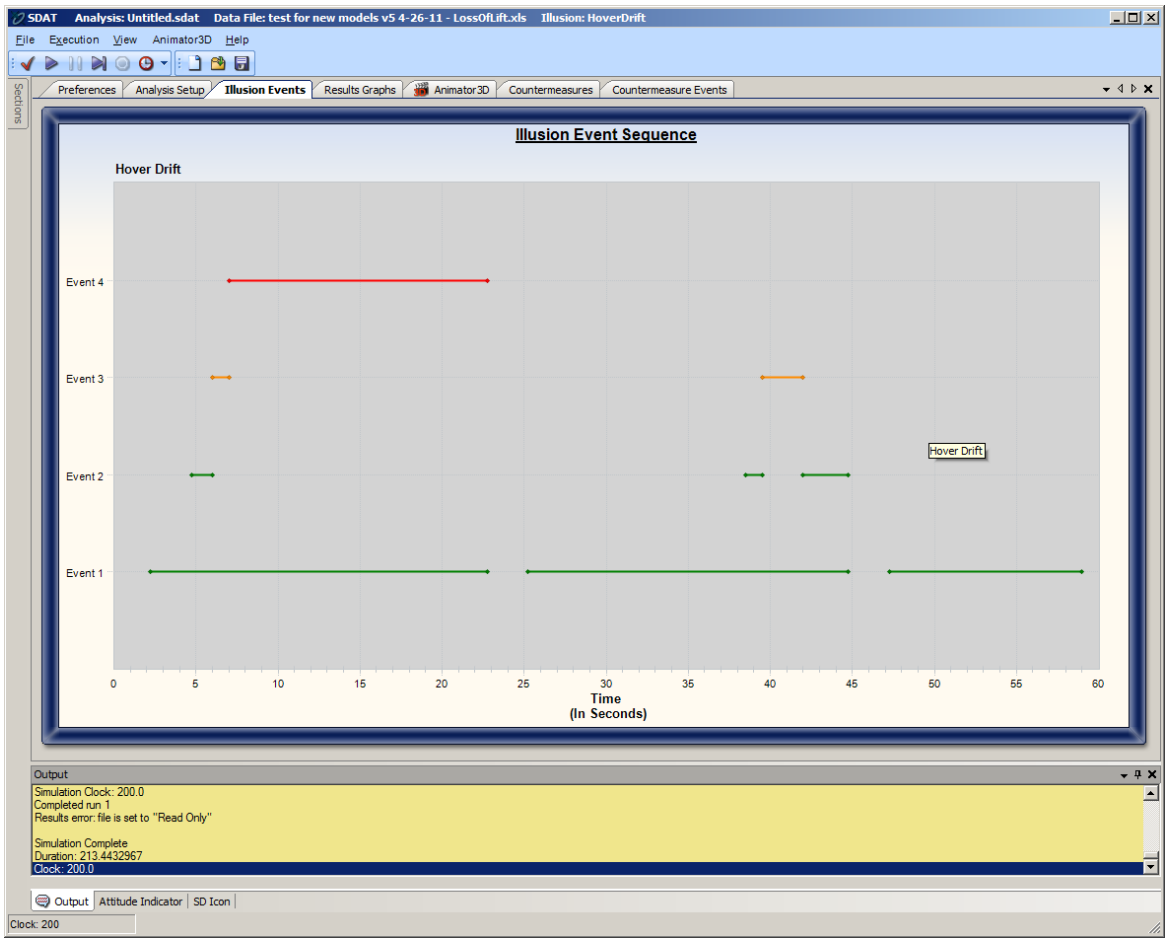

Countermeasures
We do not currently have helo countermeasures specific to this illusion model. The following is the initial idea:

- Low – visual "Check drift."
- Med – visual "Check drift" and audio and tactile cues.
- High – visual "Check drift" and audio command to "Check drift."
- Auto-recovery – engage autopilot hover mode if displacement or delta exceeds 35'.
- Auto-ejection does not apply to vertical landing vehicles.

Here is SDAT's GUI tab for this model:

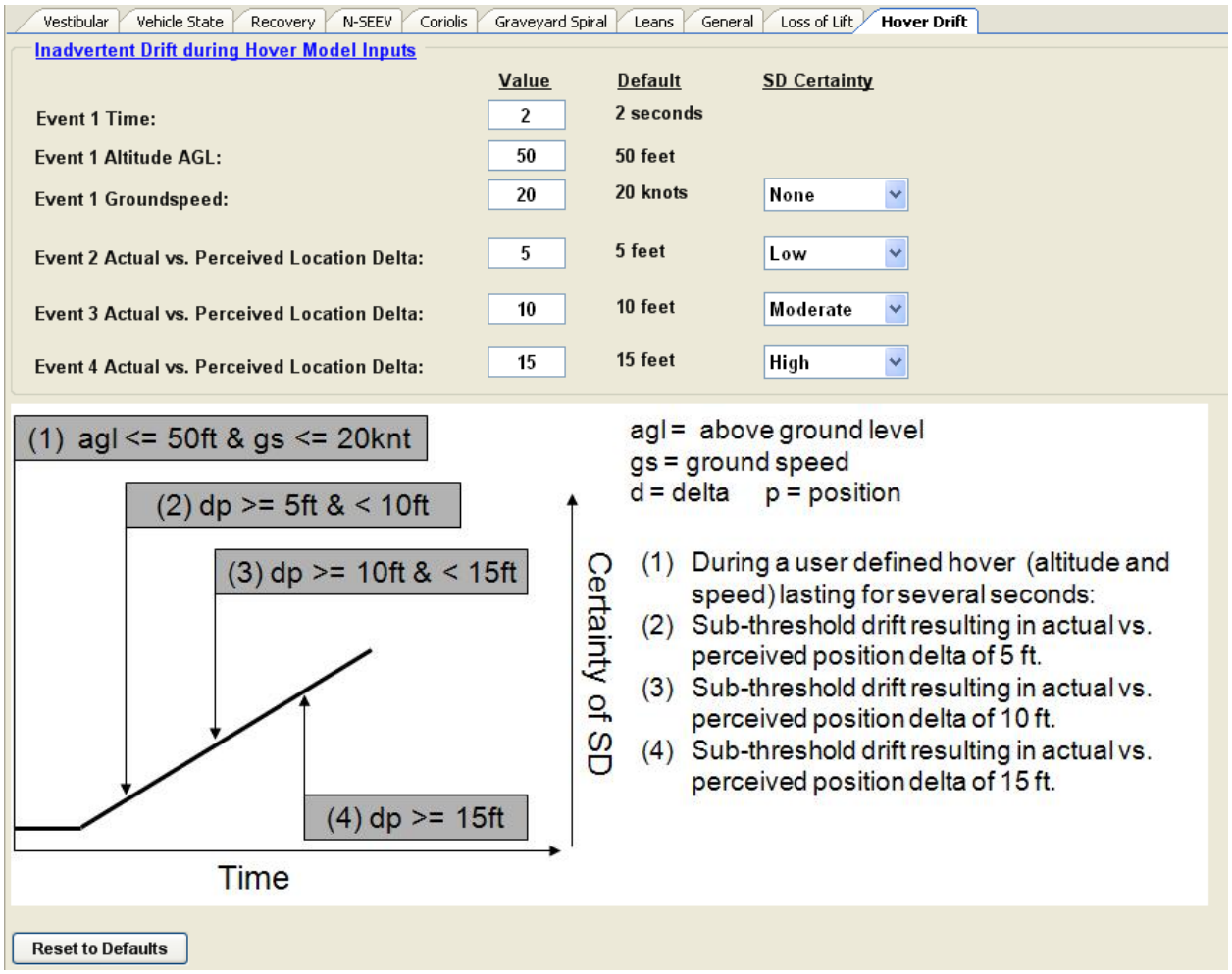

Undetected Drift during Landing

Intent – During landing, any lateral drift over a certain speed (varies by vehicle type and model) can result in a "trip" as the skids or wheels contact the surface and act as a fulcrum and the helicopter tips over, causing major damage to the helicopter and injury or death to the crew and

bystanders. Even in visual conditions, pilot distractions or fatigue or other factors could render lateral drift as undetected by the pilot. However, for use within SDAT we will still create a vestibular-based model to evaluate when the occurrence of this type of problem could be based on a vestibular illusion.

For this model, the SME suggested a user-selectable cone that looks like the figure below, where the desired drift in any direction at touchdown is 0. Some tolerances are allowed, though, as shown in the tables below the figure. We will combine these values with an evaluation of a 'hover' state (prior to landing) and a check to see if the horizontal movements (fore, aft, left & right) are below the otolith thresholds. For the purposes of this model, if the movements are above threshold, the pilot will feel them and notice the unwanted motion. This will allow us to continue our practice of using a range of vestibular threshold settings to evaluate flight data sets.

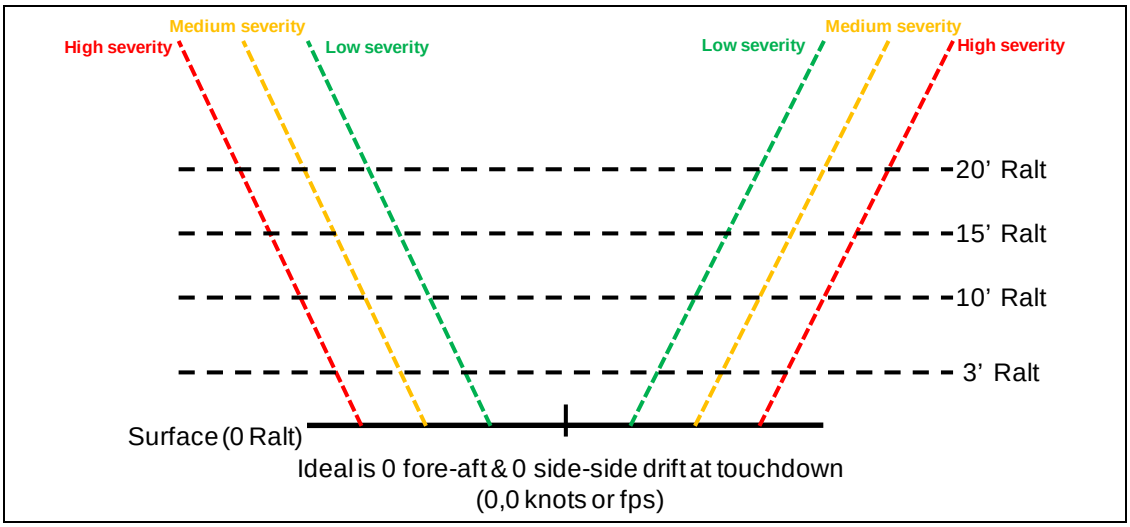

Low severity - knots			
Ralt	side-side	fore	aft
< 3 ft	0.25	0.375	0.25
3-10 ft	0.5	0.75	0.5
10.1-15 ft	1	1.5	1
15.1-20 ft	2	3	2

Low severity - feet per second (fps)			
Ralt	side-side	fore	aft
< 3 ft	0.4	0.6	0.4
3.1-10 ft	0.8	1.3	0.8
10.1-15 ft	1.7	2.5	1.7
15.1-20 ft	3.4	5.1	3.4

Medium severity - knots			
Ralt	side-side	fore	aft
< 3 ft	0.5	0.75	0.5
3.1-10 ft	1	1.5	1
10.1-15 ft	2	3	2
15.1-20 ft	3	4.5	3

Medium severity - fps			
Ralt	side-side	fore	aft
< 3 ft	0.8	1.3	0.8
3.1-10 ft	1.7	2.5	1.7
10.1-15 ft	3.4	5.1	3.4
15.1-20 ft	5.1	7.6	5.1

High severity - knots			
Ralt	side-side	fore	aft
< 3 ft	1	1.5	1
3.1-10 ft	2	3	2
10.1-15 ft	3	4.5	3
15.1-20 ft	4	6	4

High severity - fps			
Ralt	side-side	fore	aft
< 3 ft	1.7	2.5	1.7
3.1-10 ft	3.4	5.1	3.4
10.1-15 ft	5.1	7.6	5.1
15.1-20 ft	6.8	10.1	6.8

Assumptions

Acceleration vs. Speed Threshold

We are assuming that using only the otolith speed threshold is sufficient for this model. The whole model is predicated on preventing landing with too much speed. The use of the acceleration value for otolith threshold doesn't seem to be necessary and it helps to simplify the model to use only one of them.

Drift Direction and Axis

We will use only the two axes in terms of direction instead of all four directions along the two axes. Along the X axis (fore & aft), the speed values will be checked in either direction (absolute value) to compare against the threshold value. Likewise for the Y axis (side to side). This is based on the assumption that the speed value isn't accumulated via the misperception the way it would be for a SCC-based model (unperceived acceleration resulting in perceived speed accumulation over time). Rather, any speed that isn't perceived is a problem. We will, however, use a timing value to prevent initiations of sub-threshold values within high frequency data (value spikes).

Model Stages

We're using the same Event 1 for determination of Hover as used in the Hover Drift Illusion.

1. When in a hover for at least 2 seconds, where hover is defined as a low radio altitude and low groundspeed
    a. where low altitude is 50' or less AGL, and
    b. where low groundspeed is < 20 knots
    c. This version of the hover may also work for some conditions in which the vehicle is holding station over a moving object. But should still support a pre-landing condition.
    d. If hover criteria are not maintained then the illusion is reset.
2. Sub-threshold horizontal motions (otolith) occurring for 1 second followed by one of the following combinations based on the tables from above:
    a. Ground speed and lateral speeds will be used from the data set to compare with otolith threshold setting.
    b. Timing value helps to prevent data spikes. We're looking for a short period of continuous sub-threshold. This should occur as part of a regular landing sequence. So event 2 is NOT considered SD.
    c. Threshold versus speed values will be compared along each axis but direction along the axis doesn't matter. All we need is sub-threshold, not direction. The absolute value of ground speed will be used for fore/aft (X axis). The absolute value of lateral speed will be used for side-to-side (Y axis).
    d. Timing for sub-threshold along each axis will be kept separately. If super-threshold along the axis occurs then Event 2 for that axis will need to start over.
    e. Event 2 will be 'occurring' if timing requirement is met for 'either' axis.
3. Altitude and Speed combinations fitting the severity levels from the table.

a. Once Event 2 is occurring, then check to see if the criteria for speed and altitude from the tables are met. Both the altitude and speed are represented within a range of values.
    i. The altitude range within the table is the first column. The speed range is based on the values in the tables associated with the same speed range. For example:
        1. If the altitude is less than 3 feet then the speed range to check should be great than or equal to 0.25 knots and less than 0.5 knots to be of low severity.
        2. If the altitude is 10.1 to 15 feet then the speed range is greater than or equal to 2 knots and less than 3 knots for medium severity.
b. For the two lateral directions, the table provides only a single speed criterion so there is no need to check if the sub-threshold drift is left or right. For the fore-aft case, the table values are different. So while it doesn't matter which direction the vehicle is drifting in Event 2, we have to check the direction (+ or -) of ground speed to determine which value from the table to check.
c. Three different events will be represented based on the severity levels from the tables.

Units

Version 5 of the spread sheet contains data for horizontal speeds in knots and accelerations in G. While the tables above give speed values for both knots and fps, it will be easier to check model execution and during analysis if the threshold values and the speed values are in the same units. For example, if the user has set the otolith thresholds to a particular value and want to check that against the graph of speed during model execution, it will be much easier if the graphed values are in the same units. So user settings for the model will be in:

Ground Speed = knots
Lateral Speed = knots
Altitude = feet
Time = seconds

User Entered Values

Event 1: Hover

- Time: 2 seconds
- Altitude: 50 feet AGL (radio alt)
- Speed: 20 knots (ground speed)

Event 2: Otolith Threshold

- Time: 1 second

Event 3: Altitude & Speed Combination

- Given the number values represented within the tables, we may have to find a way to cut the model down some. Clearly it would be nice to be able to set things up for different types of helos or other vertical landing vehicles but the interface will be difficult.
- Also, we need to determine how best to implement these ranges. The tables provide ranges for the altitude but the associated speed ranges are a little confusing.

Model Pseudo-Code

IF Event 1 = FALSE
    Determine if Hover criteria are met
    Event 1: Hover
        If Altitude <=50ft AND Groundspeed <=20 knots
        AND both conditions are sustained for 2 seconds
        Then illusion event 1 = TRUE
IF Event 1 = TRUE
    Check ABSVALUE (Ground Speed) AND ABSVALUE (Lateral Speed) vs. Otolith Threshold
    IF one or both are sub-threshold
        THEN start timer(s) to track if sub-threshold is maintained to time criteria.
    IF timing criteria are met for either
        THEN Event 2 = TRUE and track which axis has met the criteria (perhaps both)
IF Event 2 = TRUE
    Use AGL value to find current altitude range
    AND
    Use direction of motion along axis being tracked to determine which speed column to check
    AND
    Use speed range to determine if Low, Medium or High severity has been reached
        (it is possible and reasonable to be within an altitude range and be slow enough not to meet any of the severity criteria during a good landing.)
    IF Low THEN Event 3 = TRUE
    IF Medium THEN Event 4 = TRUE
    If High THEN Event 5 = TRUE

Backing Down the Sequence

Event 1
The entire model is based on the assumption of landing so the whole model is reset at any point if the hover criteria from Event 1 are not met.

Event 2
Any above threshold speed will reset Event 2 for the specific axis. If Event 2 for an axis is FALSE then Events 3, 4 or 5 should be reset (although the requirement to check levels each time step may take care of this).

Events 3, 4 or 5 for each axis will be uniquely set at each time step in which Event 2 is still true.

There is no SDAT GUI tab for this SD illusion model because the model was not implemented in SDAT during this project.

Appendix D. Observer.dll Wrapper

Overview

We added *ObserverCppWrapperLib.dll* and *ObserverNetWrapper.dll* as intermediaries between our SDAT Excel data source, Illusion/Countermeasure Engine, and graphing outputs; and MIT's Observer dll. Unmanaged vs. managed refers to the memory management scheme used by programs and libraries in the Microsoft .NET platform. They operate differently, and to move a variable and its value from one to the other, the system needs to "marshal" the data. If we setup the wrapper class so that only basic data types (e.g., Int32, Float64, String) are sent, vs. user-defined types (e.g., class OtolithPerceivedAngle), we can let the .NET environment do the marshaling for us. Otherwise we need to setup much more advanced marshaling ourselves. Only perceptionModel_MIT_v1_win32.dll, ObserverCppWrapperLib.dll, and ObserverNetWrapper.dll are included in the install/deliverable version of SDAT.

Details

Components added to SDAT install:

- perceptionModel_MIT_v1_win32.dll
    - unmanaged C++
    - generated by MIT using Matlab tools.
- ObserverCppConsoleTestApp.exe (purely a migration/testing tool)
    - unmanaged C++
    - observer sample program ported over to visual c++
- ObserverCppWrapperLib.dll
    - unmanaged C++
    - interface with MIT-delivered perceptionModel_MIT_v1_win32.dll
    - turned ObserverCppConsoleTestApp into a dll, exposing
        - initialize()
            - allocates unmanaged MIT objects (input/output structures)
        - step()
            - copies marshaled inputs to MIT input structure and step the observer model.
        - terminate()
            - deallocates MIT objects
    - invoke ObserverStepResultsCallback()
        - copies results from MIT output structure to marshaling variables to be delivered back to ObserverNetWrapper

- ObserverNetWrapper.dll
    - managed C# assembly
    - wrap the exposed routines from ObserverCppWrapperLib in a .NET assembly to let the built-in .NET facilities do all of the data marshaling necessary.

- ObserverNetConsoleTestApp.exe (purely a migration/testing tool)
    - managed C# test program
    - mimic MIT's sample program, but coded in C# and calling the ObserverNetWrapper from a .NET environment for testing.

Appendix E. FORT Tool Details

Fundamental to the frame of reference theory and model is the notion of a **disparity** between the frame of reference of perception and that of the world (for image comparison) or of action (for control) (Wickens, Vincow, & Yeh, 2005). For example, the disparity most relevant to many aviation SD mishaps is that between perceived (ego) and actual (world) gravitational upright. In fact this is just one of a larger set of six dimensions along which a disparity can lie (pitch, roll, yaw alignment, and X, Y, Z translation). A disparity in Z occurs when the perceived altitude is different from the actual altitude; in aviation such a disparity invites the possibility of a hard landing, for example. Frame-of-reference (FOR) disparities also include the first and second derivatives of each of these six axes, yielding a total of 18 variables that could enter into a vector of *FOR disparity*. FOR disparities become even more complex in much of vehicular travel (typical of space operations) when a separate FOR can be defined for the Earth (or moon or planetary body), for the vehicle, and for the operator. Additional frames may be defined around robotic manipulators (particularly as these are mounted with cameras), and around the head as separate from the trunk; for example, when astronauts and pilots engage in off-bore-sight viewing.

The focus of FORT theory is to model the costs resulting from FOR disparities. Typically these costs can be measured as operators attempt to **transform** one FOR into another (e.g., "how do I move my control to move the probe upward?") (Wickens, 1999). Such costs are reflected in human error (if the correct transformation is not accomplished), in time costs, and in mental workload costs. The classic example of such a cost is manifest in the yaw axis when a navigator is using a north-up map to navigate in a southerly direction (Aretz & Wickens, 1992; Olmos et al., 1997). The navigator employs 2-D mental yaw rotation of 180 degrees to assure that left and right in the forward view (ego frame) correspond to desired headings on the map (world frame). The rotation showed in Figure 20 is a 90-degree rotation. Such mental rotation costs are found to increase generally monotonically with the degree of disparity, to cause added mental workload (competing with other tasks) (Wickens et al., 1996), and to occasionally lead to reversal errors in control and spatial judgments.

Six additional levels of complexity imposed on FORT theory are:

1. As noted above, there are actually 18 components along which disparities may be defined. Thus even at a simple level, one could speak of the degree of FOR disparity scaled from 0 to 18 depending on how many components are affected.
2. Disparities along different axes are not all equally serious. For example, disparities along the pitch axis are less serious than those along the yaw axis (Cizaire, 2007). Thus it is easy to follow a map, whether it is held vertically or horizontally because the transformation from vertical to horizontal is simple (Franklin & Tversky, 1990; Wickens et al., 2005). However it is considerably more demanding to navigate with a map that is rotated 90 degrees in the yaw axis (so that, for example, forward in the world is right on the map). Thus different transformation components should be weighted differently. In Figure 21, we depict the smaller mental rotation cost translating between a fore-aft axis and a vertical axis, than transformations involving the lateral (left-right) axis.
3. Also, as shown in Figure E-1, across the three rotational components of transformation (pitch, roll, yaw), the function relating human performance cost to degree of disparity is not linear, but appears to be an "S" shaped or ojival function. Again, as a straightforward

example, both vertical and lateral mental rotation costs are disproportionately small for small angles, but show non-linear increases as disparity increases toward, and then above, 90 degrees (Wickens, 1999; Hickox & Wickens, 1999; Schreiber et al., 1998).

4. Top-down knowledge-driven strategies sometimes appear to override the rotation operations. This phenomenon becomes quite prominent when mental transformations at or near 180 degrees are required, as shown in Figure E-1. Here people often adopt a verbal "left is right, right is left" or "up is down, down is up" strategy, thereby allowing shorter response times than those predicted by a full 180-degree mental rotation. For example Cizaire (2007) observed that a 180-degree rotation in pitch required no more time than a 90-degree rotation in the same axis. Such knowledge-based strategies appear to become more prominent in known and human-constructed environments, with designated walls, ceilings and floors, such as is typical when moving about a space station (Cizaire, 2007).
5. One particular FOR difference, that is also knowledge driven, is the understanding or mental model of what is "fixed" and what is "moving" on a display. Thus, in aviation, pilots have differing degrees of control effectiveness depending on whether controlling attitude with a moving aircraft or moving horizon display (Previc & Ercoline, 1999; Roscoe, 2002; Kovalenko, 1991). Confusion between the perceived FOR can cause undesirable control reversals, which could produce potentially catastrophic results in precision maneuvering (e.g., final approach to docking as described in the FORT section of the report).
6. While FOR transformations (FORT) can be costly, it is sometimes better to maintain a consistent control-display (or display-display) transformation across different systems or different components of a single system, than to require the astronaut to switch (inconsistently) from one relationship to another (Andre & Wickens, 1992).

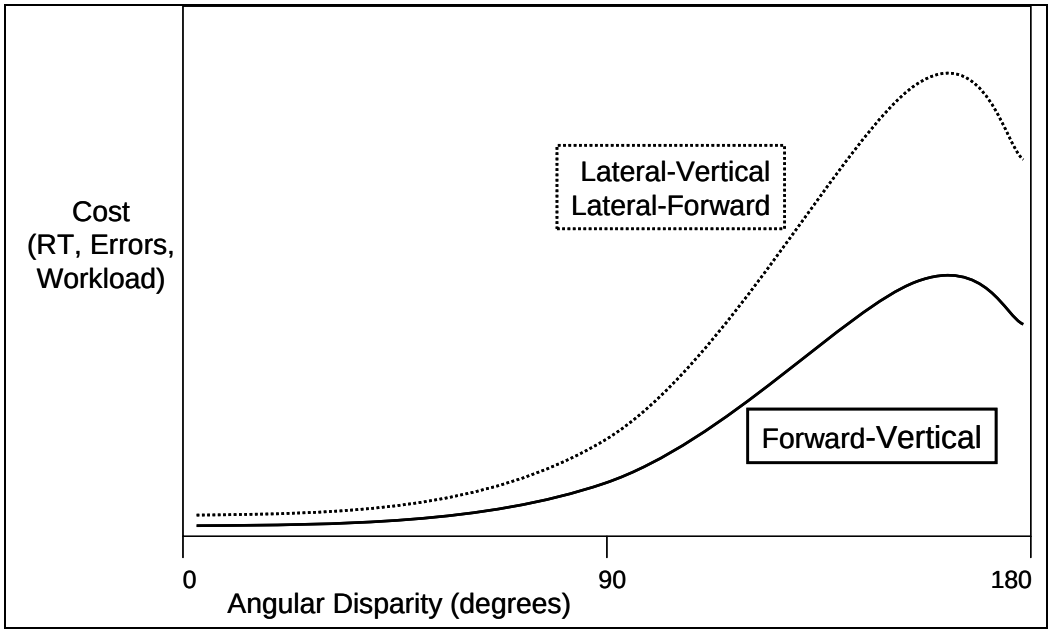

Figure E-1. Costs of frame of reference transformations.

A FORT model based upon FORT theory can serve two interacting goals. First, given any definition of spatial task requirements and specification of visual information sources (displays, and out-the-window views), it will predict the cost vector imposed by required transformations. This vector can be characterized by delays in making spatial decisions (including those necessary to exercise control), increased interference with concurrent tasks (reduced capacity for multi-tasking), and increased likelihood for errors. Second, the model can predict the effectiveness of particular display formats or augmentations in reducing or minimizing transformations, and hence minimizing workload (Gillingham & Wolfe, 1986). As a straightforward example, FORT predicts the substantial gains in flight control performance associated with synthetic vision system (SVS) displays (Alexander, Wickens, & Hardy, 2005). Such displays can be either status displays or command displays (Andre & Wickens, 1992). It is important to note that any display suite is typically required to serve more than one task. For example, a landing display must support both trajectory and speed controls, as well as obstacle awareness. FORT can help guide the designer on the choice of an appropriate display suite, or compromise display, that can minimize the aggregate FORT costs for a set of tasks (Wickens, 2000a; Wickens et al., 1996).

While formal algorithms have not yet been developed for a FORT model, the approach will be to analytically capture the curvilinear relations in Figure E-1. Net costs for simple rotations can be modeled by establishing the angular disparity along each axis and summing across axes, using a 50% weighting for forward-vertical transformations, and unity weighting for the other two transformations. The FORT cost model could be more complex by considering first and second derivatives, as well as translations. For this project at this stage, though, we will keep the cost model simple until we have more data and a greater need for the added complexity. Calculation of specific time costs will use the data reported below in FORT Research Results.

FORT Research Results

In addition to the above development of FORT theory and modeling, we accomplished the following two major goals:

1. We have surveyed the literature on mental rotation in space and using space-like tasks, and observed that:
   - Mental rotation costs in space appear to be little affected by the micro-g environment, and show roughly the same costs as on Earth, about 1-2 seconds for 180 degrees of rotation (Kanas & Manzey, 2008; Leone, 1998).
   - The cost of single axis rotations is different across axes in typical astronaut tasks (Cizaire, 2007).
   - There is an important distinction between the mental rotation of objects, and the mental rotation of self within an environment. The former is referred to as object rotation, the latter as “perspective taking” (Kozhevnikov & Hegarty, 2001). This distinction and its implications are outlined in more detail below. Importantly, the costs of self rotation are at least as great as those of object rotation, the paradigm for which the greatest amount of data are available. For example, object rotation studies have been carried out in 0-g environments (Kanas & Manzey, 2008) whereas self rotation studies have not.

2. We have examined how FORT can be integrated with a model of orientation perception, such as Observer. This application will predict online (or from an accident data base) when FOR disorientation is a likely occurrence. This will be based on three components:
   a) a "trigger event" reflected in control activity,
   b) an initial frame of reference mismatch, and
   c) dynamic FOR changes.

   These three components are elaborated upon as follows.

   (a) **Trigger event** as a control activity: Two types of control activity are strongly suggestive of FOR disorientation:
   - Control reversal. Here a control action is made that amplifies, rather than reduces, an error. To diagnose this, we need a continuous measure of the error in the relevant error-nullification (tracking) task, such as the disparity between robot manipulator and target. We also need a continuous reading of control activity, and an estimate of the time lag (e.g., transfer function) of the control system. In the absence of these three channels of information, it is possible to make a less confident assessment from the control data alone, for example, if there are high frequency reversals.
   - Control delay. FOR mismatch may also be sensed if there is a delay in moving the control, **under conditions when it should be moved** (e.g., error and error velocity of the same sign). This indicates a hesitation as the operator is trying to decide how to control. Here again, the system needs a continuous error measure.

   (b) **Pre-existing conditions**. The static FOR misalignment describes the fixed properties of a workstation, and considers the angular rotation, along the three axes of space, between the control movement, and the display movement as depicted in Figure 20. For convenience, we describe the three axes as lateral (left right), forward (fore aft), and vertical (up down), or L, F, and V. Within each axis, a geometric function of mismatch increases to 150 degrees and then decreases to 180 degrees of rotation. Furthermore, of the three axis pairings (LF, LV and FV), the first two, involving mapping to the lateral axis, are weighted twice as heavily as FV, reflecting the major left-right confusions in axis mapping. Weighted mismatch values are summed across all three axis pairs.

   (c) **Dynamic misalignment**. This term reflects the fact that FOR disorientation is amplified if mappings continue to change. For example, an astronaut manipulates a fore-aft joystick mounted to a swivel chair or space suit such that fore-aft, when facing a forward display, becomes L-R, if the workstation is swiveled 90 degrees. Dynamic misalignment at any given moment is computed exactly as static misalignment above (e.g., integrated across axes). However, a running integrator of dynamic FOR change accumulates the amount of change over the previous X minutes to assess the degree of dynamic change.

Alternatively, in the above, pre-existing conditions could just be re-defined as the momentary misalignment vector at the time of computation, with the dynamic component adding to this disorientation cost proportional to the extent of change over the past X minutes.

In implementing FORT within an orientation perception model, the idea is that the static and dynamic components will create a static and or time-varying predisposition to FOR disorientation. If this predisposition is high, then the control event classifier will be more likely to classify a given control reversal (or control absence) as evidence of FOR disorientation; or, alternatively, be likely to classify a small reversal as evidence.

Object rotation vs. perspective taking

The distinction between object mental rotation (MR) and ego perspective taking (PT) is potentially important as an ability, a strategy, and a task, although such distinction will be shown not to have any substantial impact on the currently evolving FORT model. We note at the outset that because this distinction **is** clear, we will now and henceforth refer to "misalignment cost" rather than "mental rotation" within the FORT model, as characterizing the cost when there is a disparity in frame of references. Thus, consistent with the potential importance of the MR vs. PT distinction, MR now refers to one of three possible approaches to dealing with misalignments:

1. **As an ability**. Kozhevnikov and Hegarty (2001) have shown that mental rotation and perspective taking have much in common. A high correlation (r=0.69) is found between tests of the two abilities, indicating that roughly 50% of the variance is shared between them. In contrast, the set of four tests that differ between them appear to account for only about 10% of the variance (e.g., unique to PT, not shared by MR). Thus in general, correlation **differences** between PT and navigation tasks and MR for the same navigation tasks appear, at most, to be about 0.30, and in most cases there are no such differences. The most important such difference appears to be in finding a shortcut back to the navigational starting point, which is correlated significantly with PT (r=0.30), but not with MR (r=0.11). For the other three navigation task tests, examined by the researchers, the correlations are not different.

   Another feature of the data reported by Kozhevnikov and Hegarty (2001) is that smaller disparity angles (less than 90 degrees) generally show minimal costs in either perspective taking or mental rotation, hence conforming to the general non-linear findings of performance costs with alignment differences in the FORT model.

2. **As a task**. The interesting finding from Kozhevnikov and Hegarty (2001) is that the PT task shows **more profound** costs of misalignment at large angles (160 deg) than does the MR task, as if the former are more susceptible to the classic Shepard effects, wherein two geometric figures are compared to see if one of them, rotated into alignment with the other, is identical to the other (Shepard & Metzler, 1971; Shepard & Cooper, 1982). Alternatively, it is possible that the verbally mediated reversal strategy ("left is right, right is left") which works for both tasks at 180 degrees, can also be applied more fluently with the MR task, as angles approach 180 (e.g., 160). Note that our recent research with NTU in Singapore which used a distinct PT task both in navigating within 3-D buildings (Liu, 2008) and in using hand held displays in naturalistic environments, also showed profound misalignment effects at angles nearing 180 degrees.

3. **As a strategy**. It is unclear the extent to which people can adopt the two different (PT and MR) strategies when given the identical task. However some data from Kozhevnikov and Hegarty (2001) suggest that they can, and indeed may spontaneously, shift strategy to invoke whichever one best serves the task at hand.

Applications to and relevance of the PT-MR distinction for FORT model. Most of the data from our Illinois lab from which we developed a FORT model (Wickens, 1999; Wickens, Vincow & Yeh, 2005) appear actually to have used PT tasks rather than MR tasks (Aretz, 1991; Aretz & Wickens, 1992, Wickens et al., 1996; Olmos et al., 1997; Williams, Hutchinson, & Wickens, 1996; Hofer & Wickens, 1997; Hickox & Wickens, 1999). This research dealt primarily with pilots who navigated with maps that were misaligned from the environment. It is not entirely clear (because we never asked them) whether the pilots took the **perspective** of themselves traveling southward (or eastward or westward) on a north-up map, or **mentally rotated** the map to a south-up (or east-up or west-up) perspective. However, whichever strategy was used, the costs of misalignment were typically profound. In only one study did we examine ability differences. These were not assessed by performance on PT vs. MR tests as in Kozhevnikov and Hegarty (2001), but rather by whether pilots spontaneously rotated their map, or held it north-up (about a 60-40 split). One might posit that those who held the map north-up were better able to take a different perspective. In any case, this group was superior to the map rotators in their acquisition of survey knowledge (ability to reconstruct the map of the terrain through which they had traveled). Interestingly, the two groups did not differ in their ability to draw a direct line back to their starting place (an analogy to the "short cut" task used by Kozhevnikov and Hegarty (2001)).

In conclusion, given the **more profound** misalignment costs in PT than MR observed by Kozhevnikov and Hegarty (2001), and given the substantial misalignment costs observed in most of our research in aviation (pilots in simulators), these data do not seem to mitigate the importance of the misalignment costs we have been assigning in the FORT model. Hence we will continue to use these non-linear misalignment cost functions in the model, but pay particular heed to MR vs. PT differences when the paradigm and strategy analysis allows us to do so, and when such differences might lead to divergent predictions. We remain most interested in the influence of three additional top-down factors as they may influence misalignment costs: (1) the well documented "verbal reversal strategy" (e.g., saying "up is down and down is up"); (2) the qualitative differences among the three axes of rotation (e.g., greater left-right than fore-aft confusions) highlighted by Franklin & Tversky's (1990) work; and, (3) the emerging importance of "wall-ceiling" differences and other distinct landmarks, revealed by Cizaire's dissertation (2007) and closely related grid biases, when misalignment occurs within man-made rectangular structures.

We have transformed this description of costs into a FORT computational tool, in which the user specifies the design parameters of the workspace (displays, controls, their position, movement relationships and orientation), and the model computes an overall cost function for the design.

Model Computational Penalties

Table E-1 shows the current matrix with the full set of relative penalty values associated with each possible combination of control input, display location, and display movement. The penalty

values were derived by considering the effects of various psychological factors identified via research in spatial cognition, as described in the following section. Values shown in white rows and labeled with the specific control motion refer to display movement while controlling an object. Those in yellow rows (light shading) refer to controlled viewpoint, as when movement of the control changes the viewpoint of the image generator (e.g., a camera view). Green cells (dark shading) indicate the most compatible control and display motion mapping combination within a given row.

Table E-1. FORT model penalty matrix.

AZIMUTH		0	30	60	90	120	150	180	210	240	270	300	330
TRANS	Moving												
RT	Object	4	2	1	0	1	2	4	5	4	3	4	5
	Viewpoint	2	4	5	6	5	4	2	1	1	2	1	1
FT	Object	0	1	2	4	5	4	3	4	5	4	2	1
	Viewpoint	6	5	4	3	2	2	3	2	2	3	4	5
UT	Object	0	1	2	4	5	5	4	5	5	4	2	1
	Viewpoint	6	5	4	3	2	2	3	2	2	3	4	5
ROTATE													
CVR	Object	5	3	4	1	2	3	5	6	6	5	6	6
	Viewpoint	3	5	6	7	6	5	3	2	2	3	2	2
FR	Object	1	2	3	5	6	6	5	6	6	5	3	2
	Viewpoint	6	5	4	3	2	2	3	2	2	3	4	5
CHR	Object	5	3	2	1	2	3	5	6	6	5	6	6
	Viewpoint	3	5	6	7	6	5	3	2	2	3	2	2

		DEPTH		ROTATION	
TRANS	Moving	shrinking	looming	clockwise	counter-clockwise
RT	Object	4	6	2	4
	Viewpoint	7	4	5	3
UT	Object	2	5	2	4
	Viewpoint	6	4	5	3
FT	Object	1	6	3	4
	Viewpoint	7	2	5	4
ROTATE					
CVR	Object	4	5	0	4
	Viewpoint	6	6	5	1
FR	Object	3	5	2	3
	Viewpoint	6	5	4	4
CHR	Object	4	5	1	5
	Viewpoint	6	6	6	2

Mapping Scores

In the following subsections, we describe eight psychological elements or mechanisms that contribute to the FORT model scores, prior to our discussion of how these combine in the actual FORT penalty.

Mental rotation in the frontal plane

Mental rotation relates to azimuth or compass heading rotation is associated with the alignment of translational control and display movement. It has been a hallmark in spatial cognition research since the pioneering work of Shepard and his colleagues (Shepard & Cooper, 1982; Shepard & Metzler, 1971; Shepard & Hurwitz, 1984). The mental rotation penalty follows the standard non-linear format described in Wickens et al. (2005), with small penalties up to 90 degrees of rotation, and amplified penalties above 90 degrees (Aretz, 1991; Aretz & Wickens, 1992; Zhang & Cao, 2010). For example, a right translation movement is mapped to a 90-degree azimuth movement with 0 penalty. The reason for the non-linearity is that up to 90 degrees, a rightward element on the display is always mapped to a rightward direction on the control or in the response. Once the 90-degree threshold is crossed, then right is left and left is right.

Mental rotation penalties are also structured so that direct opposite movements (e.g., right translation to 270-degree display movement, or forward translation to a 0 degree display movement) have a slightly smaller penalty than adjacent display movements (e.g., 240, 300) would impose. This is because users can often employ a verbally mediated reversal strategy to offset the incompatible spatial relation (e.g., "right is left" or "front is back"; Cizaire, 2007). Furthermore, data collected by both Gugerty and Brooks (2004) and Macedo et al (1998) indicate that the offsetting benefit of this cognitive reversal strategy spills over to angles adjacent to the 180-degree opposite angles (e.g., 160, 200).

Modulation of incompatibility penalties

In cases with a large cost of incompatibility (e.g., left-right mappings) are contrasted with those in which the cost is less (e.g., fore-aft mappings), just as the cost of incompatible mappings of the latter is reduced, so the benefits of compatible mappings in the latter are also reduced. That is, the range spanned by compatible-incompatible mappings is less, when the axis is less strongly mapped. In other words, a strong stereotype has a large cost when it is violated. For a weaker stereotype, the cost of violation is less.

Orthogonal axis offsets

A penalty is added when control movement in one plane (e.g., frontal, Y-Z) is mapped to display movement in an orthogonal plane (e.g., sagittal/horizontal X-Y or medial X-Z). Furthermore, based on the particular challenges associated with left-right mappings and left-right confusions (Franklin & Tversky, 1990), this penalty is assumed to be greater when an upward (Z) or forward (X) translation is mapped to a left-right (Y axis) movement (or vice versa), than it is for the 90-degree rotation between vertical movement and movement in depth (Chan & Hoffman, 2011). These latter mappings have the advantage of preserving the left-right mapping between display and action, whether the display (or control) surface is vertical or horizontal (DeLucia & Griswald, 2011). Indeed the former mappings ("around the corner") involving mapping lateral movement to fore-aft or up-down movements, produce a cost that is at least as great of the cost of line of sight ambiguity (see below), compared to the minimum costs of mapping fore-aft to up-down (DeLucia & Griswald, 2011). A specific example of such a mapping would occur, in Figure E-2, if the operator were exercising control laterally (Y axis) while viewing the workspace from the Y axis camera (DeLucia & Griswald,, 2011).

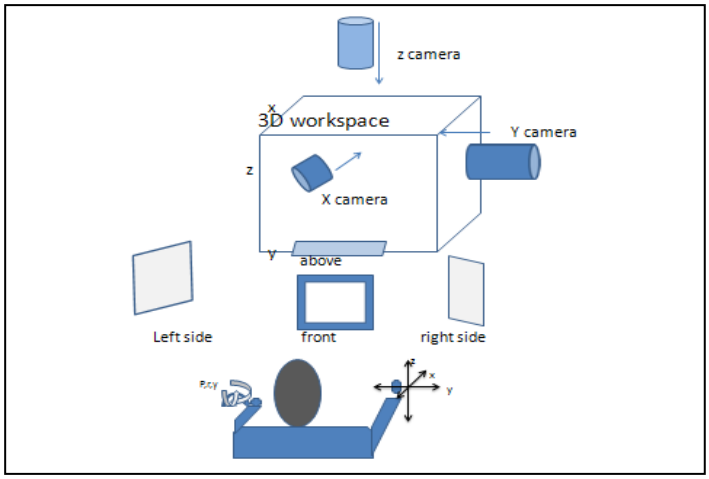

Figure E-2. Example workstation.

'Increase' population stereotypes

Data are fairly consistent that movement forward, rightward, upward and counter clockwise all correspond to increases in a quantity. However data remain more ambiguous as to the extent to which certain of these movements have a stronger stereotype than others (Chan & Hoffman, 2010). Were some consensus to emerge, it would justify placing different magnitude penalties on different movement orientations.

Translation-rotation penalties

Any time a translational control is mapped to a rotational display movement (or vice versa) there is an added penalty of 1, compared to a translation-translation pairing (e.g., translational control mapped to either display azimuth movement or depth movement), or to a rotational-rotational pair. This penalty is justified on the basis of data from Beckman (2002) examining performance in controlling the turn of a ground vehicle (rotation) by either translational or rotational movement of different controls. While, in some situations, a clockwise rotation on a frontally viewed display, is perceived equivalently to a rightward translation (Chan & Hoffman, 2011), so it may be that in this particular configuration, the translation-rotation is reduced, this qualification only holds when the focus of attention is on the top of the rotating display, or control or control is exercised on the top of the wheel.

Display movement in depth

Because of ambiguity and reduced resolution along the line of sight (Boeckman & Wickens, 2001; McGreevy & Ellis, 1986; Menchaca-Brandan et al., 2007; DeLucia & Griswald, 2011; Wickens, 2002; Wickens et al., 2005), any display that conveys movement in depth (e.g., looming, shrinking) is penalized compared with rotational or translational (compass) movement. This penalty will be applied independently of the direction of control movement that produced the display change. Naturally such a penalty will be a maximum when movement is directly parallel with the line of sight into the display, and moderated to the extent that the two angles are not parallel. While this penalty function is non-linear with angle disparity (Schreiber, Wickens et al., 1998; Boeckman & Wickens, 2001), it may be approximated by a linear function.

Moving viewpoint vs. moving object

Any control movement that moves a display viewpoint (e.g., a camera location or angle) is penalized, relative to a control movement that changes the location of an object against the fixed frame of the display. Such a penalty is assigned on the basis of the *principle of the moving part (*Johnson & Roscoe, 1972; Roscoe, 1968; Wickens & Hollands, 2000). This difference (controlled viewpoint or moving world vs. controlled object or moving object) has an opposite effect for compatible and incompatible motion relationships. For example, when controlling an object, one expects a rightward movement of the control to cause a rightward (90 degrees azimuth) movement of the object against the display frame. In contrast, when controlling the viewpoint of a camera looking at an object, one now expects the rightward movement of the control to cause a leftward movement of the object relative to the viewpoint or field of view of the display; so both of these will yield smaller penalties than their opposite direction counterparts.

Display location

As shown in Figure E-2, the displays used to control the element may be located at various azimuth and elevation angles relative to the operator. It is intuitively obvious that any display located away from the frontal plane should receive some penalty, independent of how it represents motion. Furthermore, the "visual field effect," first revealed by Worringham and Beringer (1989) and generally replicated in a series of studies by Chan and Hoffman (2010), indicates that this penalty is roughly equivalent across various motion relationships. For example, if the operator is looking toward the right display, a right-left motion depicted on that display will be most readily interpreted as a right-left motion in the 3D workspace, not a receding (forward) motion, even as, within the coordinate space of the **total workspace** (including the operators' seating and the display orientation as spatial elements)**,** that motion is actually a forward motion. Wickens et al. (2005) have referred to this as the *trunk dominance principle*, or trunk-forward bias, suggesting that people intuitively define their coordinate space around the more stable orientation of the trunk, independent of the momentary orientation of the head.

Relative penalties in the FORT model

In the above, we have identified a series of penalties for transformations. In some cases these penalties were continuous functions (e.g., increasing with visual angle offset). Furthermore, it may be the case that some penalties are greater than others. For example Chan & Hoffman (2010) report that the stereotype for "increase" is stronger with an upward than with a rightward movement, and there is ample evidence that transformations between lateral (Y axis) and either vertical (Z axis) or horizontal depth (Y axis) are substantially greater than between the latter two (DeLucia & Griswald, 2011). However at least in some cases, it appears that the magnitude of penalties within **different categories** are, within an order of magnitude, roughly equivalent. For example DeLucia's data suggest that line-of-sight ambiguity costs, and orthogonal mapping costs (from Y axis to X or Z axis) are approximately equivalent. As a consequence, and lacking nearly any data from experiments that have varied penalties orthogonally (e.g., as DeLucia did), we make the simplified assumption that: (a) all penalties are equivalent and (b) within each category, the penalties are assigned a small number of simple integer values, if there is more than one level (e.g., mental azimuth rotation) in the total FORT model described below.

Additive FORT penalties

Table E-1 presents the assignment of integer penalties for control movements, shown in the left columns, that produce different display movements, shown in the cells to the right. The table is broken into four sub-tables. At the top are penalties associated with rightward translation (RT), forward translation (FT) and upward translation (UT), as these movements produce display movements at different azimuth angles around a compass, viewed on a forward display. For example, we note that a rightward translation, producing a rightward moving (90 deg) object produces no penalty.

The specific values within the rows preserve several features of the psychological mechanisms described above. For example, moving outward from the point of maximum compatibility (parallel movement of control and display), penalties increase slowly from 0 to 60 degrees difference; they jump at a 90- (or 270-) degree orientation difference, reflecting the orthogonal mapping penalty; and then, while they continue to grow at angles beyond this, as they approach

angles directly opposite (e.g., 180-degree display movement for an upward translation) the penalty is somewhat suppressed, reflecting the verbal rehearsal strategy. Also within the table, alternate, highlighted rows, are those in which the viewpoint, rather than the depicted object moves. These penalties are all elevated by 1, reflecting a penalty for violating the principle of the moving part. They are also reversed since, for example an operator moving a viewpoint to the right (90 degrees) will expect to see the scene move to the left (270 degrees).

The second sub-table describes rotational motion in the three planes. The pattern of penalties across the columns is roughly equivalent to the pattern in the translational control motion sub-table, if it is assumed that a clockwise rotation of a vertically mounted control, corresponds to a rightward linear motion. There is an overall penalty for mapping rotation to translation, but the relative penalties within the rows remain the same. Correspondingly, it is assumed that a forward rotation of the top of a wheel rotating around the X axis corresponds to a forward translation, and here again the relative penalties are equivalent between the two sub-tables, except for the overall rotation-translation penalties. Somewhat more complex are the penalties assigned to a control rotation around a vertical axis (clockwise horizontal rotation or CHR). Here a clockwise rotation, often assumed to be an "increase" can also be seen as a movement of that part of the control closest to the operator, as a movement to the left. As a consequence of this ambiguity, the overall penalties within this row are elevated (by 1), relative to the rows above it. But since the stereotype for one direction is weaker than in those rows, the difference between compatible and incompatible azimuth movements is also reduced.

While the first two sub-tables all refer to display movement in a horizontal plane orthogonal to the user's line of sight, the left side of the bottom two tables refers to displayed movement in depth, when driven either by translational or rotational control. Two features are of note here: (1) All penalties are increased (by 1) reflecting the ambiguity (or compression) of movement parallel to the viewing axis (McGreevy & Ellis, 1986). (2) While display movement is, by definition, in the depth axis, there is no added penalty when the control moves vertically, rather in depth, because left-right mapping is not an issue, and left-right symmetry will always be preserved. However, there is a substantial penalty (of 1) when lateral movement is mapped to depth movement, because left-right has no natural mapping to fore-aft (Franklin & Tversky, 1990; DeLucia & Griswald, 2011). Finally, the right side of the bottom two tables describes rotational display motion in response to either translational (top) or rotational (bottom) motion. As before, there is an overall penalty of 1 added whenever translational motion is mapped to rotational displays, or vice versa.

A final feature of the FORT model relates to display location. As noted above, the existing data (Worringham & Beringer, 1989; Chan & Hoffman, 2010; Wickens et al., 2005) are generally consistent with the view that control display relations, with a control mounted in front of the operator, are generally unaffected by where the display is viewed (e.g., in front, to the side, above). This "visual field effect" or "trunk forward principle" justifies the assignment of penalties for off-axis viewing, to be independent of the control-display relations depicted within the context of the FORT matrix shown in Table E-1. However, to the extent that strong data do emerge suggesting that off-axis viewing may differentially reward (or punish) certain display control mappings, then off-axis penalties may be modified accordingly.

It should be noted that FORT penalties are only presented for a single axis. For multi-axis tracking when, for example, the operator may be required to move a two-axis joystick to control a cursor in all azimuths, to track a 2-D target, then the FORT penalties can be computed by simply adding (or averaging) those associated with rightward and forward translations.

Display Location Score
Finally, we note that the 'location scores' are based on some fairly straightforward heuristics supported by research: (1) Locations that preserve left-right compatibility receive small penalties. (2) Orthogonal mappings have larger penalties. (3) The orthogonal mapping that destroys left-right congruence between control and display movement receives the largest mapping penalty.

Current Limitations
As noted above, the FORT tool only computes one axis at a time, so for a multi-axis controller, separate sequencing of the tool's three steps must be undertaken. Currently there is no explicit modeling of how different axes combine (e.g., greater penalties for separate vs. multi-axis joysticks), so it is assumed that the total penalty of a set of axes is the sum of penalties over all single axes.

The tool also does not compute penalties if the position of the control is moved to the side. That is, an outward (away from body) movement of a control positioned to the right side, would have identical computation to the rightward movement of the control positioned as in panel A of the tool's GUI.

Model Exercises
While some model validation is inherent in the fact that the penalty matrix was constructed from empirical data (Small et al., 2008; Wickens et al., 2005), we have also applied or "exercised" the model explicitly to the movement relationships in a Space Shuttle docking scenario, as follows.

Exercise 1. Figure E-3 depicts a generic representation of this scenario with a side view. This representation is expanded in greater detail in each of the model exercises described below.

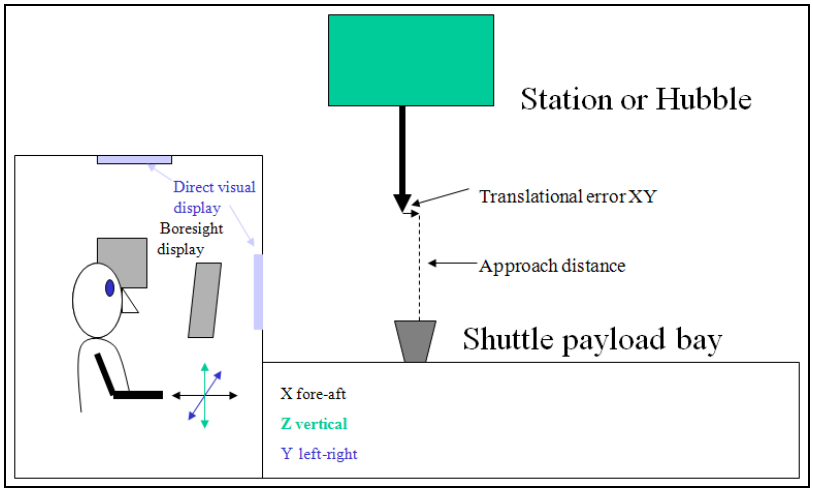

Figure E-3. Schematic representation of Shuttle docking with ISS or Hubble.

The operator is facing aft (-X direction) as the Shuttle is approaching the ISS docking port from below (+Z direction). The translational hand controller is typically set by the astronaut in the "-Z mode" to move the Shuttle (-Z motion) in response to forward movement of the translational control (-X direction).

In the following exercises, the Shuttle rendezvous is with the Hubble telescope, rather than the ISS.

Initial Hubble Rendezvous

Exercise 2. Figure E-4 shows the relative position of the Shuttle bay and Hubble space telescope during a rendezvous. In this case, the Shuttle itself is the controlled element (outlined in orange). The Hubble is represented by the green cylinder. The robotic arm (not used during initial rendezvous) is the black bar. The operator (Shuttle commander in this case) is positioned at the aft flight deck control station (left in the graphic) and facing aft (rightwards in the figure).

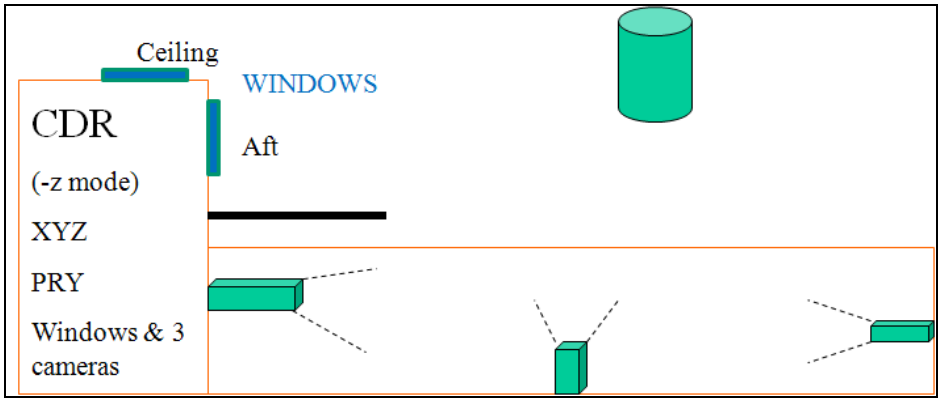

Figure E-4. Shuttle-Hubble initial rendezvous schematic. XYZ refers to the translational mode control axes; PRY (pitch, roll, yaw) refers to the rotational control axes.

The commander is flying the Shuttle from the aft control panel with the controls in the -Z mode. Based on observations of actual rendezvous video, the sequence involved mostly translational alignments but one big yaw rotation was performed. A number of displays (or viewports) could be used by the commander including direct viewing through the ceiling window and the aft window, and a display showing any of the three Shuttle bay cameras. The model was run multiple times for each of three display/viewports represented in the three matrices below. Within each of these, the different model runs represent the different axes of control. Within each matrix is the control-display mapping, and, in the right column, the mapping score for each axis. In each exercise description, we specify whether there is a moving viewpoint or a moving object.

Exercise 2.1. Ceiling window looking up at Hubble or mid-bay camera mounted in -Z, viewed in display screen (CF):

- Location score (A) = 3
- Location score (CF) = 0
- Moving viewpoint

Control Sequence	*Control Motion*	*Display Movement*	*Mapping Score*
FT → Lift	FT	Depth – looming	2
RT → Y	RT	270 deg	1
UT → X	UT	180 deg	1
CHR → Yaw	CHR	Rotation – counterclockwise	2
Mean score			1.5

Exercise 2.2. Aft window looking out at Hubble or forward bay camera in display screen (CF):

- Location score = 0
- Moving viewpoint

Control Sequence	*Control Motion*	*Display Movement*	*Mapping Score*
FT → Lift	FT	180 deg	2
RT → Y	RT	270 deg	1
UT → X	UT	Depth – shrinking	6
CHR → Yaw	CHR	Rotation – counterclockwise	2
<or>	CHR	270 deg	3
Mean score			2.8

Exercise 2.3. Aft bay camera looking at Hubble from tail of orbiter in display screen (CF):

- Location score = 0
- Moving viewpoint

Control Sequence	*Control Motion*	*Display Movement*	*Mapping Score*
FT → Lift	FT	180 deg	2
RT → Y	RT	90 deg	5
UT → X	UT	Depth – looming	4
CHR → Yaw	CHR	Rotation – clockwise	6
<or>	CHR	90 deg	6
Mean score			4.6

The mean mapping score, favoring the view through the upper window, assumes that there is equal weighting across all axes of control. In fact, however, if the commander were primarily using one (or a subset of) axes, these should be weighted more heavily in the mean score.

Final Rendezvous with Hubble

As shown in Figure E-5, the commander views a display showing the camera mounted to the end of the robotic arm. The camera is positioned viewing aft and orthogonal to the closing motion between the Hubble and the Shuttle as the latter moves upward. Control is exercised primarily by fore-aft motion of the translation controller. In the -Z mode, forward movement lifts the Shuttle toward the Hubble and aft motion descends it away. Left-right movement will move the Shuttle correspondingly. There is no need to position the Shuttle closer along the X axis as the

arm is already close enough to perform the grapple maneuver (discussed next), hence this axis is not computed.

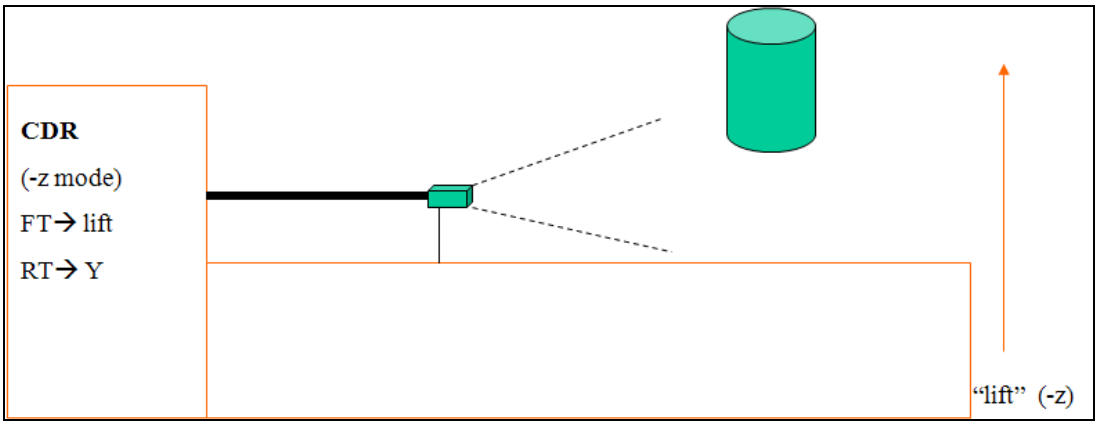

Figure E-5. Shuttle-Hubble final rendezvous schematic.

Exercise 3. Arm camera in video monitor (CF):

- Location score = 0
- Moving viewpoint

Control Sequence	***Control Motion***	***Display Movement***	***Mapping Score***
FT → Lift	FT	180 deg	2
RT → Y	RT	270 deg	1
Mean score			1.5

Robotic Arm Grapple to Hubble

As shown in Figure E-6, this task belongs to the mission specialist, again facing aft, and now controlling the robotic arm (in orange). With the Shuttle now well stabilized relative to Hubble, the arm is free to move with six degrees of freedom. The display shows the view from the camera attached to the end of the arm, as well as direct viewing through the aft- and upward-facing windows. The control sequence involves moving the end effector of the robotic arm over the grapple pin positioned at the side of the telescope.

Summary of robotic arm controls:

- X translation extends the arm away.
- Y translation moves the arm left-right.
- Z translation lifts or lowers the arm.
- Pitch, roll and yaw of the end effector are achieved by the joystick control, and produce a corresponding change in the angle of view of the effector-mounted camera.

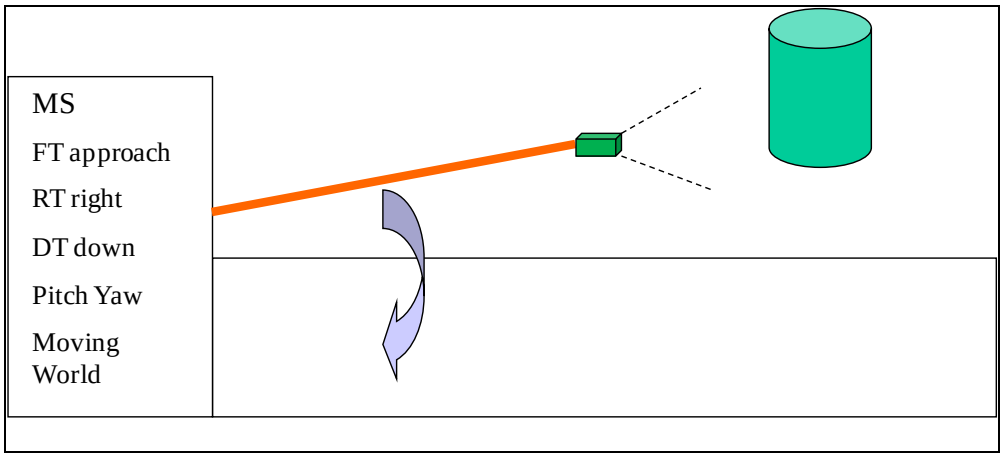

Figure E-6. Shuttle-Hubble grapple schematic. As indicated by the arrow, the arm and Hubble are actually rotated 45 degrees laterally (i.e., toward the figure's viewpoint) for the grappling coupling.

Exercise 4. Arm camera in video monitor (CF)

- Location score = 0
- Moving world or viewpoint

Control Sequence	***Control Motion***	***Display Movement***	***Mapping Score***
FT → approach	FT	Depth - Looming (toward viewer)	2
RT → right	RT	270 deg	1
UT → up	UT	180 deg	1
FR → pitch	FR	0 deg	2
CHR → yaw	CHR	270 deg	3
Mean score			1.8

In conclusion, the model exercises above have not truly validated the model by comparing outputs against actual Shuttle data. The exercises do verify that the FORT tool is working as expected. We have validated the model by applying it against data from others who have worked in areas of robotics and remote vehicle control (Gugerty & Brooks, 2004; Macedo et al., 1998). During tool development, the exercises produced plausible predictions regarding the ease of control. For the most part, all configurations appear to have been implemented without large transformations (i.e., good compatible mappings). Only one of these, Exercise 2.3, had a high penalty – a value of 4.6 given a maximum possible penalty score of 7.0. Here the cause of the high score is due to controlling an object from a viewport looking directly back at the human controller, which is similar to flying a model airplane or UAV on visual contact that is headed toward the operator, which imposes major left-right reversals or transformations.

Appendix F. Shuttle Survey Package

The package was approved by the MIT and JSC IRBs on 8/4/10. It includes a cover letter, subject information handout, consent form, and the survey.

Cover Letter

From: Thomas D. Jones {date}
To: {subject's name and address}

Subject: Shuttle entry and landing spatial orientation survey

Enclosures: *Subject Information Handout* (yours to keep), *Consent Form* (please sign and return in the enclosed envelope), *Survey* (please complete and return in the enclosed envelope)

Dear {subject's name}:

As you may already know, I've been working with Ron Small at Alion Science and Technology Corp. (Boulder, Colo) and Charles Oman of MIT on a project called ***Modeling and Mitigating Spatial Disorientation in Low G Environments***. It is funded by NASA's Human Research Program through the National Space Biomedical Research Institute. Our main focus is to develop math models to predict human spatial orientation in 0-G and upon return to Earth, and to develop potential spatial disorientation countermeasures.

A component of the project is to better understand the tilting and tumbling sensations many of us felt during Shuttle missions, especially at MECO after launch, and when we made head movements during and after return to Earth. For me, the sensations depended on G level during re-entry, and were strongest during and immediately after landing, but faded within a few hours.

Neurovestibular researchers have some ideas about what might cause the tilting and tumbling sensations; however, data are limited and incomplete. Published descriptions – such as the ones I included in *Sky Walking* – are anecdotal. So are flight surgeon and crew debriefing notes. We don't know if different people have similar sensations, or if vehicle maneuvers, as well as deliberate head movements, cause such sensations.

Certainly commanders and pilots are aware of the phenomena, and have successfully overcome any such sensations – presumably by avoiding head movements at critical times, or simply by "flying through it." Some crew members have tried making small ("trial") head movements to hasten their re-adaptation, although we don't know how useful those are.

With the imminent retirement of Shuttle, it may be many years until crews again fly a spacecraft through an approach and landing. Because you are one of the few who has flown the Shuttle, we think it is historically and scientifically important to capture your personal experiences with these sensations, and to understand how you dealt with them. Therefore, we request that you complete the enclosed survey. You may have seen earlier versions of this survey; this version incorporates feedback from initial respondents and a peer review, and therefore supersedes earlier versions.

If you agree, please read the *Subject Information Handout*, complete the *Consent Form*, and then answer the questions in the *Survey*. Please return the signed *Consent Form* and your completed *Survey* in the enclosed stamped envelope. Based upon initial samples, we estimate that the whole process will take you only 30 minutes.

Thank you for considering my request!

Best wishes,
Thomas D. Jones
281-286-7626 (office)
skywalking@comcast.net

Subject Information Handout

Subject Information Handout
Modeling and Mitigating Spatial Disorientation in Low G Environments
Shuttle entry and landing spatial orientation survey

Introduction
The principal investigator for this survey study is Ron Small at Alion Science and Technology Corp. in Boulder, Colorado, with Dr. Charles Oman of MIT as a co-investigator, and Dr. Thomas Jones as a co-investigator and the primary contact with astronaut subjects, such as you. Another Alion employee, John Keller, will help with data analyses.

We ask you to take part in this study because of your past experience as a Space Shuttle commander or pilot. Your participation is entirely voluntary.

Purpose and Background
(See Tom's cover letter.)

Number of People
We are asking as many Shuttle commanders and pilots as practical to complete our *Survey*.

Procedures
Please read through the enclosed multiple-choice *Survey*, and decide if you are willing to complete it. If you are, please sign and date where indicated on the *Consent Form*, and provide the mission data requested. We estimate that the *Survey* will take you up to 30 minutes to complete. Your participation is entirely voluntary. You may skip any question for any reason.

After you complete the survey, make a copy for your records, or we will send you a copy (depending on which line you check on the *Consent Form*). Please mail your completed *Consent Form* and *Survey* in the enclosed envelope.

Voluntary Participation
Your participation in this study is completely voluntary and you are free to withdraw your consent and terminate your participation at any time by notifying the investigator (see Questions for contact information). Your withdrawal from this study will be entirely without penalty and will not affect your participation in future studies.

Risks and Discomforts – Not applicable.

Benefits
There are no direct benefits to you from completing the *Survey*. Future benefits should include an improved knowledge of spatial disorientation during the transition from orbit to Earth and for the few days after landing.

Alternatives
The alternatives to completing the entire *Survey* are to only complete portions of it, or to not complete any of it.

Privacy and Confidentiality
Your completed *Survey* and *Consent Form* will be given an identifying code so as to protect your identity.

We will store the *Consent Forms* and *Surveys* in separate locked cabinets in a locked Alion office, with access to the full data by only four of the researchers on the project team. All *Surveys* and *Consent Forms* will be destroyed by September 1, 2014 which is three years after project completion.

Your privacy as a research subject and the confidentiality of any research data about you associated with this study will be maintained in accordance with 1) NASA Policy Directive (NPD) 7100.8, "Protection of Human Research Subjects," 2) NASA Procedural Requirements (NPR) 7100.1, "Protection of Human Research Subjects," and 3) to the extent allowed by Federal law.

Access to Research Records
Your data will be analyzed with others to determine the prevalence of illusory sensations and any statistical significance or trends. These data will not be identified by name. We may discuss data and analytical results at professional conferences or in publications. If we do, we will only report aggregate data (e.g., 28 of 34 commanders or pilots reported some orientation illusions during or immediately after Space Shuttle missions), or relevant de-identified quotes or paraphrasing (e.g., "During one of my flights, I [the commander] experienced an illusion during a head movement and so did not fly the HAC.").

Costs and Financial Considerations – Not applicable.

Payment and Reimbursement
You will not be paid to complete this *Survey*. You should have no costs associated with completing this *Survey*, other than your time.

Treatment and Compensation for Injury – Not applicable.

Questions
If you have questions, concerns or complaints about the *Survey*, please contact Dr. Thomas Jones at 281-286-7626 (office) or skywalking@comcast.net, or the project's principal investigator, Ron Small, at 303-518-5827 (cell), 303-442-6947 (office), or rsmall@alionscience.com.

You may also contact the NASA Johnson Space Center Committee for the Protection of Human Subjects (281-212-1468), or the MIT Committee on the Use of Humans as Experimental Subjects (617-253-6787). Both committees are independent of the research team and are available for questions regarding the rights and welfare of research subjects, such as you.

Consent
Your participation in this research is entirely voluntary. You have the right to decline to participate or to withdraw at any time without penalty or loss of benefits to which prospective subjects are otherwise entitled.

Your signature on the *Consent Form* indicates your agreement to participate.

Video and Photo Consent – Not applicable.

Consent Form

CONSENT TO PARTICIPATE IN SURVEY

My signature below acknowledges my voluntary participation in this research project. Such participation does not release the investigators, institutions, or granting agency from their professional and ethical responsibility to me. I have read and understand the information provided in the *Subject Information Handout* and have had my questions, if any, answered to my satisfaction. I voluntarily agree to participate in this study. I understand that I am free to retain my copy of the *Subject Information Handout* for as long as I would like.

Your printed name _____

Your signature _____ **Date** _____

Please check one:
___ Please mail me a copy of this signed *Consent Form* and my completed *Survey*.
___ I made myself a copy before I returned the *Consent Form* and *Survey*.

Your Personal Shuttle Spaceflight History:

Flight Number	**Mission** (STS number)	**Mission Month & Year**	**Duration** (days)	**Role** (Commander or pilot)
1st				
2nd				
3rd				
4th				
5th				
6th				

What is your birth date? _____ (To be used for analyses of age groups.)

Survey key number _____ (assigned by Tom or Ron)

Shuttle Survey

{Pagination is different from the distributed survey.}

Shuttle Spatial Orientation Survey
Modeling and Mitigating Spatial Disorientation in Low G Environments
NASA/NSBRI Investigators: Tom Jones, Ron Small and Charles Oman

Survey key number _____ (assigned by Tom or Ron)

Instructions: Please circle the letter in front of the appropriate answer(s), based on your ***most recent*** mission. If you recall different experiences on one or more earlier missions, please feel free to note that in the margin. So that your survey responses remain anonymous, refer to your missions by your sequential Flight Number listed on the *Consent Form*, rather than STS mission number. For example, you might indicate "1" (for your 1st flight) next to Question 1, choice b, and "2 & 3" next to choice a.

1. After launch and during main engine cut-off (MECO) did you experience any spontaneous (i.e., not induced by head motion) illusory sensations?
   a. No.
   b. Yes, but I don't recall details.
   c. Yes, I felt as though I was doing a backward summersault.
   d. Yes, I felt as though I was doing a forward summersault.
   e. Yes, I felt another sensation. Please briefly explain: _____
   f. Yes, as indicated above, and the feeling was transient (i.e., lasted a few seconds or less).
   g. Yes, as indicated above, and the feeling was sustained. If sustained, please estimate how long the sensation lasted in seconds or minutes: _____

2. During MECO did you experience any illusory sensations when you moved your head?
   a. No.
   b. Yes, but I don't recall details.
   c. Yes, I felt as though I was doing a backward summersault.
   d. Yes, I felt as though I was doing a forward summersault.
   e. Yes, I felt as though I was tumbling (i.e., like I was doing a continuous summersault, or experienced a sensation of a multi-axis rotation).
   f. Yes, I felt another sensation. Please briefly explain: _____
   g. Yes, as indicated above, and the feeling was transient (i.e., lasted a few seconds or less).
   h. Yes, as indicated above, and the feeling was sustained. If sustained, please estimate how long the sensation lasted in seconds or minutes: _____

3. During re-entry did you make any deliberate head movements to see how they felt?
   a. No.
   b. Yes.
   c. Why or why not? Please briefly explain: _____

4. Did any head movements, deliberate or not, during re-entry produce any illusory sensations? (Circle all that apply.)
   a. I experienced no illusory sensations during head movements.
   b. I recall having one or more illusory sensations when moving my head, but I don't recall details.
   c. When I pitched or rolled my head, my head seemed to tilt more than the actual motion.

d. When I pitched or rolled my head, my head seemed to tumble (i.e., like I was doing a continuous summersault, or experienced a sensation of a multi-axis rotation).
e. When I pitched or rolled my head, my head seemed to tilt less than the actual motion.
f. When I pitched or rolled my head, the tilt sensation lagged the actual motion.
g. I felt a brief translation (linear motion) in an opposite direction to my head tilt.
h. I felt a brief translation (linear motion) in the same direction as my head tilt.
i. When I yawed my head, the visual scene seemed to blur.
j. When I yawed my head, the visual scene seemed to move in the opposite direction.
k. When I yawed my head, the visual scene seemed to move in the same direction.
l. Other: _____
m. Yes, as indicated above, and the feeling was transient (i.e., lasted a few seconds or less).
n. Yes, as indicated above, and the feeling was sustained. If sustained, please estimate how long the sensation lasted in seconds or minutes: _____

5. Were there any phases of flight or maneuvers where you deliberately avoided moving your head? (Circle all that apply.)
   a. No.
   b. Yes, but I don't recall details.
   c. TAEM turns.
   d. HAC turn.
   e. Intercepting the inner glide slope.
   f. Landing flare.
   g. Rotation to nose-wheel touchdown.
   h. Rollout.
   i. Other: _____

6. When the Shuttle rolled during TAEM (i.e., all maneuvers pre-HAC), did you experience any illusory sensations? (Circle all that apply.)
   a. No.
   b. Yes, but I don't recall details.
   c. Yes, the Shuttle seemed to pitch more than indicated on flight instruments.
   d. Yes, the Shuttle seemed to roll more than indicated on flight instruments.
   e. Yes, the Shuttle seemed to pitch less than indicated on flight instruments.
   f. Yes, the Shuttle seemed to roll less than indicated on flight instruments.
   g. Yes, the Shuttle's pitch rate seemed to be more than indicated on the instruments.
   h. Yes, the Shuttle's roll rate seemed to be more than indicated on the instruments.
   i. Yes, the Shuttle's pitch rate seemed to be less than indicated on the instruments.
   j. Yes, the Shuttle's roll rate seemed to be less than indicated on the instruments.
   k. Other: _____
   l. Yes, as indicated above, and the feeling was transient (i.e., lasted a few seconds or less).
   m. Yes, as indicated above, and the feeling was sustained. If sustained, please estimate how long the sensation lasted in seconds or minutes: _____

7. When transitioning from automatic flight to manual (at about Mach 1 or just before the HAC), did you experience any illusory sensations?
   (Circle all that apply.)
   a. No.
   b. Yes, but I don't recall details.
   c. Yes, the Shuttle seemed to pitch more than indicated on flight instruments.
   d. Yes, the Shuttle seemed to roll more than indicated on flight instruments.
   e. Yes, the Shuttle seemed to pitch less than indicated on flight instruments.

f. Yes, the Shuttle seemed to roll less than indicated on flight instruments.
g. Yes, the Shuttle's pitch rate seemed to be more than indicated on the instruments.
h. Yes, the Shuttle's roll rate seemed to be more than indicated on the instruments.
i. Yes, the Shuttle's pitch rate seemed to be less than indicated on the instruments.
j. Yes, the Shuttle's roll rate seemed to be less than indicated on the instruments.
k. Other: _____
l. Yes, as indicated above, and the feeling was transient (i.e., lasted a few seconds or less).
m. Yes, as indicated above, and the feeling was sustained. If sustained, please estimate how long the sensation lasted in seconds or minutes: _____

8. When the Shuttle rolled during the HAC turn, did you experience any illusory sensations? (Circle all that apply.)
   a. No.
   b. Yes, but I don't recall details.
   c. Yes, the Shuttle seemed to pitch more than indicated on flight instruments.
   d. Yes, the Shuttle seemed to roll more than indicated on flight instruments.
   e. Yes, the Shuttle seemed to pitch less than indicated on flight instruments.
   f. Yes, the Shuttle seemed to roll less than indicated on flight instruments.
   g. Yes, the Shuttle's pitch rate seemed to be more than indicated on the instruments.
   h. Yes, the Shuttle's roll rate seemed to be more than indicated on the instruments.
   i. Yes, the Shuttle's pitch rate seemed to be less than indicated on the instruments.
   j. Yes, the Shuttle's roll rate seemed to be less than indicated on the instruments.
   k. Other: _____
   l. Yes, as indicated above, and the feeling was transient (i.e., lasted a few seconds or less).
   m. Yes, as indicated above, and the feeling was sustained. If sustained, please estimate how long the sensation lasted in seconds or minutes: _____

9. When the Shuttle intercepted the inner glide slope and decelerated, did you experience any illusory sensations? (Circle all that apply.)
   a. No.
   b. Yes, but I don't recall details.
   c. Yes, the Shuttle seemed to pitch more than indicated on flight instruments.
   d. Yes, the Shuttle seemed to roll more than indicated on flight instruments.
   e. Yes, the Shuttle seemed to pitch less than indicated on flight instruments.
   f. Yes, the Shuttle seemed to roll less than indicated on flight instruments.
   g. Yes, the Shuttle's pitch rate seemed to be more than indicated on the instruments.
   h. Yes, the Shuttle's roll rate seemed to be more than indicated on the instruments.
   i. Yes, the Shuttle's pitch rate seemed to be less than indicated on the instruments.
   j. Yes, the Shuttle's roll rate seemed to be less than indicated on the instruments.
   k. Other: _____
   l. Yes, as indicated above, and the feeling was transient (i.e., lasted a few seconds or less).
   m. Yes, as indicated above, and the feeling was sustained. If sustained, please estimate how long the sensation lasted in seconds or minutes: _____

10. During the Shuttle's landing flare, did you experience any illusory sensations? (Circle all that apply.)
    a. No.
    b. Yes, but I don't recall details.
    c. Yes, the Shuttle seemed to pitch more than indicated on flight instruments.
    d. Yes, the Shuttle seemed to roll more than indicated on flight instruments.
    e. Yes, the Shuttle seemed to pitch less than indicated on flight instruments.

f. Yes, the Shuttle seemed to roll less than indicated on flight instruments.
g. Yes, the Shuttle's pitch rate seemed to be more than indicated on the instruments.
h. Yes, the Shuttle's roll rate seemed to be more than indicated on the instruments.
i. Yes, the Shuttle's pitch rate seemed to be less than indicated on the instruments.
j. Yes, the Shuttle's roll rate seemed to be less than indicated on the instruments.
k. Yes, the Shuttle seemed higher AGL than indicated on the instruments.
l. Yes, the Shuttle seemed lower AGL than indicated on the instruments.
m. Yes, the Shuttle seemed to have a faster speed than indicated on the instruments.
n. Yes, the Shuttle seemed to have a slower speed than indicated on the instruments.
o. Other: _____
p. Yes, as indicated above, and the feeling was transient (i.e., lasted a few seconds or less).
q. Yes, as indicated above, and the feeling was sustained. If sustained, please estimate how long the sensation lasted in seconds or minutes: _____

11. During the Shuttle's rotation to nose-wheel touchdown, did you experience any illusory sensations? (Circle all that apply.)
    a. No.
    b. Yes, but I don't recall details.
    c. Yes, the Shuttle seemed to pitch more than indicated on flight instruments.
    d. Yes, the Shuttle seemed to roll more than indicated on flight instruments.
    e. Yes, the Shuttle seemed to pitch less than indicated on flight instruments.
    f. Yes, the Shuttle seemed to roll less than indicated on flight instruments.
    g. Yes, the Shuttle's pitch rate seemed to be more than indicated on the instruments.
    h. Yes, the Shuttle's roll rate seemed to be more than indicated on the instruments.
    i. Yes, the Shuttle's pitch rate seemed to be less than indicated on the instruments.
    j. Yes, the Shuttle's roll rate seemed to be less than indicated on the instruments.
    k. Other: _____
    l. Yes, as indicated above, and the feeling was transient (i.e., lasted a few seconds or less).
    m. Yes, as indicated above, and the feeling was sustained. If sustained, please estimate how long the sensation lasted in seconds or minutes: _____

12. After wheel stop, before leaving the flight deck, did head movements produce any illusory sensations? (Circle all that apply.)
    a. No.
    b. Yes, but I don't recall details.
    c. When I pitched or rolled my head, my head seemed to tilt more than the actual motion.
    d. When I pitched or rolled my head, my head seemed to tumble (i.e., like I was doing a continuous summersault, or experienced a sensation of a multi-axis rotation).
    e. When I pitched or rolled my head, my head seemed to tilt less than the actual motion.
    f. When I pitched or rolled my head, the tilt sensation lagged the actual motion.
    g. I felt a brief translation (linear motion) in an opposite direction to my head tilt.
    h. I felt a brief translation (linear motion) in the same direction as my head tilt.
    i. When I yawed my head, the visual scene seemed to blur.
    j. When I yawed my head, the visual scene seemed to move in the opposite direction.
    k. When I yawed my head, the visual scene seemed to move in the same direction.
    l. Other: _____
    m. Yes, as indicated above, and the feeling was transient (i.e., lasted a few seconds or less).
    n. Yes, as indicated above, and the feeling was sustained. If sustained, please estimate how long the sensation lasted in seconds or minutes: _____

13. During re-entry, did you experience any illusory sensations unrelated to a head movement? (Circle all that apply.)
    a. No.
    b. Yes, but I don't recall details.
    c. Yes, I experienced a spontaneous illusion. Please briefly describe the illusion: _____

    d. Yes, I experienced illusory sensations due to vehicle maneuvering, deceleration, turbulence, or gusts.
    e. Yes, I experienced illusory sensations due to visual factors (e.g., cloud bank, false horizon, etc.)
    f. Other: _____
    g. Yes, as indicated above, and the feeling was transient (i.e., lasted a few seconds or less).
    h. Yes, as indicated above, and the feeling was sustained. If sustained, please estimate how long the sensation lasted in seconds or minutes: _____

14. When flying manually, did you experience any illusory sensations unrelated to a head movement? (Circle all that apply.)
    a. Not applicable; I did not fly manually.
    b. No, I experienced no spontaneous illusory sensation when flying manually.
    c. Yes, but I don't recall details.
    d. Yes, I experienced a spontaneous illusion. Please briefly describe the illusion: _____

    e. Yes, I experienced illusory sensations due to vehicle maneuvering, deceleration, turbulence, or gusts.
    f. Yes, I experienced illusory sensations due to visual factors (e.g., cloud bank, false horizon, etc.).
    g. Yes, the Shuttle felt more sensitive than my training experiences suggested, so that I needed to deliberately reduce the size of my control inputs.
    h. Yes, the Shuttle felt less sensitive than my training experiences suggested, so that I tended to over-control it.
    i. Other: _____
    j. Yes, as indicated above, and the feeling was transient (i.e., lasted a few seconds or less).
    k. Yes, as indicated above, and the feeling was sustained. If sustained, please estimate how long the sensation lasted in seconds or minutes: _____

15. If you experienced an illusory sensation when flying manually, how easy or difficult was it to "fly through"? (Circle a single answer.)
    a. Not applicable; I did not fly manually.
    b. I experienced no illusory sensation when flying manually.
    c. I don't recall the level of difficulty.
    d. Very easy.
    e. Easy.
    f. Moderate.
    g. Difficult.
    h. Very difficult.
    i. Impossible; I had to transfer control to the other pilot or use auto-flight.

16. Referring to Question #15, if you did "fly through" an illusory sensation, which technique helped you to do so? (Circle all that apply.)
    a. I experienced no illusory sensation when flying manually.
    b. I don't recall which technique I used.
    c. Concentrating on the HUD.
    d. Concentrating on other flight instruments.

Please specify which one(s): _____

e. Verbal cues; talked to myself or with the other pilot.
f. A combination of visual and verbal techniques.
Please specify which ones: _____

g. Other: _____

17. To prevent illusory sensations and/or to improve your sense of accurate orientation, which displays, controls, procedures, and/or techniques would you enhance or add to the Shuttle? Please briefly explain your answer, if any.

18. During the post-flight walk-around, did you experience any illusory sensations? (Circle all that apply.)
    a. No.
    b. I was unable to accomplish the post-flight walk-around because of:
        i. A temporary lack of coordination.
        ii. Dizziness.
        iii. Fainting or being light-headed.
        iv. Other: _____
    c. Yes, but I don't recall details.
    d. Yes, during head movements.
    e. Yes, during body movements.
    f. If you answered Yes in d or e, please briefly explain the illusory sensation(s) you experienced:

    g. Yes, as indicated above, and the feeling was transient (i.e., lasted a few seconds or less).
    h. Yes, as indicated above, and the feeling was sustained. If sustained, please estimate how long the sensation lasted in seconds or minutes: _____

19. Immediately after landing (up to about 2 hours after landing), did you experience any illusory sensations related to a head movement?
    a. No.
    b. Yes, but I don't recall details.
    c. Yes. Please briefly explain: _____

    d. Yes, as indicated above, and the feeling was transient (i.e., lasted a few seconds or less).
    e. Yes, as indicated above, and the feeling was sustained. If sustained, please estimate how long the sensation lasted in seconds or minutes: _____

20. From about 2 to 24 hours after landing, did you experience any illusory sensations related to a head movement?
    a. No.
    b. Yes, but I don't recall details.
    c. Yes. Please briefly explain: _____

    d. Yes, as indicated above, and the feeling was transient (i.e., lasted a few seconds or less).
    e. Yes, as indicated above, and the feeling was sustained. If sustained, please estimate how long the sensation lasted in seconds or minutes: _____

21. From about wheel stop to 24 hours after landing, did you experience any difficulties with your balance or ability to walk normally (e.g., around corners or up/down stairs)?
    a. No.

b. Yes, but I don't recall details.
c. Yes. Please briefly explain: _____

22. Beyond 24 hours after landing, did you experience any illusory sensations related to head movement?
a. No.
b. Yes, but I don't recall details.
c. Yes. Please briefly explain: _____

d. Yes, as indicated above, and the feeling was transient (i.e., lasted a few seconds or less).
e. Yes, as indicated above, and the feeling was sustained. If sustained, please estimate how long the sensation lasted in seconds or minutes: _____

23. Beyond 24 hours after landing, did you experience any difficulties with your balance or ability to walk normally (e.g., around corners or up/down stairs)?
a. No.
b. Yes, but I don't recall details.
c. Yes. Please briefly explain: _____

24. In future vehicles, how do you think cockpits should be changed to improve the astronaut pilot's ability to reduce, minimize or eliminate the chances of experiencing illusory sensations (i.e., to maintain accurate spatial orientation)? (Circle all that apply.)
a. No changes needed.
b. Bright, large-format, high-contrast displays (including HUDs).
c. Layouts that minimize the need for head movements.
d. Larger, wider artificial horizon displays.
e. Larger windows.
f. Alternative head restraints; please suggest one or more: _____

g. Other procedures or techniques; please explain: _____

h. Other: _____

25. Do you have any other experiences or ideas related to spatial orientation issues during space operations that you'd like to describe? If so, please use the space below.

Thank you, again, for taking the time to complete our *Survey!*

Please return the *Survey* and signed *Consent Form* (with Your Personal Shuttle Spaceflight History and birth date) in the envelope provided.

Appendix G. Acronyms

1-D	one-dimensional
2-D	two-dimensional
3-D	three-dimensional
6-DOF	six degrees of freedom (pitch, roll, yaw, x, y, z motions)
abs	absolute value
AFRL	Air Force Research Laboratory
AGL	above ground level; height above the surface, usually in feet
aka	also known as
ASEM	*Aviation, Space and Environmental Medicine*
AsMA	Aerospace Medical Association
CDR	commander
cm	centimeter(s)
CNS	central nervous system
COTR	contracting officer's technical representative
DCM	direction cosine matrix
deg	degree(s)
.dll	dynamically linked library
DoD	Department of Defense
FAST	Function Allocation Simulation Tool
FDR	flight data recorder (aka black or orange box)
flt.	flight
FOR	frame of reference
FORT	frame of reference transformation
fpm	feet per minute (vertical speed units, typically)
g	acceleration due to gravity; 1-g at the Earth's surface
GIF	gravito-inertial force vector
GUI	graphical user interface
HAC	heading alignment circle; Space Shuttle maneuver to align with runway
HFES	Human Factors and Ergonomics Society
HUD	head-up display
IRB	institutional review board
ISS	International Space Station
JSC	NASA's Johnson Space Center
MA&D	Micro Analysis & Design operation within Alion
MECO	main engine cut-off
MIDAS	Man-Machine Integration Design and Analysis System
MIT	Massachusetts Institute of Technology
MVL	Man Vehicle Lab
NA, n/a	not applicable
NAMRL	Naval Aeromedical Research Laboratory (U.S.)
NASA	National Aeronautics and Space Administration
NSBRI	National Space Biomedical Research Institute
N-SEEV	pilot attention model (noticing - salience, effort, expectancy, value)
NTSB	National Transportation Safety Board (official aircraft accident investigators in the U.S.)
OTTR	otolith tilt-translation reinterpretation
OVAR	off-vertical-axis rotation
PhD	doctor of philosophy degree
PI	principal investigator

Q	question (as in survey question number…)
R&D	research and development
RT	response or reaction time
ROTTR	rotation otolith tilt-translation reinterpretation
SA	sensorimotor adaptation
SCC	semi-circular canal
SD	spatial disorientation
SDAT	Alion's spatial disorientation analysis tool
sec	second(s)
SM	science master's degree
SME	subject matter expert
SOAS	Alion's spatial orientation aiding system
SVV	subjective visual vertical
TAEM	terminal area energy management; Space Shuttle maneuvers (usually S turns) to lose energy prior to HAC
THC	translational hand controller
U.S.	United States
USAARL	U.S. Army Aeromedical Research Laboratory
USAF	U.S. Air Force
VAC	SDAT's vestibular attitude calculator
VLV	vertical landing vehicle
VMS	NASA Ames' vertical motion simulator
VOR	vestibular-ocular reflex
VR	virtual reality
WoW	weight on wheels (surface contact)